DEVELOPMENT AND EXPERIMENTAL TESTING OF PRESS-BRAKE-FORMED STEEL TUB GIRDERS FOR SHORT SPAN BRIDGE APPLICATIONS

Karl E. Barth, Ph.D.
Gregory K. Michaelson, Ph.D.
Robert M. Tennant

VOLUME V: FATIGUE PERFORMANCE OF UNCOATED AND GALVANIZED COMPOSITE PRESS-BRAKE-FORMED TUB GIRDERS

Submitted to the AISI Steel Market
Development Institute Short Span
Steel Bridge Alliance

ABSTRACT

FATIGUE PERFORMANCE OF UNCOATED AND GALVANIZED COMPOSITE PRESS-BRAKE-FORMED TUB GIRDERS

The Short Span Steel Bridge Alliance (SSSBA) is a group of bridge and culvert industry leaders (including steel manufacturers, fabricators, service centers, coaters, researchers, and representatives of related associations and government organizations) who have joined together to provide educational information on the design and construction of short span steel bridges in installations up to 140 feet in length. Within the SSSBA technical working group, a modular, shallow press-brake-formed steel tub girder was developed. This new technology consists of cold-bending standard mill plate width and thicknesses to form a trapezoidal box girder. The steel plate can be uncoated or galvanized steel, as each is an economical option. Once the plate has been press-brake-formed, shear studs are welded to the top flanges. A reinforced concrete deck is cast on the girder in the fabrication shop and allowed to cure, forming a composite modular unit. The composite tub girder is shipped to the bridge site, expediting construction and reducing traffic interruptions.

The increased use of the press-brake-formed tub girders has led to the recognition that long-term service life testing of different steel types in this system have not been investigated. The cold-bending of the steel plate into the desired tub-girder shape creates residual stresses in the bends of the girder. At this time, the majority of prefabricated bridge elements undergoing fatigue testing are of traditional structural shapes. It is currently unknown if the high heat of galvanization affects the residual stresses in the bends of the tub girder.

The scope of this project is to determine if hot-dip galvanization affects the fatigue performance of a cold-bent shallow press-brake-formed steel tub girder. Two composite steel tub girders were constructed, one composed of an uncoated steel tub and the second composed of a galvanized steel tub. The composite system was fatigue loaded simulating a 75-year life in a rural environment. At a predetermined number of load cycles, a Service II load was applied to the system to observe the performance of the specimen. Strain gages were applied to the webs and bottom flange of each section to determine the actual moments induced in the system. Experimental results were used to evaluate any difference in the performance of the different steels used in the composite tub girder system. Results from this project show the type of steel does not have an influence on the fatigue performance of press-brake-formed tub girders.

TABLE OF CONTENTS

LIST OF TABLES

LIST OF FIGURES

CHAPTER 1: INTRODUCTION

1.1 BACKGROUND / OVERVIEW

A technical group within the Short Span Steel Bridge Alliance (SSSBA) developed the concept of modular shallow press-brake-formed steel tub girders. The SSSBA is a group of bridge and culvert industry leaders (including steel manufacturers, fabricators, service centers, coaters, researchers, and representatives of related associations and government organizations) who have joined together to provide educational information on the design and construction of short span steel bridges in installations of up to 140 feet in length. The concept of modular shallow press-brake-formed steel tub girders consists of cold-bending standard mill plate widths and thicknesses to form a trapezoidal box girder. The steel plate can consist of either uncoated or galvanized steel. However, comparison of the fatigue performance between cold-bent tub girders consisting of different coating options has not been conducted. When the steel plate is bent into the trapezoidal box girder using a press-brake, residual stresses are created in the bends. To evaluate potential weakening caused by the galvanization process, two full scale fatigue tests of two different 38 foot cold-bent press-brake formed steel tub girders, one girder being uncoated steel and the other being hot-dip galvanized, were performed at West Virginia University.

1.2 PROJECT SCOPE & OBJECTIVES

The scope of this report was to test two composite modular press-brake-formed tub girders, one being uncoated steel and the other being galvanized. Additionally, a design example using press-brake-formed tub girders selected from optimized designs by Michaelson (2014) is included. Specifically, these objectives were assessed using the following four steps:

- A brief discussion of prior work done on press-brake-formed tub girders and their place in accelerated bridge construction
- A design example using tub girders utilizing the AASHTO LRFD Bridge Design Specifications (2014), demonstrating applications of critical limit states in press-brake-formed tub girders

- An explanation of the research methods and laboratory testing conducted on the different specimens, including a full description of the experimental investigation
- A summary of results and conclusions comparing the experimental data collected on the uncoated steel specimen and the galvanized steel specimen

1.3 REPORT ORGANIZATION

A brief overview of the organization of this report is as follows:

- Chapter 2:
  - This chapter will provide a general overview of accelerated bridge construction methods, with a more specific investigation into the research conducted on cold-bent tub girder applications at West Virginia University and elsewhere. Additionally, a summary of corrosion prevention systems is provided.
- Chapter 3:
  - This chapter contains a design example on press-brake tub girders. This includes the calculation of composite section properties and the AASHTO LRFD limit states that needed to be addressed.
- Chapter 4:
  - This chapter discusses the research methods employed during the testing program. A detailed explanation of the assembly of the composite girder and loading description is provided within.
- Chapter 5:
  - This chapter discusses the results obtained during testing. Methods used for data analysis and material properties are contained within.
- Chapter 6:
  - This chapter provides a summary of the project and recommendations for future work.
- Appendix A:
  - This appendix describes the calculations of the Service II and Fatigue I moments.
- Appendix B:
  - This appendix documents the experimental gage data obtained during the testing.

CHAPTER 2: LITERATURE REVIEW

2.1 INTRODUCTION

This chapter presents a general overview of previous research and implementation of cold-bent tub girders and their place in accelerated bridge construction. The literature review starts by discussing accelerated bridge construction and the methods proven popular to implement. A summary of previous research performed on cold-bent tub girders is presented, concluding with an in-depth review of work done at West Virginia University. Section 2.5 covers the field implementations and concurrent research performed on press-brake-formed steel tub girder bridges. Section 2.6 discusses the different corrosion protection systems, including painting, hot-dip galvanizing, and the use of weathering steel.

2.2 ACCELERATED BRIDGE CONSTRUCTION

The Every Day Counts (EDC) program was launched in 2009 by the Federal Highway Administration (FHWA) in conjunction with the American Association of State and Highway Transportation Officials (AASHTO) with the goal to accelerate the delivery of highway projects and to address the obstacles faced by limited budgets (FHWA Pamphlet, 2014). The goal of EDC is to identify and rapidly deploy innovations to shorten the project delivery procedure, improve highway safety, reduce congestion, and promote environmental sustainability. Every two years, a summit is held between the FHWA, state and local agencies, and industry stakeholders to collaboratively select innovations. State and local agencies then focus on the innovations that work best for their programs' needs and commit to finding opportunities to implement these innovations.

An innovation promoted for the 2013-2014 cycle was Accelerated Bridge Construction (ABC). ABC is a style of bridge construction, which uses innovative planning, design, materials, and construction methods to safely and cost-effectively reduce onsite construction time when building new bridges or replacing and restoring existing bridges (Culmo, 2011). ABC has become highly desirable to many states' Departments of Transportation.

When the modern highway network was under construction, most projects focused on new infrastructure, as opposed to replacing old infrastructure. These projects typically did not have traffic acting along the path which required redirection and did not occur in physically constrained spaces. This allowed more use of shored formwork and was not an inconvenience to the public for multi-month to multi-year construction projects. As a significant number of these original bridges approach and surpass their service lives, rapid bridge replacement has become a focus in the bridge construction industry. Many practices utilized in the original construction of these aging bridges are antiquated and no longer suitable or economical for current needs.

The use of ABC methods has many benefits, the most important being improved safety. Worker and motorist safety has improved by shortening travel lane restrictions by performing most construction away from traffic. Reduction of on-site construction shortens the total project delivery time, which can greatly reduce total project cost (FHWA Pamphlet, 2014). Off-site construction in a climate-controlled setting has improved the quality of bridge members. Temperature, humidity, rain, snow, and other environmental factors can have adverse effects on construction elements. To reduce environmental impacts, the EDC initiative included three particular ABC technologies in its second round of initiatives: Geosynthetic Reinforced Soil Integration Bridge Systems, Slide-In Bridge Construction, and Prefabricated Bridge Elements and Systems.

2.2.1 Geosynthetic Reinforced Soil-Integration Bridge System

Geosynthetic Reinforced Soil Integrated Bridge System (GRS-IBS) is a rapid, inexpensive method of bridge support unification of the roadway and the superstructure to create a jointless interface between the bridge and the approach (Adams et al., 2011). The three components of GRS-IBS are the reinforced soil foundation (RSF), the abutment, and the integrated approach. The RSF consists of compacted granular soil encompassed in a geotextile fabric. Using geosynthetic reinforcement in soil is an alternative to deep foundations on sub-optimal material. The abutment used in this system utilizes compacted fill with closely spaced geosynthetic material and is quicker than conventional approach slabs to install because it is placed directly on the RSF without a joint and without cast-in-place concrete. GRS-IBS is used in the approach to the bridge to transition to

the superstructure. This use of the same material in the abutment and the approach smooths the transition by removing differential settlement. A GRS-IBS cross section is seen in Figure 2.1.

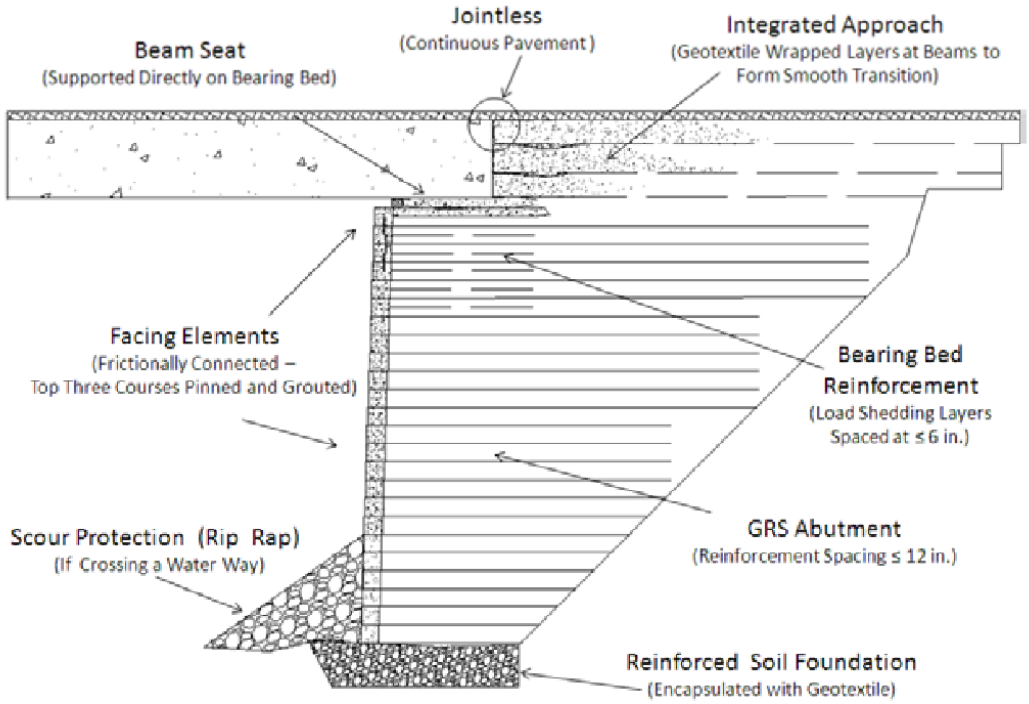

Figure 2.1: Typical GRS-IBS Cross Section (Adams et al., 2011)

2.2.2 Slide-In Bridge Construction

Slide-In Place Bridge Construction (SIBC) allows construction of a new bridge while maintaining traffic on the existing bridge during the majority of construction (FHWA, 2013). Temporary supports are constructed adjacent to the existing bridge, and the new bridge is built on these supports, as seen in Figure 2.2. Once construction of the new bridge is complete, the old bridge is closed and demolished or moved to a staging area for demolition and removal. The new bridge slides into place, approach tie-ins are constructed, and traffic reopened.

Some of the benefits of using SIBC include enhanced safety, potential reduced project costs, and improved constructability. Safety is improved by reducing the interaction between construction workers and vehicular traffic because typical phased construction requires construction of one half of the bridge, opening it to traffic, and then construction of the second

half. SIBC allows construction of the entire bridge at once, reducing the time of mobilization, concrete curing, and other phases of conventional construction. Constructability improves because more room for girders, concrete placement, and equipment access away from constant traffic are provided.

Figure 2.2: Overhead View of West Mesquite SIBC Project, Nevada (FHWA, 2013)

2.2.3 Prefabricated Bridge Elements and Systems

Prefabricated Bridge Elements and Systems (PBES) is the concept of bridge design and construction where most or all bridge components are fabricated off-site and only need to be shipped to and assembled at the construction site. The ultimate goal of PBES and ABC is to reduce construction impacts on the public. Expedient construction greatly reduces detours around the construction site and mitigate environmental effects. Off-site construction of all components necessary to build the bridge prior to on-site installation reduces time lost to conventional construction practices. Completing the majority of construction off site removes the need for on-site typical constructional aspects and wait time regarding curing.

In addition to reduced on-site construction time, PBES allows fabrication in a controlled environment, which inherently improves construction quality because bridge components are not

exposed to weather during construction. This approach affords faster construction of prefabricated modules because specialized workers will be able to use formwork multiple times instead of rebuilding forms each time an element needs reproduced. PBES also improves safety of workers by reducing time exposed to traffic while working.

2.3 Previous Applications of Cold-Bent Steel Girders

Prefabricated steel tub girders have seen a resurgence in popularity over the last few years, but they are not a new technology. Prefabricated composite tub girders were a proposed solution as early as the 1970s. Specifically, as ABC has come to the forefront of bridge design, tub girders have shown a potential for short span steel bridge applications as they can be economical and competitive at spans under 60 feet. Several other researchers have conducted studies focused on economical and rapid bridge construction utilizing cold-bent steel tub girders.

2.3.1 Prefabricated Press-Formed Steel T-Box Girder Bridge System (Taly & Gangarao, 1979)

Taly and Gangarao (1979) proposed a design for a set of cold-formed box girders suitable for spans up to 65 feet. Cold-formed girders are created by bending cold plate steel in a large capacity press-brake with the inside bend radius equal to five times the thickness of the plate. The all steel design had a stem of a trapezoidal box cold-formed from a 3/8 inch thick A-36 steel plate welded to a 3/8 inch thick steel top flange (Figure 2.3). This modular system could transfer load to adjacent girders through continuous welds provided at the junctions of the flanges. The advantages of such a system include, but are not limited to, high torsional stiffness of closed sections, increased effectiveness in distributing a load, and increased effectiveness for bridges on horizontal curves.

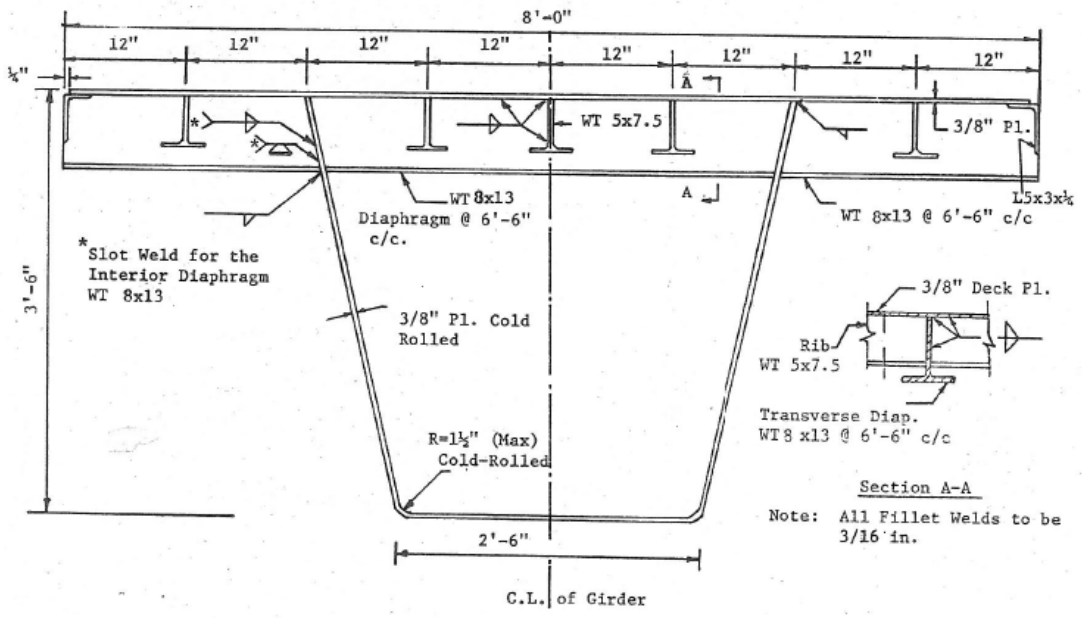

Figure 2.3: Taly and Gangarao's Proposed All-Steel Section (Taly & Gangarao, 1979)

The other major advantage of this system is its ability to be constructed off site. The superstructure is fabricated in pieces under controlled conditions so quality of the individual members and structure as a whole increases. A cold-bent system, opposed to a system of welded plates in the form of a box, reduces the amount of fabrication by eliminating another step in the construction process. The low weight of the all steel system, approximately 11 tons for a 65 foot long girder with a depth of 42 inches, allows the use of low capacity equipment for handling, transportation, and erection.

An alternative to the all steel system was proposed by Taly and Gangarao using a 5 inch thick precast, prestressed concrete deck instead of a 3/8 inch thick steel plate as seen in Figure 2.4. Composite action would be developed through shear studs welded to the top flanges of the cold-bent section. At the time, the AASHTO specifications did not provide design criteria for the design of members using a press brake or composite box girders. Therefore, the researchers evaluated their designs against the 1977 American Iron and Steel Institute (AISI) specifications.

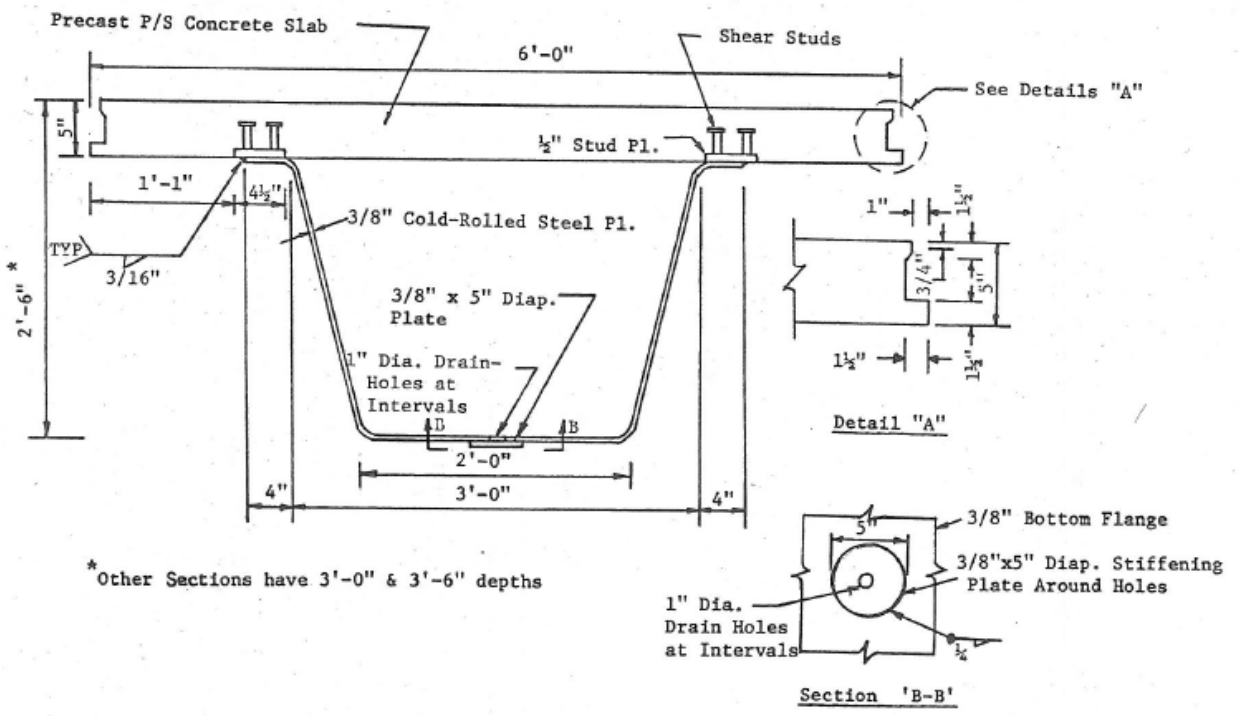

Figure 2.4: Taly and Gangarao's Composite Section (Taly & Gangarao, 1979)

2.3.2 Composite Girders with cold Formed Steel U-sections (Nakamura, 2002)

Nakamura (2002) envisioned a continuous multi-span system utilizing a cold-bent steel girder with a reinforced concrete deck. The system behaves as a typical composite section over span centers but is in negative bending over the intermediate supports of a continuous girder. This negative bending places the reinforced concrete deck in tension and creates potential for buckling of the bottom flange over the support.

To overcome this susceptibility of buckling, the U-section is filled with concrete and pre-stressed by prestressed concrete bars to increase the strength against the negative bending moment. Typical prestressed girders require formwork and scaffolding to pour the concrete but these U-Sections act as a mold, which further reduces fabrication costs. This concrete over the support increases the vertical reaction over the pier but does not increase the moment because the concrete is poured over the intermediate supports and not over midspans. Figure 2.5 shows Nakamura's proposed bridge system with an exposed cross-section over a midspan with concrete only in the deck section.

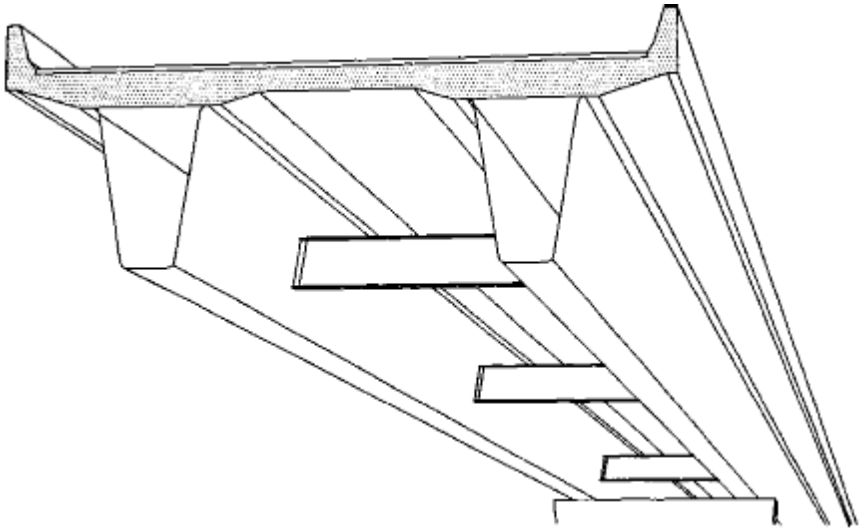

Figure 2.5: Nakamura's Proposed Bridge System (Nakamura, 2002)

Nakamura carried out bending tests to investigate the behavior of the proposed design. These tests confirmed the system behaved as a composite beam at span centers and behaved as a prestressed beam over the intermediate supports with the filled concrete restricting the buckling of the steel plates in compression. The researcher concluded the modified tub-girder system had sufficient bending strength and deformation capacity and deemed the design to be feasible and economical. A shortcoming of the design is the requirement of more steel than a typical plate girder section; however, the fabrication cost is more dominant than the material cost, suggesting the total construction cost could be lowered.

2.3.3 Folded Plate Girders (Developed at the University of Nebraska)

Researchers at the University of Nebraska have performed testing on cold-bent steel tub girders with a composite reinforced concrete deck. Figure 2.6 shows the system where an inverted tub-girder has flanges bent inward and a concrete deck poured on the wider center flange, opposed to the previous systems where the deck was cast on smaller exterior flanges. Glaser (2010) specifically investigated the constructability of the girder. During construction, a bridge is in its

least stable condition due to not having the concrete to join the members together; it is important the bridge components exhibit both adequate strength and stability non-compositely during this critical stage (Glaser, 2010). The researcher performed a flexure test of the non-composite beam to simulate the loads present during construction. The system displayed stability and ductility through testing because there were no measurable permanent deformations in the girder at loads equivalent to those experienced during construction. Advantages of this system include a safer work area due to the wider top flange and easier access for maintenance and inspection by the bottom being open.

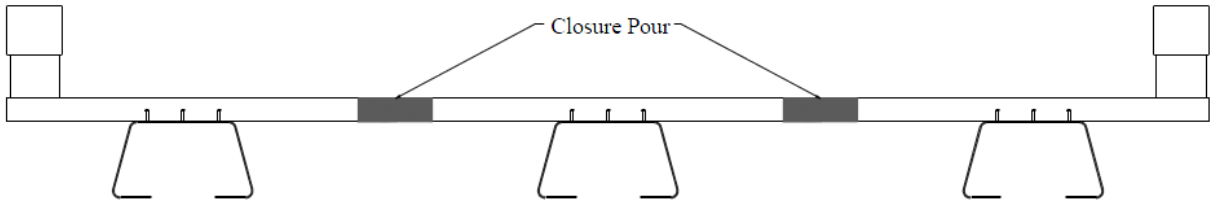

Figure 2.6: System Proposed at the University of Nebraska (Burner, 2010)

Another researcher at the University of Nebraska, Burner (2010), subjected the composite inverted tub girder to fatigue loading and investigated the rebar details in closure regions between adjacent slabs. Based on the fatigue testing, the inverted girder withstood the equivalent of 75 years of traffic without a significant loss in stiffness. The bends of the tub girder, which contain residual stresses from the cold-bending, did not experience any change in behavior through fatigue testing. The optimum rebar detail was found to be hooked bars because they do not pose the same concrete cover issues found with headed bars. Headed bars can be difficult to obtain due to their specialized fabrication where hooked bars do not require specialized fabrication details.

2.3.4 Texas Department of Transportation Rapid Economical Bridge Replacement

The Texas Department of Transportation (TxDOT) developed a highly construable, light, and efficient shallow trapezoidal steel box girder for the FM 3267 bridge on a six lane stretch of I-35 located 75 miles north of Austin, Texas (Chandar et al., 2010). The tub girder consisted of a

five foot wide bottom flange welded to two three foot deep webs, as seen in Figure 2.7, with two rows of shear studs welded to the top flanges. The shear studs connected the trapezoidal box girder to the cast-in-place concrete deck. Due to the lightweight nature of box girders, each girder was directly supported by individual columns, removing the need for a bent cap and reducing construction time.

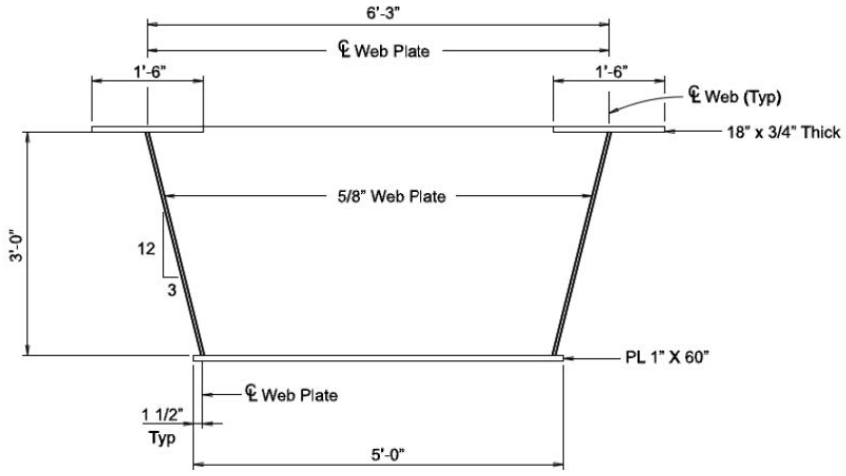

Figure 2.7: TxDOT Trapezoidal Box Girder for Rapid Bridge Replacement (Chandar et al., 2010)

The bridge consisted of six shallow box girders with a combined width of 78 feet with four spans of lengths of 45 feet, 100 feet, 100 feet, and 65 feet respectively. The box girder section was designed for a 100 foot section, and the 45 foot and 65 foot sections used the same larger section reducing design time. While ABC methods were implemented in design, conventionally fabricated steel tub girders, comprised of welded plate sections, were employed as opposed to girders formed using cold-bending.

2.3.5 MDOT Prefabricated Composite Steel Box-Girder Systems for Rapid Bridge Construction

The Michigan Department of Transportation (MDOT) was interested in a completely prefabricated composite steel box girder which could be shipped to the construction site where only placement and post-tensioning would be required to complete construction (Burgueño &

Pavlich, 2008). As seen in Figure 2.8, the system consists of a press-formed or cold-bent steel plate connected to a cast-in-place or precast deck by shear studs. The goal was to gain knowledge of this modular system by performing multiple finite element analyses to address the global system response of the system to applied loads, the localized behavior of joints, and the effect of reduced post tensioning on both the global system and the joints. Researchers found issues including fatigue deficiencies with cold-bent plates, efficiency of box sections, and difficulty with internal inspection of the girder. However, they addressed each concern and found the system to be a feasible option in the short span bridge market and a rapid construction alternative.

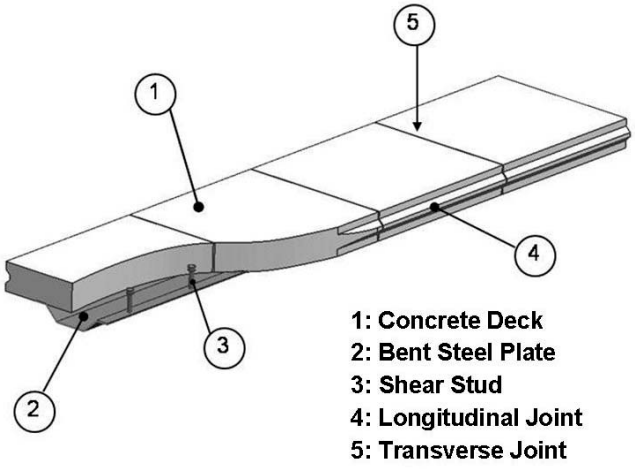

Figure 2.8: MDOT Proposed Bridge System (Burgueno & Pavlich, 2008)

2.3.6 Con-Struct Prefabricated Bridge System

The Con-Struct Prefabricated Bridge System was established in 2004 as an answer to the growing demand for ABC products (Con-Struct Pamphlet). The system, as seen in Figure 2.9, is a prefabricated composite bridge consisting of a shallow steel tub girder and a concrete deck. The concrete deck is cast on the steel tub girder when the girder is cambered. Cambering the girder in this fashion increases the serviceability of the system. Designs of this system are valid up to 60 feet in length and are available in various classes for different desired service lives. The Con-Struct system has been implemented by states such as Minnesota, Missouri, and Michigan.

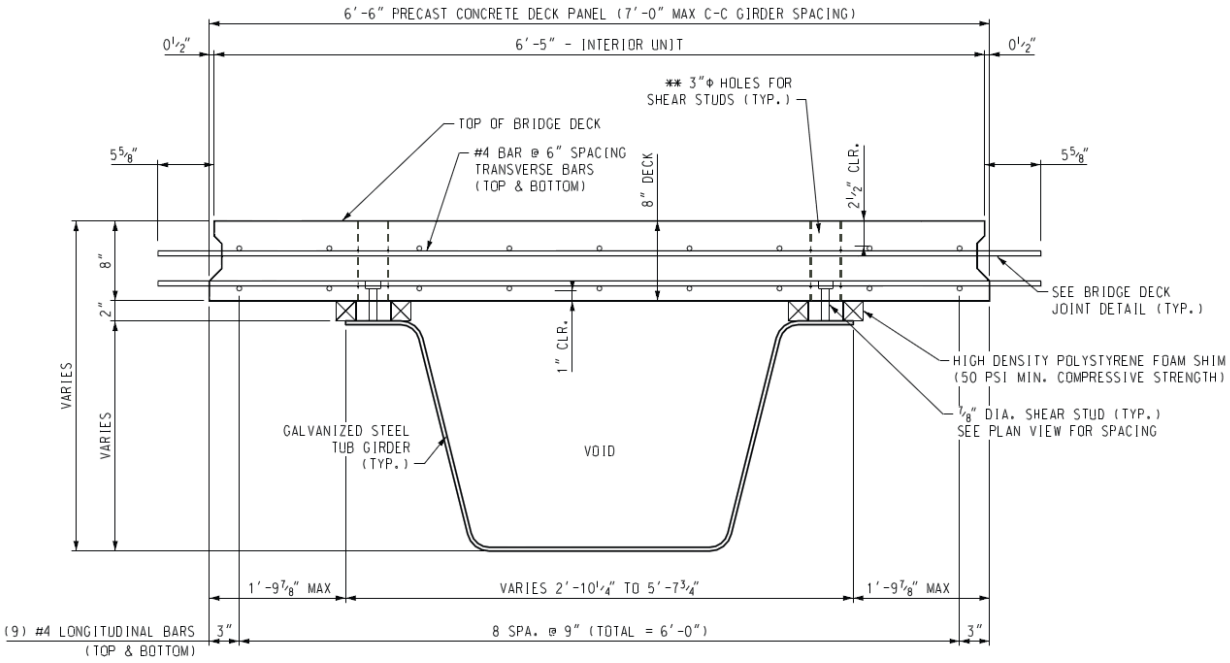

Figure 2.9: Typical Interior Con-Struct Cross Section

2.4 PREVIOUS RESEARCH AT WVU ON PRESS-BRAKE-FORMED STEEL TUB GIRDERS

2.4.1 Development and Feasibility Assessment of Shallow Press-Brake-Formed Steel Tub Girders for Short-Span Bridge Applications (Michaelson 2014)

The SSSBA developed the notion of a shallow press-brake-formed tub girder consisting of cold-bending standard mill plate width and thickness. In the design, shear studs are welded on the upper flanges and a reinforced concrete deck is cast on top of the newly formed girder. This process takes place in a fabrication shop and the concrete cures creating a composite unit. This modular unit can be shipped to the construction site allowing for quicker construction.

To design the tub-girders, Michaelson (2014) first developed a spreadsheet to compute the section properties of any configuration of different bent plate sizes. In this study, three different standard plate thicknesses were considered: 7/16, 1/2, and 5/8 inch. Six different standard plate widths were evaluated: 60, 72, 84, 96, 108, and 120 inch. The bottom flange width and depth of web were varied to find the optimum design while keeping other variables, such as slope of the

web, inside bend radii, and top flange widths, constant. The optimum design was assessed by comparing total girder depth to yield moment of the composite section. Figure 2.10 displays an example of the comparison of total girder depth to yield moment and shows the optimum depth of an 84 inch wide standard mill plate.

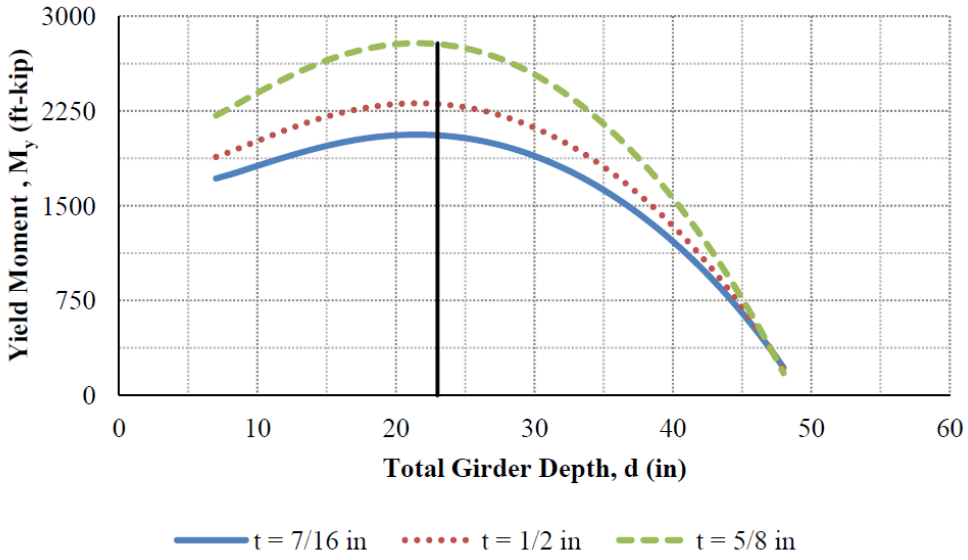

Figure 2.10: Design Comparison of 84" Wide Plate (Michaelson, 2014)

Physical flexural testing was performed on the composite and non-composite modular tub girders to confirm the performance and capacity of the units. Specimens were simply supported and flexural testing occurred in three-point bending. Two girders were tested non-compositely without the reinforced concrete deck or shear studs welded to the top flanges and two were tested with the reinforced concrete deck cast on top. Each of the four specimens tested was made from 84 inch wide x 7/16 inch thick x 280 inch long plate. This plate was chosen for testing because it created the largest tub-girder which could be tested to ultimate failure using a 330-kip servo hydraulic actuator. The deck thickness was shortened from eight inches to six inches to ensure failure could be reached. The composite section's failure was controlled by ductility where the concrete deck crushed under a load of approximately 300 kip and 3.1 inches of midspan deflection. The non-composite sections failed as the tub-girders began to exhibit significant lateral deflection and twist.

Michaelson also performed two separate analyses to evaluate the behavior and capacity of the proposed system. Finite element analysis (FEA) was used and results were compared against experimental data to assess legitimacy and precision. A comparison of the FEA and experimental results can be seen in Figure 2.11. A strain-compatibility assessment evaluated the flexural capacity of the press-brake tub girder. An iterative approach was used to predict the ultimate capacity of the section in positive flexure. The approach proved adequate in determining the capacity of the composite section.

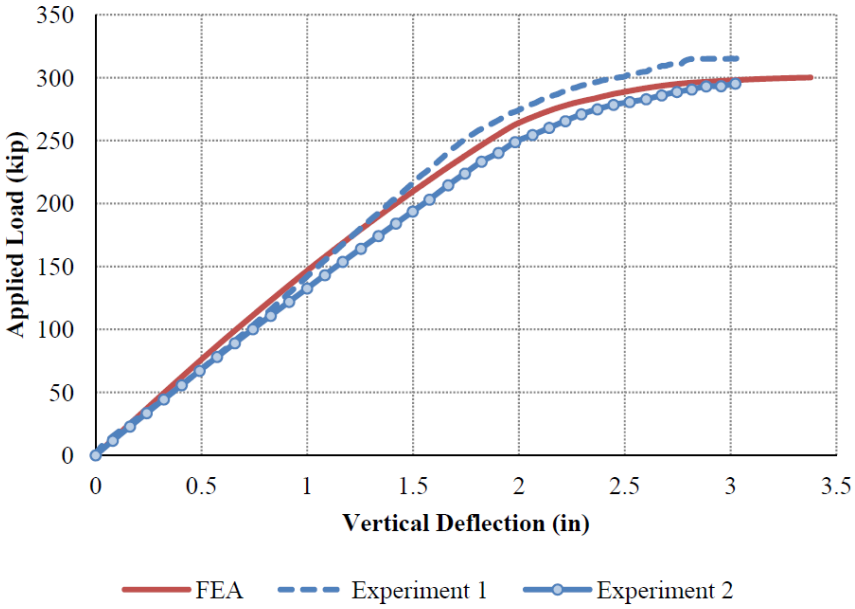

Figure 2.11: Comparison of Experimental and Analytical Results (Michaelson, 2014)

Behavioral studies were employed to assess the applicability of AASHTO Load and Resistance Factor Design (LRFD) specifications for the system. The nominal flexural capacity calculations from the specifications were slightly conservative for determining the capacity of the system. An assessment of non-composite stability behavior showed other means of construction were possible, such as a cast-in-place concrete deck. The loads present during construction were found to be substantial for an open press-brake-formed tub girder. The finishing machine and other torsional loads, such as eccentric concrete loads, proved the girder was susceptible to lateral torsional buckling under one third of the load applied to the composite section. However, stay-in-place metal formwork greatly improved the performance of the non-composite system.

Michaelson addressed the feasibility and compared the proposed system to traditional options for short span bridges. A set of girders were proposed by eliminating plates which are not regularly manufactured. It was found that widths of 72, 96, and 120 inch are industry standard and most producers in the United States produce 1/2 inch thick plate steel. Four standardized systems were found to be economically competitive for different spans with live load distribution factors equal to 1.0. The author stated further research assessing live load distribution factors for tub girders may further increase economic competitiveness.

2.4.2 Experimental Evaluation of Non-Composite Shallow Press-Brake-Formed Steel Tub Girders (Kelly 2014)

In conjunction with Michaelson, Kelly (2014) assessed the feasibility of a cast-in-place concrete deck in contrast to shipping a cured modular composite unit. While pouring the concrete deck, the non-composite steel open section must support the construction load including the wet concrete. Two girders were non-compositely tested under three-point bending. Before testing began, an initial tilt was noticed in both girders. Figure 2.12 shows the inclination of the webs at points across the length of the girder where no inclination should exist. The galvanized specimen had a much higher initial twist than the weathering steel specimen due to fabrication errors prior to hot dip-galvanization.

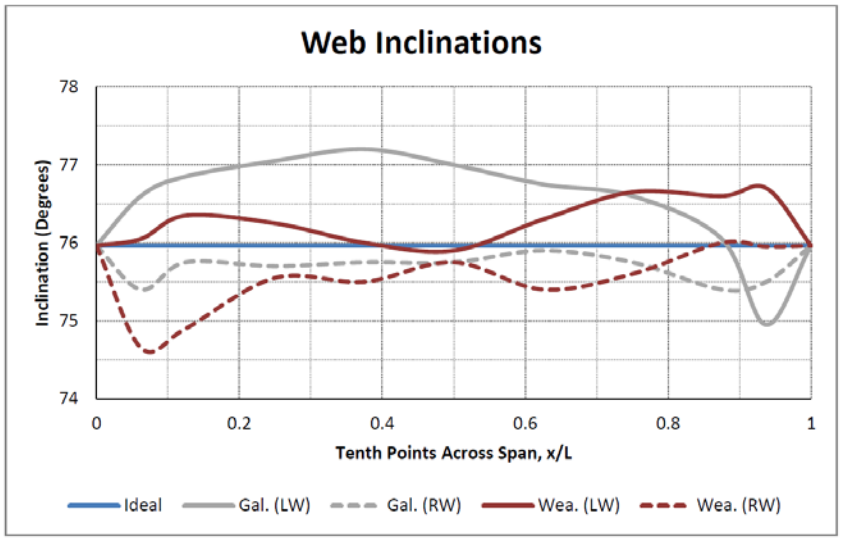

Figure 2.12: Web Inclinations (Kelly, 2014)

The first-order lateral torsional buckling capacity of the tub girder was calculated to 10,590 in-kip corresponding to a point load at mid-span of 92.3 kip. The weathering steel specimen deflected linearly up to a loading of 94 kip, consistent with the calculated limit, when it suddenly failed in lateral torsional buckling, as seen in Figure 2.13. The testing of the galvanized steel specimen performed similarly until a critical loading of 33 kip, when it suddenly failed in lateral torsional buckling. The loss of capacity was attributed to the second-order effects relating to initial fabrication imperfections prior to galvanization.

Figure 2.13: Lateral Torsional Buckling (Kelly, 2014)

2.4.3 Evaluation of Modular Press-Brake-Formed Tub Girders with UHPC Joints (Kozhokin, 2016)

Durable connections are needed to join modular prefabricated bridge elements and systems together. Ultra-high performance concrete (UHPC) is a cementitious material containing Portland cement, silica fume, quartz flour, fine silica sand, high-range water reducer, water, and steel fibers. Kozhokin (2016) tested the structural performance of modular press-brake-formed tub girders connected by UHPC. Two techniques can be used to create an exposed aggregate finish for the

slab edge. The first technique involved applying a retarder to the shear key formwork and wire brushing the concrete. The other technique included gluing a 3/4 inch stone to the formwork to create voids in the concrete slab edge after formwork removal. After testing both techniques, the form retarder and wire brushing to remove concrete paste produced the better results and was used during construction of the full-scale model, as seen in Figure 2.14.

Figure 2.14: Concrete Surface after Wire-Brushing (Kozhokin, 2016)

The UHPC joint was poured between two modular press-brake-formed tub girders with a reinforced concrete deck cast on top. After the two modular units were combined with UHPC along the length of the specimens, a 67.43 kip cyclic load was applied to induce the Fatigue I moment over 2,737,500 cycles. The Fatigue I load combination reflects the load found to be representative of the maximum stress range of the truck population for infinite fatigue life design. The load was applied in the center of one of the press-brake formed tub girders through a 20 inch x 10 inch x 1 inch plate to replicate a truck tire contact area. At a predetermined amount of cycles, the fatigue loading halted and a static load was applied, inducing a Service II moment, to see if the twin tub girder unit began to act abnormally.

After 1,635,000 cycles, the concrete deck failed by punching shear directly under the load application. The actuator was moved to the center of the other girder and a 30 inch x 18 inch x 1/2

inch plate was used under the actuator to help spread the load and to avoid the punching shear failure seen previously. Loading of the second girder continued through 2,800,000 cycles with only a single shear crack propagating across the UHPC joint from the failed deck region (Figure 2.15). Material testing of the concrete determined the compressive strength of the deck concrete was only 3,000 psi after 28 days, which contributed to the punching shear failure. The UHPC joint performed satisfactorily throughout subsequent testing transferring stresses from one girder to the other.

Figure 2.15: Shear Crack Propagated Across UHPC Joint (Kozhokin, 2016)

2.5 CURRENT IMPLEMENTATIONS OF PRESS-BRAKE-FORMED STEEL TUB GIRDERS

2.5.1 Amish Sawmill Bridge in Buchanan County, Iowa

County Engineer Brian Keierleber, P.E. managed construction of the first bridge designed, constructed, and opened to traffic utilizing press-brake-formed steel tub girders (Gibbs, 2017). Demolition of the old bridge began late in the summer of 2015 and the construction of the new bridge was complete in December of 2015. Four galvanized tub girders, made from 96 inch wide by 1/2 inch thick plate were bent before being shipped to the site. Contractors chose to use a 31 foot 3 inch wide by 8 1/2 inch thick cast-in-place concrete deck. In addition to utilizing tub girders, the New Amish Sawmill Bridge used GRS-IBS consisting of GRS abutments with a galvanized sheet piling face. Researchers from West Virginia University and Marshall University traveled to Iowa to perform testing when construction was completed (Figure 2.16).

Figure 2.16: New Amish Sawmill Bridge (Gibbs, 2017)

Experimental testing was performed on site by researchers while FEA was performed on a model of the bridge. The purpose of the testing was to investigate if AASHTO specifications could safely be applied to press-brake-formed tub girders. Comparing results from the live load field test to the finite element model analysis shows the live load distribution factors (LLDFs) were very close, but the actual bending stresses in the field test bottom flanges were much lower than the finite element model. This was attributed to differing boundary conditions. The Amish Sawmill Bridge design included integral abutments, but the finite element model utilized simply supported boundary conditions. Simply supported conditions were used in the model because there are not proper methods in current practices to replicate integral abutments. When comparing the LLDFs from the load test and the finite element model with AASHTO specifications, the AASHTO specifications were considerably higher (Figure 2.17). From this study, it was determined LLDFs calculated using specifications from AASHTO may be used for press-brake-formed tub girders with the understanding that the method is very conservative.

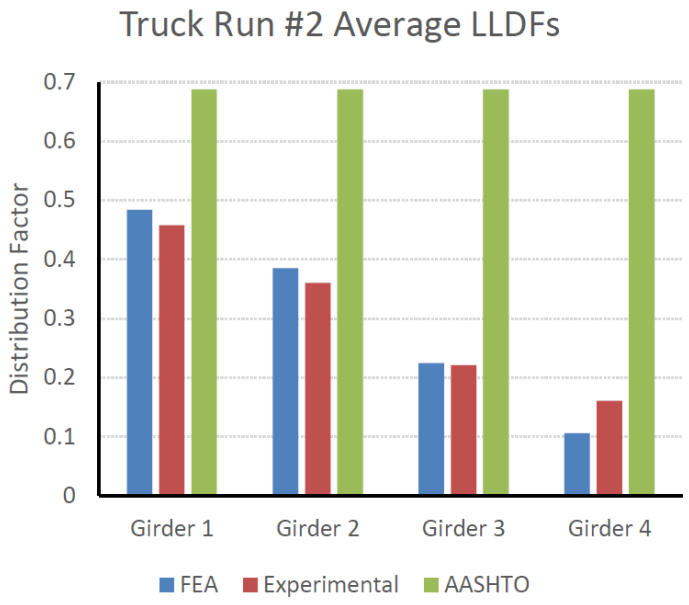

Figure 2.17: FEA v. Experimental v. AASHTO LLDFs (Gibbs, 2017)

2.5.2 Cannelville Road Bridge in Muskingum County, Ohio

The new Cannelville Road Bridge, opened on May 27, 2017, was the first press-brake-formed tub girder in Ohio. The bridge consisted of a thin, lightweight Sandwich Plate System (SPS) bolted to the girders in a fabrication shop, so the modular unit could be rapidly assembled at the construction site. The bridge contained two modules, each consisting of two tub girders joined by the SPS deck and cross bracing between the tub girders. The entire system was hot-dipped galvanized, extending the life of the bridge up to 100 years. Both modules were lifted and placed on their abutments in only 22 minutes (Figure 2.18). The entire bridge construction, including removal of the old bridge and abutments, driving of new foundations, pouring of new abutments, and erection of the superstructure, was accomplished in 26 days.

Figure 2.18: Modular SPS Deck/Tub Girder System Being Lowered in Place

2.6 CORROSION PROTECTION SYSTEMS

2.6.1 Corrosion Process

When deciding which material to be used in the construction of steel bridge girders, the designer must consider corrosion protection systems. Corrosion of steel is an electrochemical process which occurs in stages. Parts of the steel surface act as anodes and others act as cathodes (Figure 2.19.) Ferrous ions enter solution on anodic areas where free electrons are released. These electrons move to cathodic areas on the surface of steel where they combine with oxygen ions to form hydroxyl ions. These hydroxyl ions react with ferrous ions forming rust at the anodic areas of the surface. Steel corrosion can only occur when both oxygen and water are present simultaneously. With time, new anodic areas form on a steel surface creating areas for further corrosion (Corus, 2004).

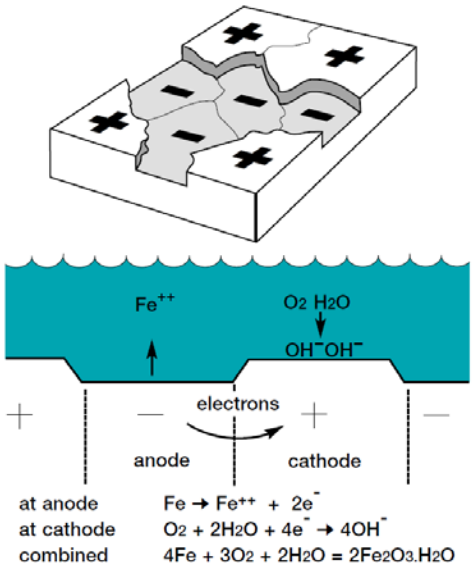

Figure 2.19: Schematic Representation of the Corrosion Process (Corus, 2004)

The principle factors determining the rate of corrosion of steel in air are time of wetness, atmospheric pollution, and localized corrosion, such as bimetallic and crevice corrosion. Time of wetness is the amount of time steel is exposed to water. Steel would not need a protective system in a dry environment, such as the interior of a heated building, due to lack of water, or in a completely submerged environment due to lack of oxygen. Atmospheric pollution refers to contaminants, such as sulfates, chlorides, and dust. Sulfates originate from the combustion of fossil fuels, such as sulfur bearing oils and coal. The sulfur dioxide gas emitted from the combustion of fossil fuels reacts with water in the atmosphere to create sulfurous and sulfuric acids. Sulfur dioxide typically originates in industrial environments. Chlorides are typically found in marine environments because the highest concentrations of chlorides are found in coastal regions. Sulfates and chlorides increase corrosion rates of steel by producing soluble salts, which are themselves corrosive, concentrated in pits on the steel surface. Bimetallic corrosion occurs when two different metals are joined together in an electrolyte causing an electrical current to pass between them and corrosion to occur on the anodic metal. Some metals, such as nickel and copper, cause steel to corrode whereas other metals, such as zinc, preferentially corrode when joined with steel. The further apart the joined metals are in the galvanic series, the greater the tendency of bimetallic corrosion as seen in Figure 2.20 (Ghavamian et al., 2015).

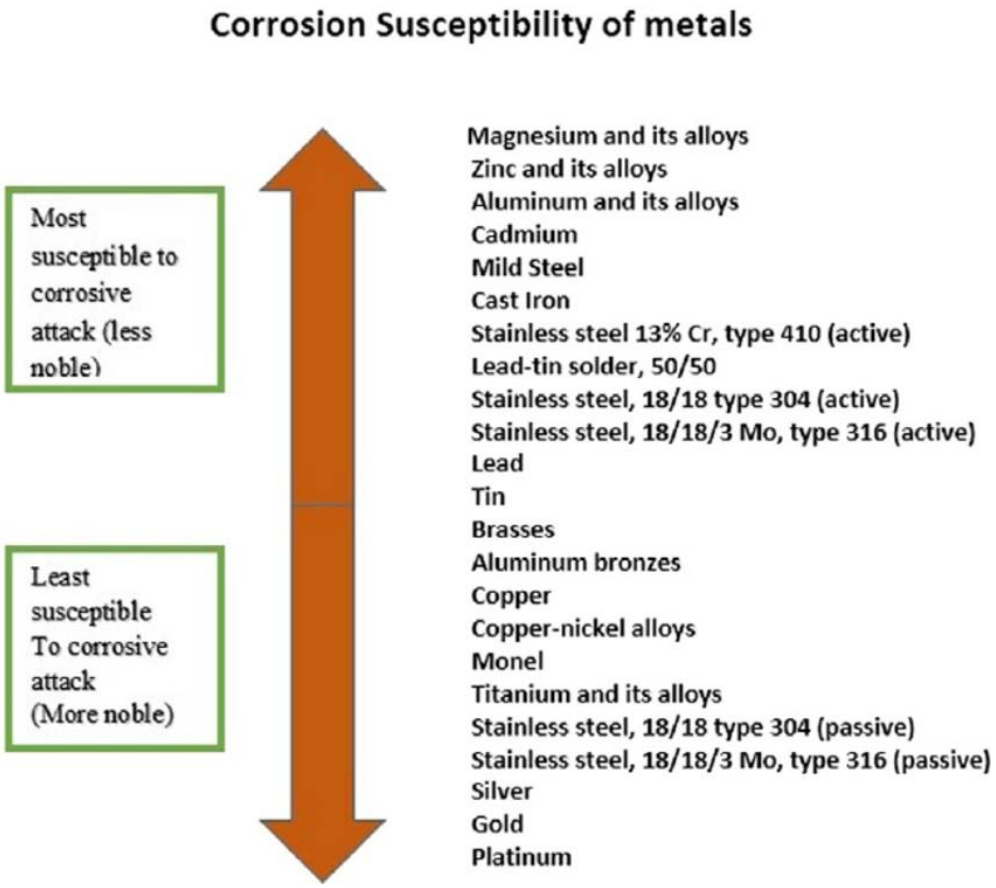

Figure 2.20: Galvanic Series (Ghavamian et al., 2015)

Design detailing, welding, and surface debris can cause crevices in steel surfaces. Oxygen in the crevice is used by the corrosion process and cannot be replaced. The entrance to the crevice becomes cathodic because the cathode reaction demands oxygen. The tip of the crevice becomes the anode in the reaction causing high corrosion at that localized point.

2.6.2 Painting Systems

Protective paint systems conventionally consist of primer, undercoat(s), and finish coats (Figure 2.21). However, two coat systems combining undercoats and finishing coats are now available.

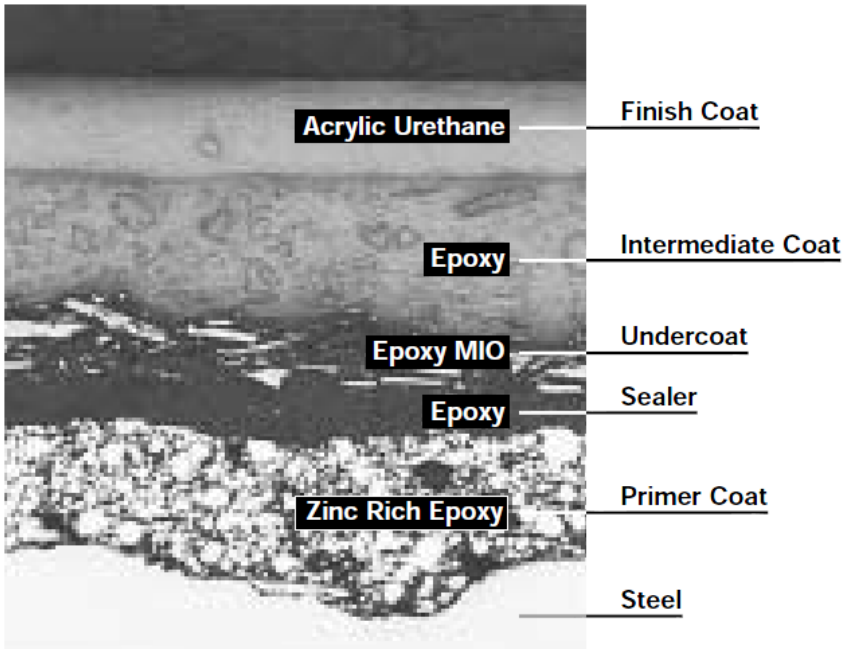

Figure 2.21: Conventional Protective Paint System (NPL, 2000)

Primers for steel surfaces are usually required to provide some corrosion inhibition. These primers are applied directly on the cleaned steel surface, wetting the surface and providing good adhesion for subsequent applied coats. There are two basic types of primer, the first being pigmented with metallic elements anodic to steel. An opening in this coating exposes the steel substrate causing the anodic metallic element to sacrificially oxidize protecting the steel. The other type of primer is typically an epoxy, which relies on its high adhesion and chemical resistance properties. Adhesion of this primer is highly dependent on a thoroughly clean surface to prevent under rusting at mechanical breaks.

Undercoats, or intermediate coats, are applied to build thickness of the paint system. Longer system life is generally dependent on the thickness of the system, so several coats may need to be applied. Highly pigmented undercoats decrease permeability of the paint system to

oxygen and water. Laminar pigments, such as iron oxide, reduce or delay moisture penetration in humid environments and improve the tensile strength of the paint.

The finish coat provides the surface resistance and appearance of the system. The finish must provide the first line of defense against all environmental conditions, such as condensation as on the undersides of bridges, highly polluted atmospheres in chemical plants, impact and abrasion at floor or road levels, and bacteria and fungi in food factories and farms.

Paints are composed of three main components: pigment, binder, and solvent. Pigments are finely ground inorganic or organic powders dispersed in the binder, which is typically oil or resin. The solvent, typically water, dissolves the binder and when the solvent evaporates, a film layer remains on the surface as a protective coating. Paint systems consist of multiple layers of different paints serving different purposes.

The current standard for bridge coating is a three-coat system consisting of an inorganic zinc-rich primer, an epoxy midcoat, and a urethane topcoat (IOZ/E/U). Thousands of bridges constructed since the mid-1960s are coated with a zinc-rich primer paint as part of a paint system and are in excellent condition (Kline, 2009). Many structures, such as the Golden Gate Bridge in San Francisco, California, the Windgap Bridge near Pittsburgh, PA, and the Martin Luther King Bridge in Richmond, Virginia, consist of a zinc-rich primer, epoxy midcoat, and a urethane topcoat. The costs of this painting system, in 2009 dollars, is approximately $5.50 for the initial blast cleaning, surface preparation, and prime coating in the shop and application of the second and third layers at the construction site and two touch-ups over the bridge life.

As bridge coating technology continued to evolve in the 1990s, advancements in binder technology allowed a reduction in the number of coating layers from three coats to two coats with the use of high-build, two-coat polyaspartic urethane (PAS) coating systems (Olson et al., 2017). PAS coating systems reduce the overall cost of painting with corrosion protection similar to the conventional three-coat systems. PAS systems utilize a similar zinc-rich primer as three-coat systems, but the epoxy and polyurethane layers are replaced by a high-build PAS topcoat. The difference between the two systems can be seen in Figure 2.22.

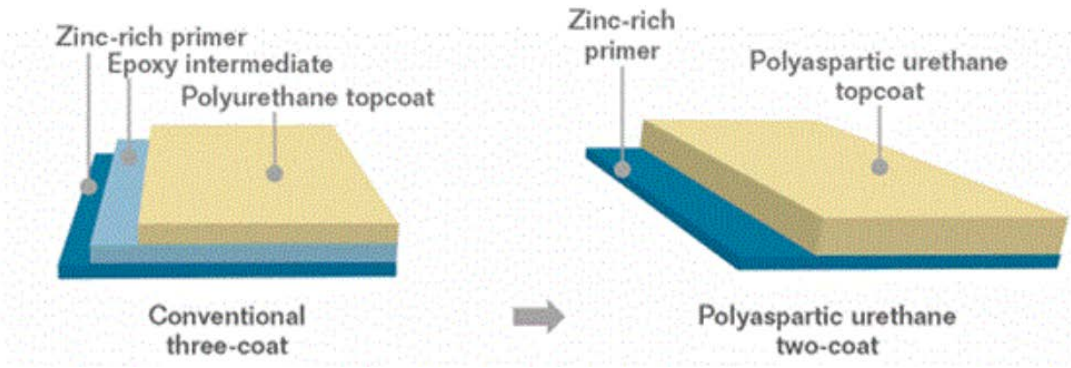

Figure 2.22: Comparison between 2-Coat and 3-Coat Systems (Olsen et al., 2017)

2.6.3 Weathering Steel

Weathering steels have a carbon content of less than 0.2% and have alloying elements (Copper, Cromium, Nickel, Phosphorus, Silicon, and Manganese) consisting of 3-5%. The chemical composition of steel alloys is specifically formulated to rapidly form a layer of rust that provides a protective coating (AZO Materials, 2016). Copper and nickel act as the main alloys contributing to corrosion resistance by bonding the protective oxide layer to the underlying steel. The steel oxidizes because the system rusts slowly and the accumulated rust layer creates the coating to slow future corrosion. Bridges built with weathering steel can last up to 120 years with little maintenance because of this slow corrosion rate. Repeated wet/drying cycles are essential to create the optimum dense and adherent rust layer. Unwanted corrosion can occur in poorly detailed areas with crevices. The desired patina cannot form in crevices where water can collect.

The desired oxidation process occurs over several years before steady-state stabilization of the surface occurs with a tightly bonded coating. Phosphorus and sulfur contribute to formation of the patina layer by creating low-solubility phosphates and sulfates developed between underlying steel and the protective oxidized layer. Phosphorous specimens form a protective passive film over the steel, preventing the ingress of moisture supporting formation of a dense patina layer. Phosphorus can have a detrimental effect on the mechanical strength of the steel by effecting the alloy grain structure, so low level boron or carbon are added to the steel restoring required grain boundaries. Large amounts of non-metal oxides can result in acidification of the aqueous layer, which hinders patina formation.

Chlorides are typically the largest concern in the United States as contamination may result from runoff of deicing salts applied to roadways or proximity of the structure to marine environments having high atmospheric chloride levels (Barth & McConnell, 2010). The most desirable situation for weathering steel is where the steel is perpetually dry, so no corrosion will occur, but this is unrealistic. The best approach to long-term maintenance of weathering steel structures is to minimize its exposure to moisture. Proper design details are highly encouraged, such as the use of a continuous reinforced concrete deck to prevent water from reaching the girders, the removal of joints wherever possible, and the use of integral or semi-integral abutments. Periodical inspection and maintenance for cracks, open joints, and debris in the drainage system can drastically improve the structures life and reduce future corrosion.

2.6.4 Hot-Dip Galvanization

Hot-Dip Galvanizing is a process involving dipping steel into a container of molten zinc to form a corrosion protection layer surrounding the underlying steel. The process consists of three basic steps: surface preparation, galvanization, and inspection. Zinc will not react with a dirty surface, which leads to many cases of premature failure. To avoid this, three surface preparation steps are needed. The first step of the surface preparation process is to submerge the steel member in a hot alkali solution, mild acidic bath, or biological cleaning bath to remove organic contaminants. The second step is removal of mill scale and iron oxides from the steel surface by submerging the specimen in a heated sulfuric acid or ambient hydrochloric bath. Abrasive cleaning using blasted air with sand, metallic shot, or grit onto the steel can be done in addition to or without the previous step. The final surface preparation step is to remove any remaining rust and to deposit a layer of zinc using a zinc ammonium chloride solution. After the surface preparation, displayed in Figure 2.20, the material is completely immersed in a molten bath of 98% minimum pure zinc kept between 815°-850° Fahrenheit. The zinc reacts with iron in the steel to form metallurgically bonded zinc-iron intermetallic alloy layers. A layer of impact resistant pure zinc typically tops the intermediate alloy layers. The specimen being galvanized is slowly removed from the zinc bath while carefully draining or vibrating the excess zinc. After completion of galvanization, it is required to inspect the specimen for defects.

Figure 2.23: Dipping of Steel in Molten Zinc (American Galvanizers Association, 2018)

The coating developed during the galvanization process is metallurgically bonded to the steel. The zinc reacts with the iron in the steel to form a series of zinc-iron alloy layers during the reaction in the molten bath. Figure 2.23 shows a cross-section of the galvanized steel coating showing the typical layers of steel, alloys, and the top zinc layer. The hardness of each layer is expressed as a Diamond Pyramid Number (DPN) in Figure 2.23. The hardness of the Zeta, Delta, and Gamma layers are harder than the underlying steel providing abrasive resistance. The Eta layer, being more ductile, provides protection from impacts.

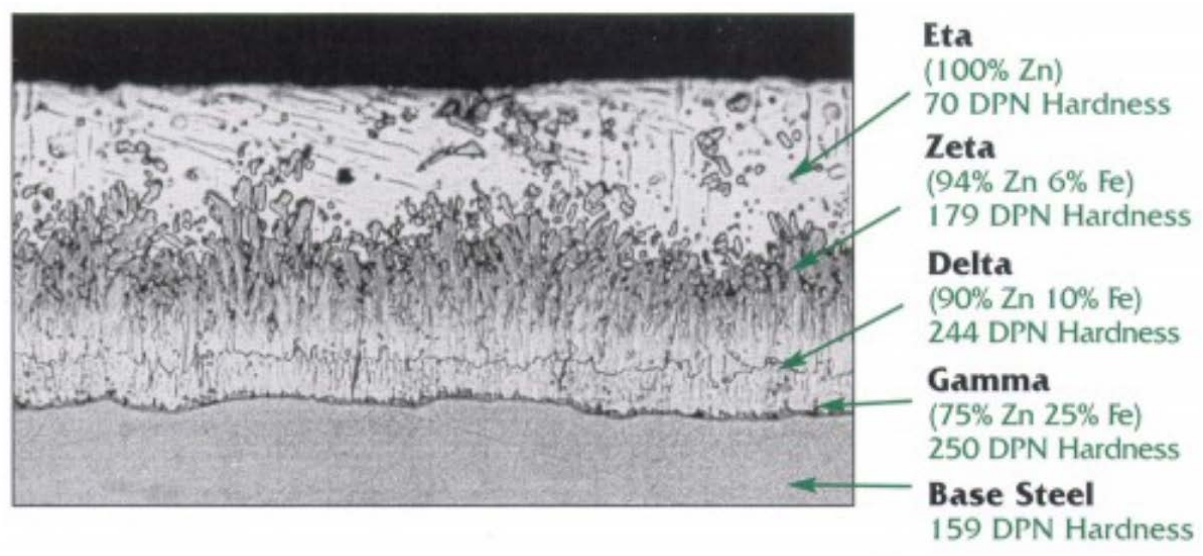

Figure 2.24: Cross Section of Galvanized Steel Coating (American Galvanizers Association, 2018)

CHAPTER 3: TUB GIRDER DESIGN EXAMPLE

3.1 INTRODUCTION

The goal of utilizing tub girders is to develop a set of standardized designs that increases the efficiency of short span steel bridge design. Michaelson (2014) optimized the design used in this chapter. Efforts were made by Michaelson to include technical feedback from all aspects of steel construction, including, but not limited to, accounting for plate availability, upper bounds of girder length, and erection issues.

The girder was designed according to the 2014 AASHTO LRFD Bridge Design Specifications. It should be noted that in this design suite, once the girder was optimized for readily available plate sizes, a design review was conducted by evaluating limit state checks by reducing the overall plate width by two inches. This was performed to aid in potential fabrication practices where the plate is cut to be perfectly square. AASHTO LRFD specifications are referred to consistently throughout this chapter when discussing tables, articles, and equations.

3.2 BRIDGE LAYOUT

As shown in Figure 3.1, the bridge being evaluated is designed for a clear roadway width of 28 foot 4 inch including two 12 foot travel lanes and two 26 inch shoulders. The bridge has two Jersey-style barriers that are 19 inches wide. To accommodate the lanes and shoulders, the bridge in this design evaluation consists of four girders spaced at eight feet with 3 foot 9 inch overhangs. An 8.5 inch thick concrete deck is employed, which includes a 1/2 inch sacrificial wearing surface (i.e. an integral wearing surface (IWS)), and a 2 inch haunch measured from the top of the top flanges to the bottom of the deck. In addition, the bridge is designed for a simple span of 60 feet with no skew or super elevation in the girder layout.

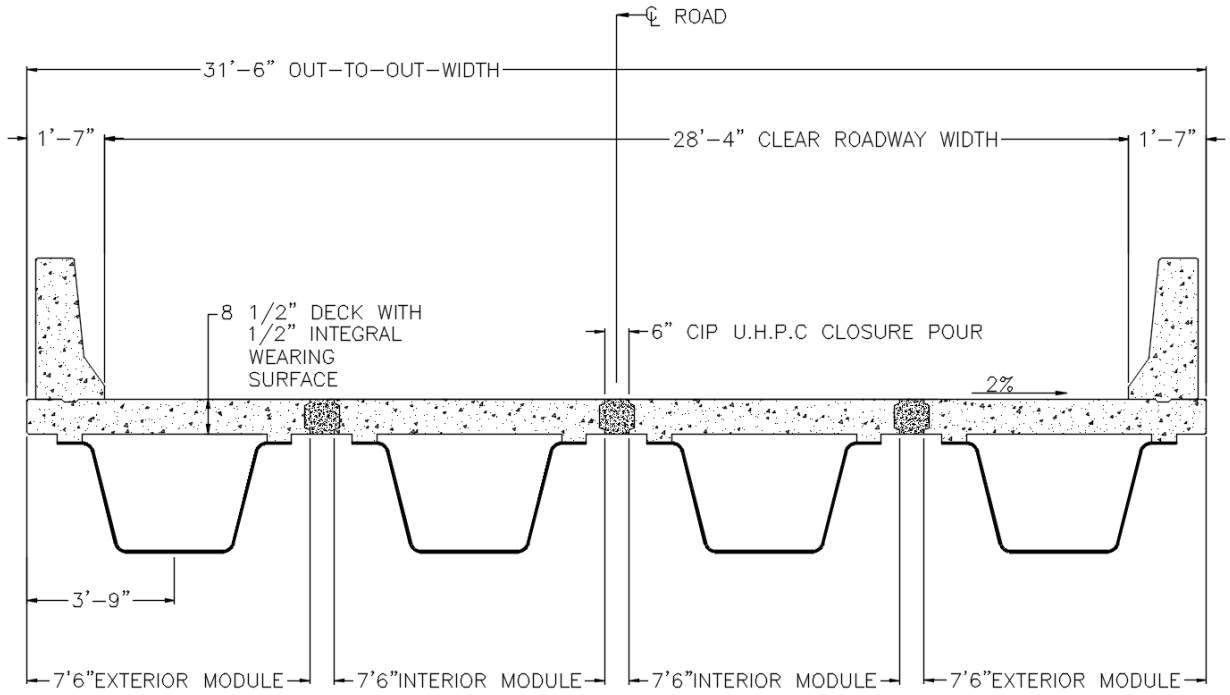

Figure 3.1: Typical Bridge Cross Section

3.3 GIRDER GEOMETRY

AASHTO Section 6.11-BOX-SECTION FLEUXRAL MEMBERS refers heavily back to ASSHTO Section 6.10-I-SECTION FLEXURAL MEMBERS; therefore, many articles and equations in this chapter are from Section 6.10 by reference of the corresponding Article in Section 6.11. As stated in AASHTO Article 6.10.1.1.1, the elastic stress at any location on the composite section due to the applied loads shall be equal to the sum of the stresses caused by the loads applied separately to the non-composite steel section, the short-term composite section, and the long-term composite section. For calculating flexural stresses, the concrete deck is transformed to an equivalent area of steel using the modular ratio *n*, where *n* = eight for this bridge. For loads applied to the short-term composite section, the concrete is transformed by dividing the concrete's effective flange width by *n*. For loads applied to the long-term composite section, the concrete is transformed by dividing the concrete's effective flange width by *3n*.

AASHTO Article 4.6.2.6.1 states the effective flange width of a concrete deck shall be taken as the tributary width to compute the effective flange width. Barrier rails are often not structurally continuous, so the added deck width allowed by AASHTO Equation 4.6.2.6.1-1 is not included. Therefore, for the bridge layout in this evaluation the effective flange width for the girders is 96 inches. Tables 3.1 through 3.3 are used to calculate the section properties used in the limit state evaluations later in this chapter. The locations of each parts centroid and moments of inertia are specifically used in the determination of the composite flexural and shear capacities of the tub girders.

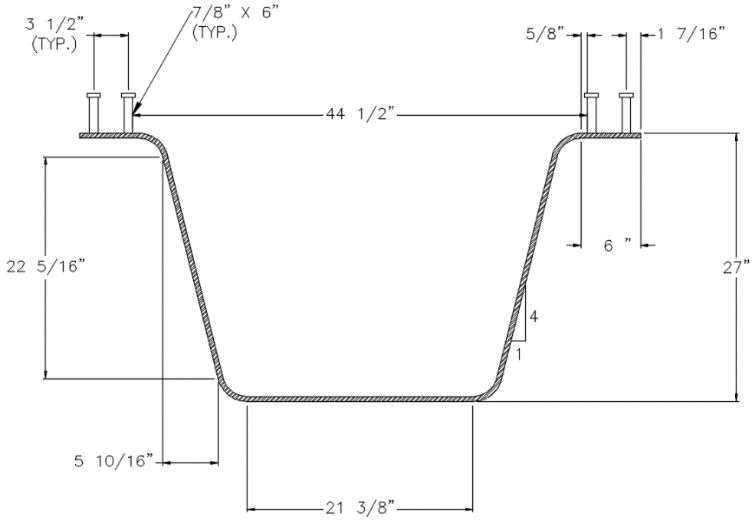

Figure 3.2: Girder Cross-Section

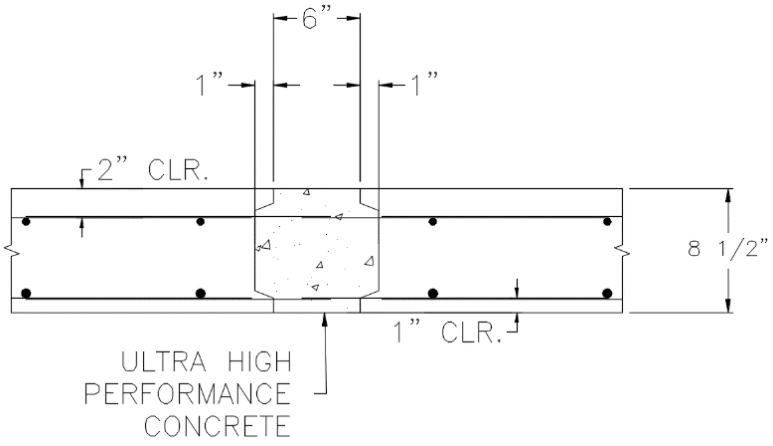

Figure 3.3: Joint Detail

Table 3.1: Non-Composite Section Properties

Noncomposite Section

Part	A (in^2)	y (in)	Ay (in^3)	I_{X-C} (in^4)	d_Y (in)	I_{X-X} (in^4)
BF	10.7	0.25	2.7	0.2	11.9	1520.9
LR_1	1.8	1.0	1.8	0.8	11.2	229.3
LR_2	1.8	1.0	1.8	0.8	11.2	229.3
W_1	11.5	13.5	155.4	478.5	-1.3	498.6
W_2	11.5	13.5	155.4	478.5	-1.3	498.6
TR_1	1.8	26.0	47.4	0.8	-13.8	349.9
TR_2	1.8	26.0	47.4	0.8	-13.8	349.9
TF_1	3.0	26.8	80.3	0.1	-14.6	637.0
TF_2	3	26.8	80.3	0.1	-14.6	637.0
Σ =	47		572.4			4950.5

Table 3.2: Short Term Composite Section Properties

Short Term Composite Section

Part	A (in^2)	y (in)	Ay (in^3)	I_{X-C} (in^4)	d_Y (in)	I_{X-X} (in^4)
Girder	47	12.2	572.4	4950.5	14.0	14133.4
Deck	96	33	3168	512	-6.8	5007.8
Σ =	143		3740.4			19141.24

Table 3.3: Long Term Composite Section Properties

Long Term Composite Section

Part	A (in^2)	y (in)	Ay (in^3)	I_{X-C} (in^4)	d_Y (in)	I_{X-X} (in^4)
Girder	47	12.2	572.4	4950.5	8.4	8293.6
Deck	96	33	1056	170.66667	-12.4	5080.9
Σ =	143		1628.4			13374.577

The concrete deck attaches to the steel press-brake-formed tub girder using 6 inch long and 7/8 inch diameter shear studs welded to the top flanges of the girder. In the cross-section, there are two shear studs spaced 3 1/2 inches on each flange. They are spaced every 12 inches along the entire span of the girder.

3.4 LOADS & LOAD COMBINATIONS

For this set of design evaluations, the following permanent and transient loads are used for evaluation:

- DC = dead load of structural components and nonstructural attachments
  - Divided into two components: DC1 which is applied to the non-composite section and DC2 which is applied to the composite section
- DW = dead load of wearing surface and utilities
- IM = vehicular dynamic load allowance
  - Serves to amplify the vehicular components of the HL-93 live load (i.e. the truck and tandem)
  - For the fatigue limit state, IM = 15% (AASHTO Table 3.6.2.1-1)
  - For all other limit states, IM = 33% (AASHTO Table 3.6.2.1-1)
- LL = vehicular live load
  - The HL-93 vehicular live load is defined in AASHTO Article 3.6.1.2
    - Vehicular live loading on the roadways of bridges shall consist of a combination of the Design Truck + Design Lane Load -OR- Design Tandem + Design Lane Load
  - Note that the fatigue load shall be one design truck or axles but with a constant spacing of 30.0 feet between the 32.0-kip axles (AASHTO Article 3.6.1.4.1)

The following load combinations are assessed using the permanent and transient loads mentioned previously with values for load factors derived from AASHTO Tables 3.4.1-1 and 3.4.1-2, unless otherwise specified. The ductility factor (η_D), redundancy factor (η_R), and the operational importance factor (η_I), are taken to be 1.00 for this set of design calculations.

- Strength I: basic load combination relating to the normal vehicular use of the bridge without wind
  - 1.25DC + 1.50DW + 1.75(LL + IM)
- Strength IV: load combination relating to very high dead load to live load force effect ratios

    - 1.50DC + 1.50DW
- Service I: load combination associated with evaluation of live load deflections (Article 3.4.2.2)
    - 1.00(LL + IM)
- Service II: load combination intended to control yielding of steel structures due to vehicular live load
    - 1.00DC + 1.00DW + 1.30(LL + IM)
- Fatigue I: fatigue load combination related to infinite load-induced fatigue life
    - 1.50(LL + IM)

The following loads were taken for all calculations in this design evaluation:

- Unit weight of concrete (γ_c) = 0.150 kcf
- Compressive strength of concrete (f'c) = 4.0 ksi
- Modular ratio of normal weight concrete (n = 8) (AASHTO Article C6.10.1.1.1b)
    - These values correspond to normal weight concrete.
- Unit weight of steel (γ_s) = 0.490 kcf
- Steel stay-in-place formwork (SIP) unit weight = 0.015 ksf
- Future waring surface = 0.025 ksf
- Weight of concrete Jersey barrier = 0.304 kip/ft

3.4.1 Component and Attachment Dead Load (DC)

The dead load of structural components and nonstructural attachments are computed as follows. Loads such as the slab, the Jersey-style barriers, and the SIP formwork are assumed to be equally distributed to all the girders.

Noncomposite Dead Load (DC1):

$$Slab = \frac{0.150}{4}\left[\left(\frac{8.5}{12}\right)\left(31 + \frac{6}{12}\right)\right]$$ 0.837 kip/ft

$$Haunch = 0.150\left[\left(\frac{2 \times 6.0}{12}\right)\left(\frac{2.0}{12}\right)\right]$$ 0.025 kip/ft

$$SIP = 0.015\left[\frac{55.21 - 2 \times 6.0}{12}\right]$$ 0.054 kip/ft

$$Girder = \frac{0.490}{144}(47.0)$$ 0.160 kip/ft

$$\boldsymbol{Total = 0.837 + 0.025 + 0.054 + 0.160}$$ **1.076 kip/ft**

Composite Dead Load (DC2):

$$Barrier = \frac{2}{4}(0.304)$$ 0.152 kip/ft

$$\boldsymbol{Total = 0.304}$$ **0.304 kip/ft**

The dead load of the future wearing surface is applied across the clear roadway width of 28 foot 4 inch. Loads are assumed to be equally distributed to all the girders.

Wearing Surface Dead Load (DW):

$$Wearing\ Surface = \frac{0.025}{4}\left(\frac{340}{12}\right)$$ 0.177 kip/ft

$$\boldsymbol{Total = 0.177}$$ **0.177 kip/ft**

3.5 MULTIPLE PRESENCE FACTORS & LIVE LOAD DISTRIBUTION

Multiple presence factors account for the probability of coincident live loadings and are listed in AASHTO Article 3.6.1.1.2. These factors are included in the empirical equations listed in AASHTO Article 4.6.2.2. The engineer must use the multiple presence factors when employing lever rule or special analysis. Note: Multiple presence factors are not applied when evaluating the fatigue limit state. These factors are listed in Table 3.4.

Table 3.4 Multiple Presence Factors (AASHTO, 2014)

Number of Lanes Loaded	Multiple Presence Factor, m
1	1.20
2	1.00
3	0.85
>3	0.65

Live load distribution factors were employed to determine live loads on individual girders instead of a complex three-dimensional analysis. As stated in AASHTO Article 4.6.2.2, these factors are only applicable if the bridge meets certain parameters. Parameters for this bridge, including their range of applicability, which can be found in AASHTO Article 4.6.2.2, are as follows:

- $0.5 \leq \frac{N_L}{N_b} \leq 1.5$
  - N_L = Number of Lanes = 2
  - N_b = Number of Beams = 4

The parameters fall within the range of applicability found in AASHTO Article 4.6.2.2. Using these parameters, distribution factors for the analysis are found using Equations 3.1 and 3.2:

Live Load Distribution Factor:

$$DF_{LL} = 0.05 + 0.85\frac{N_L}{N_b} + \frac{0.425}{N_L} = 0.688 \qquad \text{Eq. 3.1}$$

Fatigue Live Load Distribution Factor:

$$DF_{Fat} = \frac{DF_{LL}}{m} = 0.573 \qquad \text{Eq. 3.2}$$

To determine the distribution factor for live load deflections, all girders are assumed to deflect equally and the appropriate multiple presence factor shall be applied. For this bridge, with a clear roadway width of 28 foot 4 inches, this equates to two design lanes (AASHTO Article 3.6.1.1.1). With a multiple presence factor of 1.00 for two loaded lanes (AASHTO Article 3.6.1.1.2), the distribution factor appears in Equation 3.3:

$$g = 1.00\left(\frac{2}{4}\right) = 0.500 \qquad \text{Eq. 3.3}$$

3.6 STRUCTURAL ANALYSIS

The tables in this section contain the moments, shears, and deflections resulting from structural analysis of the girder. Analyses were generated using the commercial software package LEAP CONSYS (2008), which idealizes the structure as a simple span line girder. Tables 3.5 through 3.7 show the moments, shears, and deflections from the applied dead and live loads. Tables 3.8 and 3.9 determine which Live Load Case controls, either the design truck or the design tandem, and distribute the moments and shears from the bridge system to the girders. Tables 3.10 through 3.12 factor the moments and shears calculated in the previous tables to determine the maximum shears and moments needed in the limit state evaluations. Tables 3.13 through 3.15 perform similar procedures for evaluations of deflection and fatigue cases.

Table 3.5: Unfactored/Undistributed Moments (ft-kip)

x (ft)	x/L	Dead Load Moments			Live Load Moments							
					Truck		Lane		Tandem		Fatigue Truck	
		DC_1	DC_2	DW	(+)	(-)	(+)	(-)	(+)	(-)	(+)	(-)
0	0	0	0	0	0	0	0	0	0	0	0	0
6	0.1	174.3	24.6	28.7	321.6	0	103.7	0	260	0	257.6	0
12	0.2	309.9	43.8	51.0	556.8	0	184.3	0	460	0	428.8	0
18	0.3	406.7	57.5	66.9	705.6	0	241.9	0	600	0	540.8	0
24	0.4	464.8	65.7	76.5	790.4	0	276.5	0	680	0	585.6	0
30	0.5	484.2	68.4	79.7	800.0	0	288.0	0	700	0	544.0	0
36	0.6	464.8	65.7	76.5	790.4	0	276.5	0	680	0	585.6	0
42	0.7	406.7	57.5	66.9	705.6	0	241.9	0	600	0	540.8	0
48	0.8	309.9	43.8	51.0	556.8	0	184.3	0	460	0	428.8	0
54	0.9	174.3	24.6	28.7	321.6	0	103.7	0	260	0	257.6	0
60	1	0	0	0	0	0	0	0	0	0	0	0

Table 3.6: Unfactored/Undistributed Shears (kip)

x (ft)	x/L	Dead Load Shears			Live Load Shears							
					Truck		Lane		Tandem		Fatigue Truck	
		DC_1	DC_2	DW	(+)	(-)	(+)	(-)	(+)	(-)	(+)	(-)
0	0	32.3	4.6	5.3	60.7	0	19.2	0	48.3	0	50.13	0
6	0.1	25.8	3.6	4.2	53.6	-3.2	15.6	-0.2	43.3	-3.3	42.93	-3.2
12	0.2	19.4	2.7	3.2	46.4	-6.4	12.3	-0.8	38.3	-8.3	35.73	-6.4
18	0.3	12.9	1.8	2.1	39.2	-11.7	9.4	-1.7	33.3	-13.3	28.8	-10.1
24	0.4	6.5	0.9	1.1	32.0	-18.1	6.9	-3.1	28.3	-18.3	22.4	-14.1
30	0.5	0	0	0	24	-24.0	4.8	-4.8	23.3	-23.3	18.13	-18.1
36	0.6	-6.5	-0.9	-1.1	18.1	-32.0	3.1	-6.9	18.3	-28.3	14.13	-22.4
42	0.7	-12.9	-1.8	-2.1	11.7	-39.2	1.7	-9.4	13.3	-33.3	10.13	-28.8
48	0.8	-19.4	-2.7	-3.2	6.4	-46.4	0.8	-12.3	8.3	-38.3	6.4	-35.7
54	0.9	-25.8	-3.6	-4.2	3.2	-53.6	0.2	-15.6	3.3	-43.3	3.2	-42.9
60	1	-32.3	-4.6	-5.3	0	-60.7	0	-19.2	0	-48.3	0	-50.1

Table 3.7: Unfactored/Undistributed Deflections (in)

x (ft)	*x/L*	*Live Load Deflections*			
		Truck		*Lane*	
		(+)	*(-)*	*(+)*	*(-)*
0	0	0	0	0	0
6	0.1	0.24	0	0.11	0
12	0.2	0.52	0	0.2	0
18	0.3	0.72	0	0.27	0
24	0.4	0.84	0	0.32	0
30	0.5	0.88	0	0.34	0
36	0.6	0.84	0	0.32	0
42	0.7	0.72	0	0.27	0
48	0.8	0.52	0	0.2	0
54	0.9	0.24	0	0.11	0
60	1	0	0	0	0

Table 3.8: Unfactored/Distributed Moments (ft-kip)

x (ft)	*x/L*	*1.33Truck + Lane*		*1.33Tandem + Lane*		DF	*LL + IM*	
		(+)	(-)	(+)	(-)		(+)	(-)
0	0	0	0	0	0	0.688	0	0
6	0.1	531.4	0	449.5	0	0.688	365.3	0
12	0.2	924.9	0	796.1	0	0.688	635.8	0
18	0.3	1180.4	0	1039.9	0	0.688	811.5	0
24	0.4	1327.7	0	1180.9	0	0.688	912.8	0
30	0.5	1352.0	0	1219.0	0	0.688	929.5	0
36	0.6	1327.7	0	1180.9	0	0.688	912.8	0
42	0.7	1180.4	0	1039.9	0	0.688	811.5	0
48	0.8	924.9	0	796.1	0	0.688	635.8	0
54	0.9	531.4	0	449.5	0	0.688	365.3	0
60	1	0	0	0	0	0.688	0	0

Table 3.9: Unfactored/Distributed Shears (kip)

x (ft)	*x/L*	*1.33Truck + Lane*		*1.33Tandem + Lane*		DF	*LL + IM*	
		(+)	(-)	(+)	(-)		(+)	(-)
0	0	100.0	0	83.4	0	0.688	68.7	0
6	0.1	86.8	-4.4	73.2	-4.6	0.688	59.7	-3.1
12	0.2	74.0	-9.3	63.3	-11.9	0.688	50.9	-6.4
18	0.3	61.5	-17.3	53.7	-19.5	0.688	42.3	-11.9
24	0.4	49.5	-27.2	44.6	-27.5	0.688	34.0	-18.7
30	0.5	36.7	-36.7	35.8	-35.8	0.688	25.2	-24.6
36	0.6	27.2	-49.5	27.5	-44.6	0.688	18.9	-30.7
42	0.7	17.3	-61.5	19.5	-53.7	0.688	13.4	-36.9
48	0.8	9.3	-74.0	11.9	-63.3	0.688	8.1	-43.5
54	0.9	4.4	-86.8	4.6	-73.2	0.688	3.2	-50.3
60	1	0	-100.0	0	-83.4	0.688	0	-57.3

Table 3.10: Strength I Moments (ft-kip)

x (ft)	*x/L*	*1.25DC* $_1$	*1.25DC* $_2$	*1.50DW*	*1.75LL + IM*		*Strength I*	
					(+)	(-)	(+)	(-)
0	0	0	0	0	0	0	0	0
6	0.1	217.9	30.8	43.0	639.4	0	931.0	291.7
12	0.2	387.4	54.7	76.5	1112.7	0	1631.3	518.5
18	0.3	508.4	71.8	100.4	1420.1	0	2100.7	680.6
24	0.4	581.0	82.1	114.7	1597.4	0	2375.2	777.8
30	0.5	605.3	85.5	119.5	1626.6	0	2436.9	810.2
36	0.6	581.0	82.1	114.7	1597.4	0	2375.2	777.8
42	0.7	508.4	71.8	100.4	1420.1	0	2100.7	680.6
48	0.8	387.4	54.7	76.5	1112.7	0	1631.3	518.5
54	0.9	217.9	30.8	43.0	639.4	0	931.0	291.7
60	1	0	0	0	0	0	0	0

Table 3.11: Strength I Shears (kip)

x (ft)	*x/L*	*1.25DC 1*	*1.25DC 2*	*1.50DW*	*1.75LL + IM*		*Strength I*	
					(+)	(-)	(+)	(-)
0	0	40.4	5.7	8.0	120.3	0	174.3	54.0
6	0.1	32.3	4.6	6.4	104.5	-5.4	147.7	37.9
12	0.2	24.2	3.4	4.8	89.0	-11.2	121.4	21.2
18	0.3	16.1	2.3	3.2	74.0	-20.9	95.7	0.8
24	0.4	8.1	1.1	1.6	59.5	-32.7	70.3	-21.9
30	0.5	0	0	0	44.2	-43.1	44.2	-43.1
36	0.6	-8.1	-1.1	-1.6	33.0	-53.7	22.2	-64.5
42	0.7	-16.1	-2.3	-3.2	23.4	-64.7	1.8	-86.3
48	0.8	-24.2	-3.4	-4.8	14.3	-76.1	-18.2	-108.5
54	0.9	-32.3	-4.6	-6.4	5.6	-88.1	-37.6	-131.3
60	1	-40.4	-5.7	-8.0	0	-100.4	-54.0	-154.4

Table 3.12: Service II Moments (ft-kip)

x (ft)	*x/L*	*1.00DC 1*	*1.00DC 2*	*1.00DW*	*1.30LL + IM*		*Service II*	
					(+)	(-)	(+)	(-)
0	0	0	0	0	0	0	0	0
6	0.1	174.3	24.6	28.7	474.9	0	702.6	227.6
12	0.2	309.9	43.8	51.0	826.6	0	1231.2	404.6
18	0.3	406.7	57.5	66.9	1055.0	0	1586.0	531.1
24	0.4	464.8	65.7	76.5	1186.6	0	1793.6	607.0
30	0.5	484.2	68.4	79.7	1208.4	0	1840.6	632.3
36	0.6	464.8	65.7	76.5	1186.6	0	1793.6	607.0
42	0.7	406.7	57.5	66.9	1055.0	0	1586.0	531.1
48	0.8	309.9	43.8	51.0	826.6	0	1231.2	404.6
54	0.9	174.3	24.6	28.7	474.9	0	702.6	227.6
60	1	0	0	0	0	0	0	0

Table 3.13: Service I Deflections (in)

x (ft)	*x/L*	*Truck*		*0.25Truck + Lane*		DF	*Service I*	
		(+)	(-)	(+)	(-)		(+)	(-)
0	0	0	0	0	0	0.5	0	0
6	0.1	0.32	0	0.19	0	0.5	0.16	0
12	0.2	0.69	0	0.37	0	0.5	0.35	0
18	0.3	0.96	0	0.51	0	0.5	0.48	0
24	0.4	1.12	0	0.60	0	0.5	0.56	0
30	0.5	1.17	0	0.63	0	0.5	0.59	0
36	0.6	1.12	0	0.60	0	0.5	0.56	0
42	0.7	0.96	0	0.51	0	0.5	0.48	0
48	0.8	0.69	0	0.37	0	0.5	0.35	0
54	0.9	0.32	0	0.19	0	0.5	0.16	0
60	1	0	0	0	0	0.5	0	0

Table 3.14: Fatigue I Moments (ft-kip)

x (ft)	*x/L*	*LL + IM*		DF	*1.50(LL + IM)*	
		(+)	(-)		(+)	(-)
0	0	0	0	0.573	0	0
6	0.1	296.2	0	0.573	254.6	0
12	0.2	493.1	0	0.573	423.8	0
18	0.3	621.9	0	0.573	534.5	0
24	0.4	673.4	0	0.573	578.7	0
30	0.5	625.6	0	0.573	537.6	0
36	0.6	673.4	0	0.573	578.7	0
42	0.7	621.9	0	0.573	534.5	0
48	0.8	493.1	0	0.573	423.8	0
54	0.9	296.2	0	0.573	254.6	0
60	1	0	0	0.573	0	0

Table 3.15: Fatigue I Shears (kip)

x (ft)	*x/L*	*LL + IM*		DF	*1.50(LL + IM)*	
		(+)	(-)		(+)	(-)
0	0	57.7	0	0.573	49.5	0
6	0.1	49.4	-3.7	0.573	42.4	-3.2
12	0.2	41.1	-7.4	0.573	35.3	-6.3
18	0.3	33.1	-11.7	0.573	28.5	-10.0
24	0.4	25.8	-16.3	0.573	22.1	-14.0
30	0.5	20.9	-20.9	0.573	17.9	-17.9
36	0.6	16.3	-25.8	0.573	14.0	-22.1
42	0.7	11.7	-33.1	0.573	10.0	-28.5
48	0.8	7.4	-41.1	0.573	6.3	-35.3
54	0.9	3.7	-49.4	0.573	3.2	-42.4
60	1	0	-57.7	0.573	0	-49.5

3.7 LIMIT STATE EVALUATIONS

The limit states pertaining to the performance of the tub girders are discussed in this section. It should be noted, for all limit states, according to AASHTO Article 6.5.4.2, the resistance factor for flexure (ϕ_f) and for shear (ϕ_v) are both taken to be 1.00. The hybrid factor (R_h) is taken as 1.00 since the girders are fully comprised of 50-ksi steel.

3.7.1 Cross Section Proportion Limits (AASHTO Article 6.11.2)

The girders in this design evaluation were evaluated to meet the cross-section proportion limits of AASHTO Article 6.11.2. These limits are divided into two main categories: web proportions and flange proportions.

For webs without longitudinal stiffeners, the following limits are employed from AASHTO Articles 6.10.2.1.1:

$$\frac{D}{t_w} \leq 150 \qquad \text{Eq. 3.4}$$

Where:

D = Depth of web (in)

t_w = Thickness of web (in)

$$\frac{26}{0.5} \leq 150$$

$$52 \leq 150 \ \therefore OK$$

The following limits are employed for flange proportions:

$$\frac{b_f}{2t_f} \leq 12.0 \qquad \text{Eq. 3.5}$$

Where:

b_f = width of flange (in)

t_f = thickness of flange (in)

$$\frac{6}{2 * 0.5} \leq 12.0$$

$$6 \leq 12.0 \ \therefore OK$$

$$b_f \geq D/6 \qquad \text{Eq. 3.6}$$

$$6 \geq \frac{26}{6}$$

$$6 \geq 4.33 \therefore OK$$

Note the top flange of the tub girder is continuously supported during fabrication and construction. AASHTO Equation 6.11.2.2-3 ensures some restraint will be provided by the flanges against web shear buckling. This restraint is provided by the reinforced concrete deck, which is cast directly on the flange.

3.7.2 Constructability

The tub girder is continuously supported during fabrication and construction. No constructability checks are required because no significant loading occurs during the fabrication of the modular unit.

3.7.3 Service Limit State

The service limit state evaluated according to Article 6.11.4 heavily refer to Articles 6.10.4.1 (governing elastic deformations) and 6.10.4.2 (governing permanent deformations).

3.7.3.1 Permanent Deformations

The intent of the service limit state is to limit stresses and deformations under regular operating conditions. This is accomplished by limiting the levels of stress the member experiences to prevent localized yielding. As per AASHTO Article 6.11.4, the provisions of AASHTO Article 6.10.4 and its respective equations apply, except the f_l term in Equation 3.8 shall equal zero.

For the top steel flange of composite sections:

$$f_f \leq 0.95 R_h F_{yf} \qquad \text{Eq. 3.7}$$

For the bottom steel flange of composite sections:

$$f_f + \frac{f_l}{2} \leq 0.95 R_h F_{yf} \qquad \text{Eq. 3.8}$$

Where:

f_f = flange stress at the section under consideration due to the Service II loads calculated without consideration flange lateral bending (ksi)

f_l = flange lateral bending stress at the section under consideration due to the Service II loads determined as specified in AASHTO Article 6.10.1.6 (ksi)

R_h = hybrid factor determined as specified in AASHTO Article 6.10.1.10.1

F_{yf} = specified minimum yield strength of a flange (ksi)

The first step in evaluating the girders' performance under permanent deformation limits is to determine the girders' service level stresses. This will be derived from gravity and vehicular loadings, as lateral loads are not being considered at the service limit state in this design evaluation.

From the analysis results, the following Service II moments, from Table 3.12, were found:

$$1.00M_{DC1} = 484.2\ ft\ kip$$

$$1.00M_{DC2} = 68.4\ ft\ kip$$

$$1.00M_{DW} = 79.65\ ft\ kip$$

$$1.30M_{LL+IM} = 1208.35\ ft\ kip$$

Using these moments, Service II stresses for the top and bottom flange are found in Equations 3.9 and 3.10. The distances from the centroid and the moments of inertia for each portion of load corresponding to the non-composite, short-term composite, and long-term composite sections can be found in Tables 3.1 through 3.3.

Top Flange:

$$f_f = \frac{(484.2)(12)(14.82)}{4950.48} + \frac{(68.4+79.65)(12)(6.39)}{13374.58} + \frac{(1208.35)(12)(0.84)}{19141.24} = 18.88 \text{ ksi} \quad \text{Eq. 3.9}$$

$$f_f \leq 0.95 R_h F_{yf}$$

$$18.88 < 0.95(1.0)(50) \Rightarrow 18.88ksi < 47.5\ ksi\ \therefore OK(Ratio = 0.398)$$

Bottom Flange:

$$f_f = \frac{(484.2)(12)(12.18)}{4950.48} + \frac{(68.4+79.65)(12)(20.61)}{13374.58} + \frac{(1208.35)(12)(26.16)}{19141.24} = 36.85 \text{ ksi} \quad \text{Eq. 3.10}$$

$$f_f + \frac{f_l}{2} \leq 0.95 R_h F_{yf}$$

$$36.85 + \frac{0}{2} < 0.95(1.0)(50) \Rightarrow 36.85ksi < 47.5\ ksi\ \therefore OK(Ratio = 0.776)$$

Therefore, according to Equations 3.7 and 3.8 respectively, the flanges are shown to meet the requirements for permanent deformations at the service limit state.

3.7.3.2 Elastic Deformations

Many states' Departments of Transportation and owner agencies choose to invoke optional live load deflection criteria meant to ensure user comfort in addition to the limit states set forth for permanent deformations. This optional limit is also evaluated. AASHTO Article 2.5.2.6.2 states deflection criteria that may be used. For bridges subjected to vehicular loads only, a limit of *L*/800 is specified (Figure 3.4). For a span length of 60 feet, this equates to a live load deflection of 0.9

inches. From analysis results, a maximum live load deflection of 0.585 inches was determined. Therefore, this meets elastic deformation requirements (Ratio = 0.650).

- Vehicular load, general Span/800,
- Vehicular and pedestrian loads Span/1000,
- Vehicular load on cantilever arms..... Span/300, and
- Vehicular and pedestrian loads on cantilever arms Span/375.

Figure 3.4: Live Load Deflection Limits (AASHTO, 2014)

3.7.4 Fatigue Limit State

The intent of the fatigue limit state is to control crack growth under cyclic loading conditions by limiting the range of live load stress (Δf) to which the steel members are subjected. Specifically, load induced fatigue categories must satisfy the limit shown in Equation 3.6. For the limit, the load factor (γ) and the nominal fatigue resistance ($(\Delta F)_n$) associated with the fatigue limit state are a function of the number of stress cycles to which the girder is subjected.

$$\gamma(\Delta f) \leq (\Delta F)_N \qquad \text{Eq. 3.11}$$

Where:

γ = load factor specified in AASHTO Table 3.4.1-1 for the fatigue load combination

(Δf) = force effect, live load stress range due to the passage of the fatigue load as specified in AAASHTO Article 3.6.1.4 (ksi)

$(\Delta F)_n$ = nominal fatigue resistance as specified in AASHTO Article 6.6.1.2.5 (ksi)

AASHTO Article 6.11.5 states the provisions of AASHTO Article 6.10.5 apply where AASHTO Article 6.10.5.1 requires fatigue be investigated in accordance with AASHTO Article 6.6.1, which states the live load stress range be less than the fatigue resistance. The $(\Delta F)_n$ varies based on the fatigue category to which a particular member or detail belongs. The nominal fatigue resistance is taken using the following equations:

For the Fatigue I load combination (infinite life):

$$(\Delta F)_n = (\Delta F)_{TH} \quad \text{Eq. 3.12}$$

For the Fatigue II load combination (finite life):

$$(\Delta F)_n = \left(\frac{A}{N}\right)^{\frac{1}{3}} \quad \text{Eq. 3.13}$$

$$N = (365)(75)n(ADTT)_{SL} \quad \text{Eq. 3.14}$$

Where:

A = constant taken from AASHTO Table 6.6.1.2.5-a (ksi^3)

n = number of stress range cycles per truck pass taken from AASHTO Table 6.6.1.2.5-2

$(ADTT)_{SL}$ = single-lane $ADTT$ as specified in AASHTO Article 3.6.1.4

$(\Delta F)_{TH}$ = constant-amplitude fatigue threshold taken from AASHTO Table 6.6.1.2.5-6 (ksi)

For this design evaluation, the detail is the bottom bend in the steel plate. According to AASHTO Table 6.6.1.2.3-1 Section 1, this detail is listed with a fatigue category B. Fatigue category B is chosen to be conservative because it is unknown if the steel used will be galvanized or weathering steel and otherwise meets the description in described in Section 1.2 of Table 6.6.1.2.3-1. For a fatigue category B, a constant amplitude fatigue threshold, $(\Delta F)_{TH}$ = 16 ksi (AASHTO Table 6.6.1.2.5-3), is obtained.

Values for cycles per truck passage (*n*) are listed in AASHTO Table 6.6.1.2.5-2. For a simple-span girder with a span length larger than 40 feet, *n* is taken as 1.0.

To determine the single-lane average daily truck traffic ($(ADTT)_{SL}$), a value of the average daily truck traffic (*ADTT*) is assumed. For this design example, an *ADTT* of 4000 trucks per day was assumed. AASHTO Table 3.6.1.4.2-1 lists *p* values, which are fractions of *ADTT* that can be expected in a single lane. For a two-lane bridge, $p = 0.85$. Therefore, according to Equation 3.15, $(ADTT)_{SL}$ can be easily evaluated.

$$(AADT)_{SL} = p(AADT) = 0.85\left(4000\frac{trucks}{day}\right) = 3400\frac{trucks}{day} \qquad \text{Eq. 3.15}$$

AASHTO Table 6.6.1.2.3-2 lists ADTT values, which are equivalent to infinite life. Specifically, AASHTO Article 6.6.1.2.3 states that when the actual $(ADTT)_{SL}$ value is larger than that listed in the table, the detail in question shall be designed for the Fatigue I load combination for infinite life. For a fatigue category B, a value of 860 trucks per day is listed. Therefore, the details chosen for these design evaluations are evaluated for the Fatigue I load combination for infinite life.

From the previously determined Factored Fatigue I moments, a maximum moment of 578.7 ft-kip was determined from Table 3.14. Since the structure being analyzed is a simple span bridge, a minimum fatigue moment of zero was found. Therefore, a fatigue stress range can be found for both the top flange and bottom flange by determining the stress resulting from the calculated moment in Equations 3.16 and 3.17, respectively. As shown in the following check for fatigue, the bends in the tub girder perform satisfactorily. The distances from the flange being analyzed can be calculated and the short-term composite moment of inertia can be found in Tables 3.1 and 3.2.

Top Flange:

$$\gamma(\Delta f) = \frac{578.7(12)(0.84)}{19141.24} = 0.31ksi \qquad \text{Eq. 3.16}$$

$$0.31ksi < 16.0ksi \therefore OK(Ratio = 0.019)$$

Bottom Flange:

$$\gamma(\Delta f) = \frac{578.7(12)(26.16)}{19141.24} = 9.49ksi$$ Eq. 3.17

$$9.49ksi < 16.0ksi \therefore OK(Ratio = 0.593)$$

3.7.5 Strength Limit State

The intent of the strength limit state is to ensure the structure has adequate strength and stability when subjected to maximum factored loads. For a composite section in positive flexure, sections must meet flexural resistance requirements and the ductility requirement outlined in AASHTO Article 6.10.7.3. The section must have adequate shear capacity under the maximum factored loads. The computation of the girder's flexural resistance, shear resistance, and ductility are discussed in Section 3.3 Girder Geometry, along with the factored loads and force effects these sections must withstand.

3.7.5.1 Flexure

For flexure, in order to determine a section's capacity, a determination must be made whether the section is classified as compact or noncompact. For this determination, the section's plastic moment capacity must be calculated. The plastic moment capacity of the section is evaluated according to the provisions of AASHTO Article D6.1. For this evaluation, the reinforcement in the concrete slab is conservatively neglected.

The first step in determining the section's plastic moment capacity is to determine the plastic forces in each of section's components, as seen in Equations 3.18 through 3.23.

$$P_S = 0.85f'_c b_s t_s = 0.85(4)(96)(8.00) = 2611.2\ kip$$ Eq. 3.18

$$P_{TF} = F_y A_{TF} = (50)(12) = 300\ kip$$ Eq. 3.19

$$P_{TB} = 2F_y A_{bend} = 2(50)(1.8) = 182.3\ kip$$ Eq. 3.20

$$P_W = F_y A_W = 2(50)(11.5) = 1151.1\ kip$$ Eq. 3.21

$$P_{BB} = 2F_y A_{bend} = 2(50)(1.8) = 182.3\ kip$$ Eq. 3.22

$$P_{BF} = F_y A_{BF} = (50)(10.7) = 534.3\ kip$$ Eq. 3.23

Where:

P_S = plastic compressive force in concrete deck (kip)

f'_c = minimum specified 28-day compressive strength (ksi)

b_s= effective width of concrete deck (in)

t_s = thickness of concrete deck (in)

P_{TF} = plastic force in top flange of steel girder (kip)

F_y = yield strength of steel used in steel girder (ksi)

A_{TF} = cross sectional area of top flange (in^2)

P_{TB} = plastic force in top bend of steel girder (kip)

A_{TB} = cross sectional area of top bend (in^2)

P_W = plastic force in web of steel girder (kip)

A_W = cross sectional area of web (in^2)

P_{BB} = plastic force in bottom bend of steel girder (kip)

A_{BB} = cross sectional area of bottom bend (in^2)

P_{BF}= plastic force in bottom flange of steel girder (kip)

A_{BF} = cross sectional area of bottom flange (in^2)

Next, the location of the plastic neutral axis (PNA) must be determined. AASHTO Table D6.1 gives a straightforward procedure, using Equations 3.24 and 3.25, on determining the location of the PNA and is adopted in this design example.

Case I (PNA is in the web)

$$P_{BF} + P_{BB} + P_W \geq P_{TB} + P_{TF} + P_S \qquad \text{Eq. 3.24}$$

$$1867.7 < 3093.5 \therefore PNA\ is\ not\ in\ the\ web$$

Case II (PNA is in the top flange)

$$P_{BF} + P_{BB} + P_W + P_{TB} + P_{TF} \geq P_S \qquad \text{Eq. 3.25}$$

$$2350 < 2611.2 \therefore PNA\ is\ not\ in\ the\ top\ flange$$

Therefore, the PNA is in the concrete slab and its location measured from the top of the structural slab (Y) is found in Equation 3.26:

$$\bar{Y} = (t_s)\left[\frac{P_{BF} + P_{BB} + P_W + P_{TB} + P_{TF}}{P_{Slab}}\right] \qquad \text{Eq. 3.26}$$

$$\bar{Y} = (8)\left[\frac{534.3 + 182.3 + 1151.1 + 182.3 + 300}{2611.2}\right] = 7.20in$$

Next, the distances of the individual components from the location of the PNA are computed.

$$d_S = 7.20 - \left(\frac{8.00}{2}\right) = 3.200in$$

$$d_{TF} = (8.00 - 7.20) + 2.00 + (27.00 - 26.75) = 3.05in$$

$$d_{TB} = (8.00 - 7.20) + 2.00 + (27.00 - 26.00) = 3.78in$$

$$d_W = (8.00 - 7.200) + 2.00 + (27.00 - 13.50) = 16.30in$$

$$d_{BB} = (8.00 - 7.20) + 2.00 + (27.00 - 1.00) = 28.82in$$

$$d_{BF} = (8.00 - 7.20) + 2.00 + (27.00 - 0.25) = 29.55in$$

Where:

d_S = distance from the plastic neutral axis to centroid of concrete slab (in)

d_{TF} = distance from the plastic neutral axis to centroid of top flange (in)

d_{TB} = distance from the plastic neutral axis to centroid of top bend (in)

d_W = distance from the plastic neutral axis to centroid of web (in)

d_{BB} = distance from the plastic neutral axis to centroid of bottom bend (in)

d_{BF} = distance from the plastic neutral axis to centroid of bottom flange (in)

The plastic moment of the composite section (M_p) is then evaluated using Equation 3.27.

$$M_p = \left(\frac{\overline{Y^2}P_s}{2t_s}\right) + [P_{TF}d_{TF} + P_{TB}d_{TB} + P_W d_W + P_{BB}d_{BB} + P_{BF}d_{BF}] \quad \text{Eq. 3.27}$$

$$M_p = \left(\frac{(7.200)^2 * 2611.2}{2(8.00)}\right) + [(300)(3.050) + (182.3)(3.782) + (1151.1)(16.300) + (182.3)(28.818) + (543.3)(29.550)]$$

$$M_p = 49870.2\ in\ kip = 4155.9\ ft\ kip$$

For a composite section in positive flexure to be considered compact, according to AASHTO Article 6.10.6.2.2, the section must meet three requirements. The first requirement states the minimum yield strengths of the flanges must not exceed 70.0 ksi, which is met by the 50 ksi steel used throughout this design example. The second requirement is that the web satisfies AASHTO Article 6.10.2.1.1, which was evaluated earlier in Section 3.7.1 Cross Section Proportion Limits. The third requirement is that the section satisfies the web slenderness limit found in Equation 3.12.

$$\frac{2D_{cp}}{t_w} \leq 3.76\sqrt{\frac{E}{F_{yc}}} \qquad \text{Eq. 3.28}$$

Where:

D_{cp} = depth of the web in compression at the plastic moment determined in AASHTO Article D6.3.2 (in)

t_w = thickness of web (in)

E = modulus of elasticity of steel (ksi)

F_{yc} = minimum compression strength of compression flange (ksi)

It was previously determined the PNA was in the concrete slab. Therefore, D_{cp} = 0, satisfying the third requirement. Since AASHTO Article 6.10.6.2.2 requirements have been met, this section is classified as compact. For compact composite sections in positive flexure, AASHTO Article 6.10.7.1.2 states the nominal flexural resistance (M_n) is computed using Equations 3.29 and 3.30:

If $D_p \leq 0.1\ D_t$, then:

$$M_n = M_p \qquad \text{Eq. 3.29}$$

Otherwise:

$$M_n = M_p\left(1.07 - 0.7\frac{D_p}{D_t}\right) \quad \text{Eq. 3.30}$$

Where:

D_p = distance from the top of the concrete deck to the neutral axis of the composite section at the plastic moment (in)

D_t = total depth of the composite section (in)

M_n = nominal flexural resistance (kip-in)

$$D_p = \bar{Y} = 7.20\ in$$

$$D_t = 8.00 + 2.00 + 27.00 = 37.00\ in$$

$$0.1D_t = 3.70\ in$$

$$D_p > 0.1D_t$$

Therefore, solving Equation 3.30:

$$M_n = 4155.9\left(1.07 - 0.7\frac{7.20}{37.0}\right) = 3880.7\ ft\ kip$$

To satisfy strength limit state requirements, the section must satisfy the following relation:

$$M_u + \frac{1}{3}f_l S_{xt} \leq \phi_f M_n \quad \text{Eq. 3.31}$$

Where:

ϕ_f = resistance factor for flexure specified in AASHTO Article 6.5.4.2

f_l = flange lateral bending stress determined as specified in AASHTO Article 6.10.1.6 (ksi)

M_n = nominal flexural resistance of the section determined as specified in AASHTO Article 6.10.1.6 (kip-in)

M_u = bending moment about the major-axis of the cross-section determined as specified in AASHTO Article 6.10.1.6 (kip-in)

M_{yt} = yield moment with respect to the tension flange determined as specified in AASHTO Article D6.2 (kip-in)

S_{xt} = elastic section modulus about the major axis of the section to the tension flange (in^3)

Due to wind forces and other lateral loads being neglected at the finished state, $f_l = 0$. From the moments generated for this girder, a maximum Strength I bending moment of 2436.9 ft-kip was found, as seen in Table 3.10, indicating this girder meets strength limit state requirements of the modified Equation 3.31 for flexure.

$$M_u \leq \phi_f M_n$$

$$2436.9\ ft\ kip < 1.00(3880.7\ ft\ kip) \therefore OK(Ratio = 0.628)$$

3.7.5.2 Shear

The provisions of AASHTO Article 6.11.9 are applied to determine whether sections meet strength limit state requirements for shear. The first step in finding shear is to determine the plastic shear capacity of the web, which is found using Equation 3.32. Note that *D* in AASHTO Article 6.10.9 shall be taken as the depth of web plate measured along the slope.

$$V_p = 0.58F_{yw}Dt_w \qquad \text{Eq. 3.32}$$

$$V_p = 0.58(50)(23.02)(0.5) = 333.8\ kip$$

Where:

V_p = plastic shear force (kip)

The plastic shear capacity of the web is then modified by *C* to obtain the nominal shear resistance. *C* is the ratio of shear-buckling resistance to shear yield strength and is a function of the slenderness of the web. For this computation, a shear buckling coefficient (*k*) is introduced. However, as this web is unstiffened, *k* is taken as a constant value equal to 5.0. Therefore, *C* is determined using Equation 3.33.

$$\frac{D}{t_w} \leq 1.12\sqrt{\frac{Ek}{F_{yw}}} \qquad \text{Eq. 3.33}$$

$$\frac{23.02}{0.5} \leq 1.12\sqrt{\frac{(29000)(5.0)}{(50)}}$$

$$46.0 \leq 60.3$$

Therefore:

$$C = 1.0$$

The nominal shear capacity (V_n) is then determined using Equation 3.34.

$$V_n = V_{cr} = CV_p \qquad \text{Eq. 3.34}$$

$$V_n = (1.0)(333.8) = 333.8kip$$

From the shears generated for this girder, a maximum Strength I shear of 196.5 kip was found in Table 3.11. Equation 3.35 indicates the girder meets strength limit state requirements for shear.

$$V_u \leq \phi_v V_n \qquad \text{Eq. 3.35}$$

$$174.3kip \leq (1.0)(333.8kip) \therefore OK(Ratio = 0.522)$$

Where:

ϕ_v= resistance factor for shear specified in AASHTO Article 6.5.4.2

V_n = nominal shear resistance (kip)

V_u = shear in the web at the section under consideration due to the factored loads (kip)

3.7.5.3 Ductility

An additional ductility requirement is placed on composite sections in positive flexure. Specifically, sections shall meet the requirements in Equation 3.36.

$$D_p \leq 0.42 D_t \qquad \text{Eq. 3.36}$$

$$7.20 \leq (0.42)(37.0)$$

$$7.20in \leq 15.4in \ \therefore OK(Ratio = 0.463)$$

For this requirement, using previously determined values, the section performs satisfactorily.

3.7.6 Shear Connectors

The fatigue shear resistance of an individual shear stud (Z_r) is based on the Fatigue I load combination because the $(ADTT)_{SL}$ is greater than 960 trucks per day. Equation 3.37 is used to calculate the fatigue shear resistance of an individual shear stud. The diameter of the shear studs used in this design example (d) are 7/8 inch.

$$Z_r = 5.5d^2 \qquad \text{Eq. 3.37}$$

$$Z_r = 5.5\left(\frac{7}{8}\right)^2 = 4.21\ kip$$

The next step in determining the maximum distance between shear studs is to determine the first moment of the deck with respect to the neutral axis of the composite section (Q). The distance from the centroid of the deck to the centroid of the composite section is 6.84 inches and the transformed area of the deck is 47 in^2.

$$Q = (6.84in)(47in^2) = 656.96in^3$$

The Vertical Shear Force Range Under the Applicable Fatigue Load (V_f) is found by finding the difference between the maximum and the minimum shears for each tenth point along the span, as seen in Table 3.16.

Table 3.16: Calculation of Vertical Shear Force Range

x (ft)	*x/L*	*1.50(LL + IM)*		**V_f (kip)**
		(+)	(-)	
0	0	49.5	0.0	49.5
6	0.1	42.4	-3.2	45.6
12	0.2	35.3	-6.3	41.6
18	0.3	28.5	-10.0	38.5
24	0.4	22.1	-14.0	36.1
30	0.5	17.9	-17.9	35.8
36	0.6	14.0	-22.1	36.1
42	0.7	10.0	-28.5	38.5
48	0.8	6.3	-35.3	41.6
54	0.9	3.2	-42.4	45.6
60	1	0.0	-49.5	49.5

The Longitudinal Fatigue Shear Range per Unit Length (V_{fat}) is calculated using the Vertical Shear Force Ranges at tenth points by evaluating Equation 3.38. The Horizontal Fatigue Shear Range per Unit Length (V_{sr}) is simply the same as the Longitudinal Fatigue Shear Range per Unit Length because the radial shear due to curvature may be conservatively neglected for box sections as stated in AASHTO Section C6.11.10, as seen in Equation 3.39.

$$V_{fat} = \frac{V_f Q}{I} \quad \text{Eq. 3.38}$$

Where:

V_f = vertical shear force range under the applicable fatigue load

I = moment of inertia of the short-term composite section (in^4)

$$V_{sr} = \sqrt{\left(V_{fat}\right)^2 + \left(F_{fat}\right)^2} \quad \text{Eq. 3.39}$$

Therefore, the maximum pitch (p), or distance between shear studs, required to meet fatigue requirements, at tenth points, for shear studs is calculated using Equation 3.40. The minimum pitch values at tenth points can be seen in Table 3.17.

$$p \leq \frac{nZ_r}{V_{sr}} \quad \text{Eq. 3.40}$$

Where:

n = number of shear connectors in a cross-section

Table 3.17: Calculation of Minimum Pitch

x (ft)	*x/L*	Stresses (ksi)			***p* (in)**
		V_{fat}	H_{fat}	V_{sr}	
0	0	1.700	0	1.700	9.91
6	0.1	1.565	0	1.565	10.76
12	0.2	1.429	0	1.429	11.79
18	0.3	1.321	0	1.321	12.75
24	0.4	1.239	0	1.239	13.59
30	0.5	1.230	0	1.230	13.69
36	0.6	1.239	0	1.239	13.59
42	0.7	1.321	0	1.321	12.75
48	0.8	1.429	0	1.429	11.79
54	0.9	1.565	0	1.565	10.76
60	1	1.700	0	1.700	9.91

Linear interpolation reveals a 12 inch pitch occurs at approximately 13.33 feet or 160 inches. A pitch of 9 inches will be used on the girder until 13.5 feet or 162 inches from the center-line of bearing from either side. A 12 inch pitch will be used on the central region of the beam as seen in Figure 3.5. The pitch layout allows for 70 rows of studs and a total of 280 studs per girder.

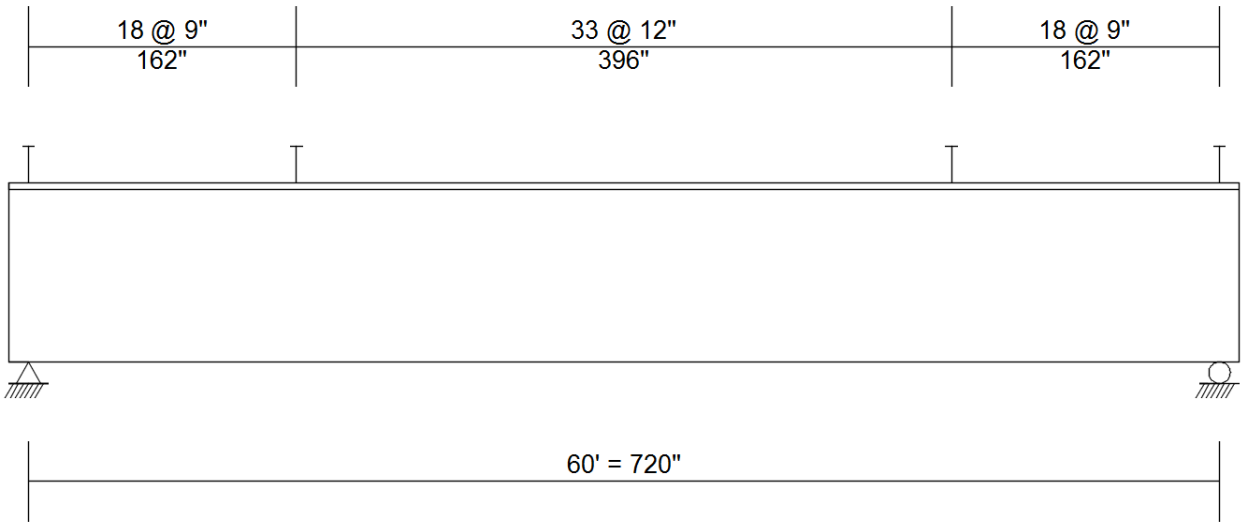

Figure 3.5: Shear Stud Spacing

3.8 PERFORMANCE SUMMARY

A tabulated summary of the girder's performance ratios is presented in Table 3.18. As shown, the girder performs satisfactorily under all evaluated design checks, with the permanent deformation at the service limit state governing (Ratio = 0.776).

Table 3.18: Performance Ratio Summary

Service Limit State	
Elastic Deformations	0.650
Permanent Deformations	
Top Flange	0.398
Bottom Flange	0.776
Fatigue Limit State	
Bends in Plate Steel	
Top Flange	0.019
Bottom Flange	0.593
Strength Limit State	
Moment	0.628
Shear	0.522
Ductility	0.463

3.9 AASHTO EQUATION REFERENCES

Table 3.19 details a summary of the equations referenced in the chapter along with their respective AASHTO equation and page numbers.

Table 3.19: Equation Legend (AASHTO, 2014)

Chapter 3	AASHTO 7th Edition	AASHTO 7th Edition Page Number
Equation 3.1	Table 4.6.2.2.2b-1	4-37
Equation 3.3	Article 2.5.2.6.2	2-11
Equation 3.4	Equation 6.11.2.1.2-1	6-179
Equation 3.5	Equation 6.11.2.2-1	6-180
Equation 3.6	Equation 6.11.2.2-2	6-180
Equation 3.7	Equation 6.10.4.2.2-1	6-130
Equation 3.8	Equaiton 6.10.4.2.2-2	6-130
Equation 3.11	Equation 6.6.1.2.2-1	6-34
Equation 3.12	Equation 6.6.1.2.5-1	6-48
Equation 3.13	Equaiton 6.6.1.2.5-2	6-48
Equation 3.14	Equation 6.6.1.2.5-3	6-48
Equation 3.16	Equation 3.6.1.4.2-1	3-31
Equation 3.26	Table D6.1-1	6-325
Equation 3.27	Table D6.1-1	6-325
Equation 3.28	Equation 6.10.6.2.2-1	6-135
Equation 3.29	Equation 6.10.7.1.2-1	6-140
Equation 3.30	Equation 6.10.7.1.2-2	6-140
Equation 3.31	Equation 6.10.7.1.1-1	6-139
Equation 3.32	Equation 6.10.9.2-2	6-153
Equation 3.33	Equation 6.10.9.3.2-4	6-154
Equation 3.34	Equation 6.10.9.2-1	6-153
Equation 3.35	Equation 6.10.9.1-1	6-151
Equation 3.36	Equation 6.10.7.3-1	6-143
Equation 3.37	Equation 6.10.10.2-1	6-158
Equation 3.38	Equation 6.10.10.1.2-3	6-156
Equation 3.39	Equation 6.10.10.1.2-2	6-156
Equation 3.40	Equation 6.10.10.1.2-1	6-156
Figure 3.4	Section 2.5.2.6.2	2-12
Table 3.4	Table 3.6.1.1.2-1	3-20

CHAPTER 4: EXPERIMENTAL TESTING

4.1 INTRODUCTION

This chapter is an overview of the experimental testing completed to assess the fatigue performance of uncoated versus galvanized steel. A brief description of each specimen consisting of a steel-brake-formed tub girder with a reinforced concrete deck is provided herein. An instrumentation plan of the strain gages and linear variable displacement transducers (LVDTs) and a determination of load applied is provided.

4.2 OVERVIEW OF TESTING PROGRAM

To verify the fatigue performance of modular tub girders, testing was performed at the Major Units Laboratory at West Virginia University. Fatigue testing conducted on two simply supported composite press-brake-formed tub girder specimens occurred in three-point bending as shown in Figures 4.1 and 4.2.

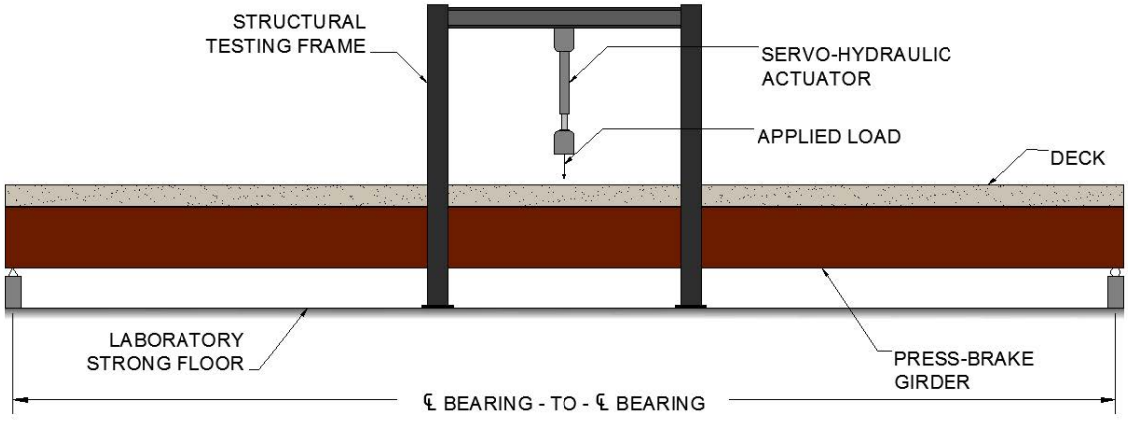

Figure 4.1: Test Setup Schematic

Figure 4.2: Isometric View of Typical Test Setup

Two-inch round diameter bars located under bearing plates, placed 37.5 feet between centerline of bearing to center line of bearing, simulated simply supported boundary conditions. One of the round bars was welded to the plate underneath, simulating a pinned boundary condition (Figure 4.3), and the other round bar was placed in a small groove allowing horizontal displacement, simulating a roller boundary condition (Figure 4.4). The two-inch diameter bars were supported by 6 inch x 24 inch x 2 inch plate steel, which were in turn supported by 12 inch x 24 inch x 2 inch plate steel. Four threaded rods connected the 12 inch x 24 inch x 2 inch plate, through two 6 inch x 6 inch hollow structural sections filled with concrete, to the support system shown in Figure 4.5. Lateral bracing at the support locations prevented unintentional rotation using equal leg angles connecting the specimen to the lateral-resisting steel frame. 1/2 inch thick steel plate welded to the tub girder operated as connection plates for the lateral bracing elements. Figure 4.5 shows a complete setup of the lateral resisting system.

Figure 4.3: View of Pinned Boundary Condition

Figure 4.4: View of Roller Boundary Condition

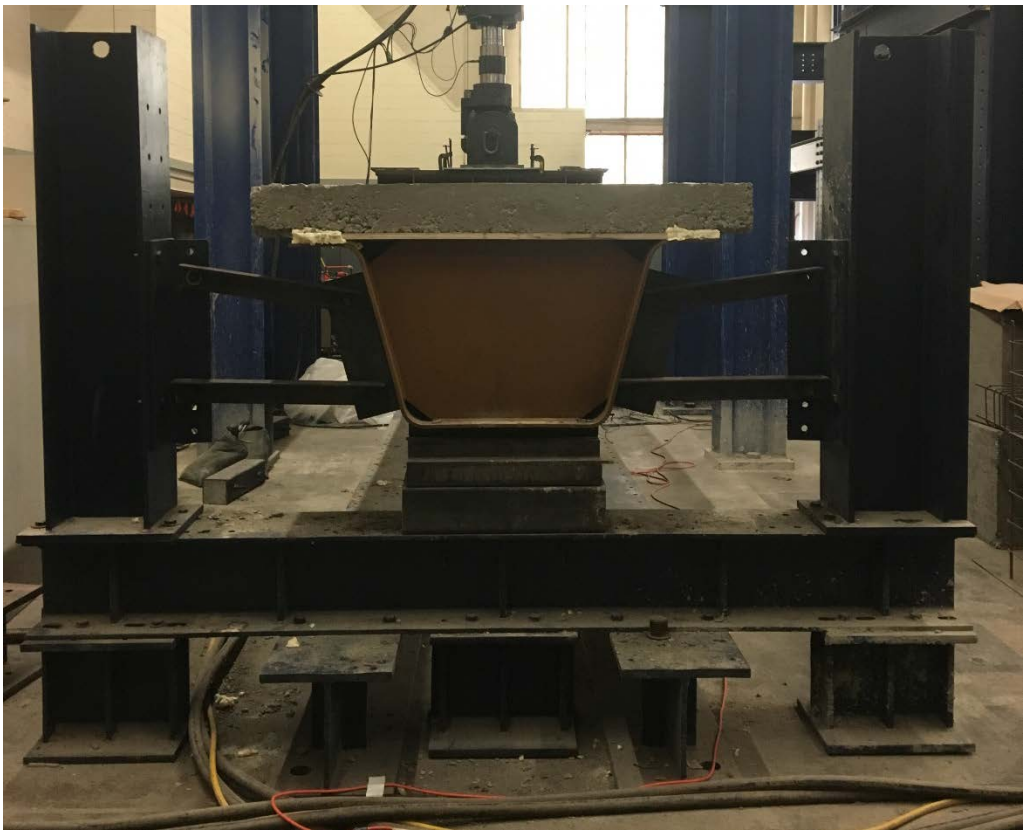

Figure 4.5: Lateral Bracing System

4.3 SPECIMEN DESCRIPTIONS

Michaelson (2014) found the optimum cross-section of an 84 inch x 7/16 inch plate for this press-brake-formed tub girder to have a 23 inch depth and a 6 inch top flange width. The girder was bent by being placed in a large capacity press-brake and cold-bent with the inside bend radius equal to five times the thickness of the plate. After the plate was bent into the shape (Figure 4.6), two rows of 7/8 inch by 4 inch shear studs were welded onto each 6 inch wide top flange. 3/4 inch bearing plates were then welded three inches from the end of the tub girder to prevent potential premature buckling during testing, as seen in Figures 4.7 and 4.8. Table 4.1 shows the non-composite section properties of the 84 inch x 7/16 inch press-brake-formed tub girder (Kozhokin 2016). One specimen consisted of uncoated HPS-50 steel and the other consisted of HPS-50 steel hot dip galvanized prior to its arrival at the laboratory.

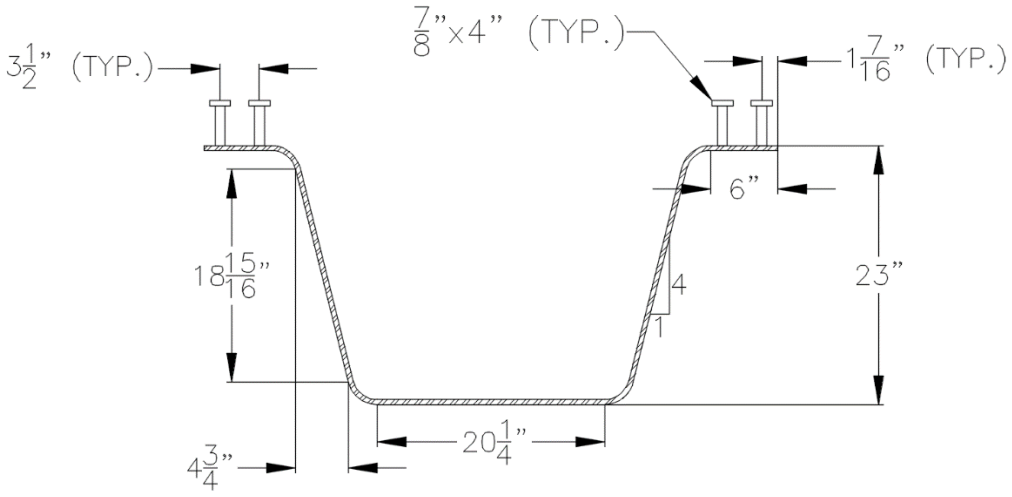

Figure 4.6: Press-Brake Tub Girder Cross Section

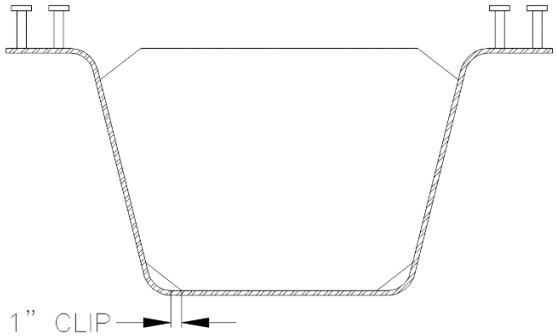

Figure 4.7: Press-Brake Tub Girder with End Diaphragm

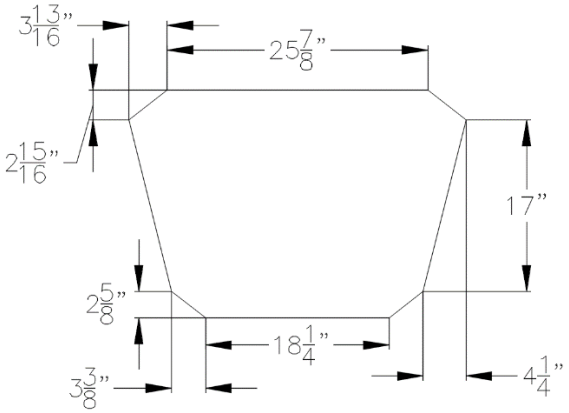

Figure 4.8: End Diaphragm

Table 4.1: Press-Brake-Formed Tub Girder Non-Composite Section Properties

Property	Value
A (in^2)	36.75
L (in)	444
E (ksi)	29,000
G (ksi)	11,154
I_x (in^4)	2893.1
I_y (in^4)	8049.6
I_{open} (in^4)	2.3447
I_{closed} (in^4)	69,000
I_w (in^6)	139,952
β_x (in)	-19.704

4.4 INSTRUMENTATION

4.4.1 Instruments

Two types of bondable foil strain gages measured the strain in the tub girder: uniaxial linear pattern on the bottom flange and rectangular rosettes on the webs. The uniaxial strain gages recorded strain in one direction while the rectangular rosettes recorded axial strain and shear at each gage location. LVDTs measured the vertical deflections at various locations. The strain gages and LVDTs connected to a Micro-Measurements Model 5100 Scanner, which in turn utilized StrainSmart software (Micro-Measurements, 2010) to record the strain and displacement data. An MTS Model 201.70 330-kip servo hydraulic actuator applied the load to the system.

4.4.2 Layout of Strain Gages

Six uniaxial strain gages, placed along the top and bottom of the bottom flange of the tub girder measured the extreme tensile stresses in the system. Twelve rectangular rosettes, placed along the interior and exterior of the webs, captured the bending and shear strains. The eighteen strain gages employed during testing are shown in Figure 4.9. The gages were placed at 46 inches,

twice the girder depth, away from the load application to avoid strain concentration effects of the load. The nine strain gages on the interior face of the girder can be seen in Figure 4.10. The interior gages where then covered with two inch insulation board for protection during the concrete pour (Figure 4.11). The exterior gages were covered in a roll of plastic for protection from regular laboratory operations.

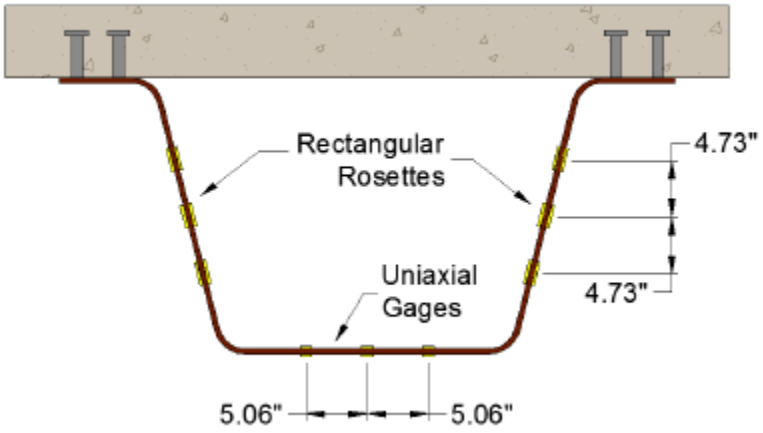

Figure 4.9: Strain Gage Layout

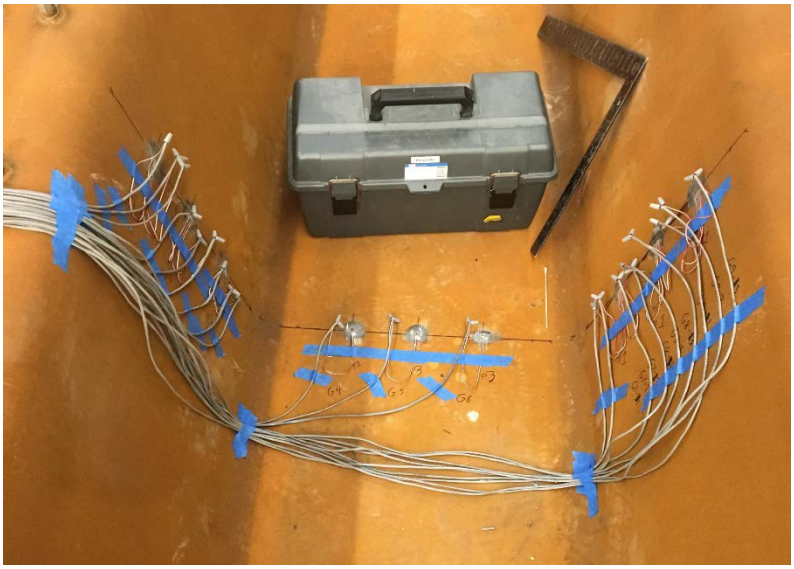

Figure 4.10: Exposed Strain Gages

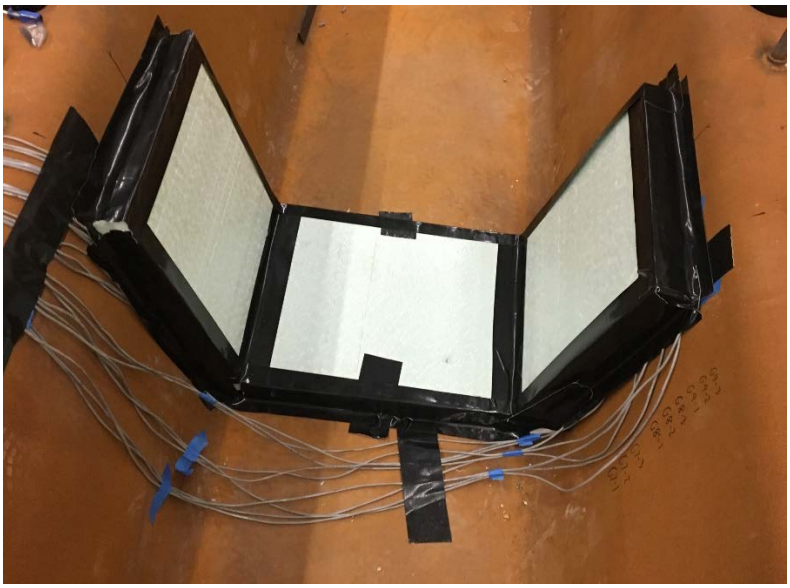

Figure 4.11: Covered Strain Gages

4.4.3 Layout of LVDTs

Three LVDTs along the length of the girder measured vertical deflections. One LVDT was located at mid-span and the other two were placed at quarter points on the girder. These LVDTs were placed in the center of the bottom flange. By placing the LVDTs under the bottom flange, consideration of torsional deflections from the flanges were neglected.

4.5 TEST SPECIMEN ASSEMBLY

4.5.1 Concrete Formwork

Concrete formwork was placed in and around the 38 foot long tub girders. 2 inch x 4 inch dimensional lumber was cut to fit inside the girders to support the stay in place plywood (Figure 4.12). Expanding spray foam sealed locations not completely enclosed by the frame work, such as where the wires connecting the interior strain gages entered the tub girder. During construction for industry, the plywood forms would be replaced with SIP metal formwork.

Figure 4.12: Supports Inside the Girder

Most exterior forms were reused from previous testing performed by Michaelson (2014) and Kozhokin (2016), but their specimens were 35 feet long where the specimens tested for this study were 38 feet long. This difference necessitated additional framework construction. 2 inch x 8 inch lumber was cut to produce a 6 inch deep concrete deck and was placed around the top of the formwork. The forms allowed a 4.5 inch overhang on either side of the steel tub girder for the concrete deck. The formwork was braced using large concrete blocks as dead-man anchors. Repeated use of the forms created a bow in the formwork, requiring the use of additional bracing as seen in Figure 4.13

Figure 4.13: Completed Concrete Formwork

4.5.2 Reinforcing Bars

AASHTO Article 9.7.2 was used to design the reinforcement pattern with the empirical deck method. The bottom mat of reinforcing steel bars consisted of #5 rebar with a bottom cover of one inch. The top mat of reinforcement consisted of #4 rebar placed two inches above the bottom mat, creating a top cover of two inches. The longitudinal rebar of both layers was spaced at 12 inches with an edge space of two inches. The transverse bars had a spacing of 12 inches, which coincided with the placement of the shear studs and the typical edge spacing of two inches. The reinforcement pattern can be seen in Figure 4.14.

Figure 4.14: Placement of Reinforcing Steel

4.5.3 Concrete Deck Pour

Approximately two days prior to the concrete pour, the outer formwork was coated in form release. This allowed the easy removal of the forms for reuse in future tests without significant damage to the concrete deck. Once the concrete arrived on site, four 6 inch diameter cylinders were poured for future compressive strength testing. A one yard concrete bucket attached to an overhead ten ton crane (Figure 4.15) delivered the wet concrete from the truck to the pour location. The concrete was vibrated after each successive pour from the bucket to minimize air pockets and honey combing.

Figure 4.15: Concrete Bucket Lowering into Position

The entire pouring process lasted approximately two hours for each deck placement. The concrete cured before the formwork was stripped from the composite unit. The deck was inspected for any damage from the removal of the formwork and only minimal localized damage occurred at locations where forms were pried away from the deck. The completed concrete deck is seen in Figure 4.16. The concrete was allowed to cure for at least 28 days prior to loading.

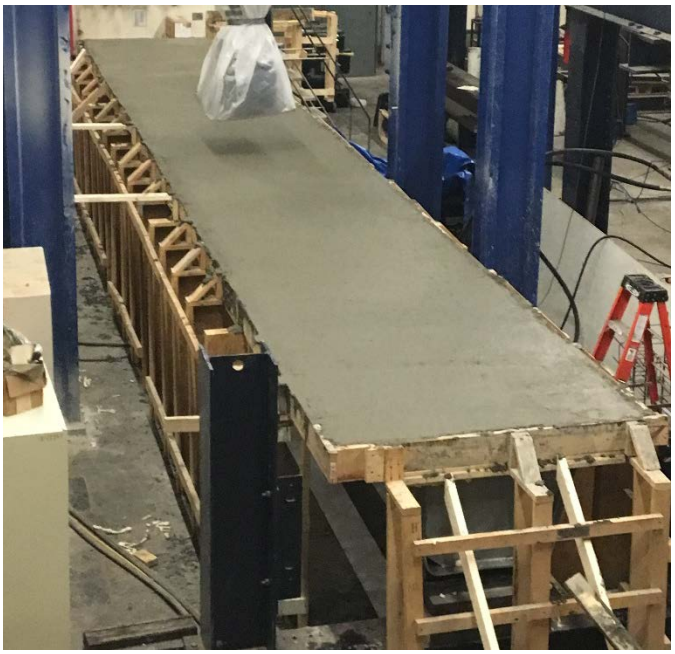

Figure 4.16: Poured Concrete Deck

4.6 LOAD CONFIGURATION

The induced load was applied at the mid-span of the system by an MTS 330-kip servo-hydraulic actuator mounted to a large steel structural frame bolted to the floor of the major unit's laboratory (Figure 4.17). A large spreader beam was attached to the head of the actuator using large C-clamps to avoid localized concrete crushing due to concentrated load effects. An elastomeric pad was placed between the spreader beam and the concrete deck, as seen in Figure 4.17. Elastomeric bearing pads consist of alternating layers of neoprene, an industrial grade rubber, and steel strips. These bearing pads aid in transfer of load from the spreader beam to the deck.

Figure 4.17: Load Applied to the System

4.7 LOAD MAGNITUDE DETERMINATION

4.7.1 Load Determination Overview

The loads required to induce the Service II and Fatigue I moments needed to be calculated prior to testing of the specimen. The Service II load combination is intended to control yielding of steel structures due to vehicular live loads and is determined using AASHTO Tables 3.4.1-1 and 3.4.1-2.

$$\text{Service II} = 1.0DC + 1.0DW + 1.3(LL + IM) \qquad \text{Eq. 4.1}$$

The Fatigue I load combination is related to infinite load-induced fatigue life and is determined using AASHTO Tables 3.4.1-1 and 3.4.1-2.

$$\text{Fatigue I} = 1.75(LL + IM) \qquad \text{Eq. 4.2}$$

The terms used in AASHTO LRFD Article 3.3.2 for Equations 4.1 and 4.2 were previously defined in Section 3.4 Loads and Load Combinations.

4.7.2 Magnitude of Applied Loads

A static load of 92.50 kip was applied to the uncoated steel specimen to induce the Service II moment. The MTS 330-kip servo-hydraulic actuator applied a cyclic load of 68.30 kip to induce the Fatigue I moment. For the galvanized steel specimen, a static load of 93.00 kip was applied to induce the Service II moment. The actuator applied a cyclic load of 68.50 kip to induce the Fatigue I moment. Procedures outlining the calculation of these loads are described in Appendix A.

4.7.3 Number of Cycles

Three assumptions were made to determine the number of fatigue cycles:

1. The average daily traffic (ADT) was 800 vehicles.
2. The bridge was in a non-interstate rural environment.
3. The Design Life was 75 years

AASHTO Table C3.6.1.4.2-1 was used to determine 15% of the ADT are trucks due to the rural non-interstate environment where the bridge is located. With two lanes available to trucks, AASHTO Table 3.6.1.4.2-1 expresses the $(ADTT)_{SL}$ is equal to 85% of the $ADTT$ (p = 0.85). The number of fatigue cycles, assuming a 75 year design life, was determined as follows:

Number of Cycles = 800 (ADT) x 0.15 (representing 15% truck traffic) x 0.85 (p) x 365 (Days/Year) x 75 (years) = 2,792,250 Cycles

4.8 TESTING PROCEDURE

4.8.1 Procedure for Fatigue Testing

As discussed in Section 4.4 Instrumentation, nine strain gages were used on the interior of the tub girder and nine strain gages were used on the outside of the tub girder at a distance of 46 inches from midspan. Three LVDTs placed under the bottom flange of the girder were located at quarter points of the span to measure vertical deflections.

The fatigue loading frequency of the uncoated steel girder was kept constant at 0.5 hertz. The fatigue loading frequency for the galvanized steel girder initially began at 0.5 hertz, but through the cyclic loading the actuator began to no longer meet the required loading of 68.48 kip, so the frequency was slowed at 0.01 hertz increments until the load range needed to reach the Fatigue I moment was attained. Typically, the actuator needed to be slowed by 0.01 hertz after each static loading of the Service II load.

A static base test was conducted before fatigue loading began. Five LVDT and the strain gage readings were taken before any load was applied by the actuator. The load was increased in ten 9.30 kip intervals to reach the Service II loading. Every five minutes, five readings were recorded and the load was increased. The five minute wait insured the system had settled and removed any vibration effects from the previous increase in loading. The loading to 93 kip occurred twice and the readings from the strain gages and LVDTs were averaged. The static testing previously described was conducted at a predetermined number of cycles: 1e5; 2e5; 3e5; 5e5; 7e5; 9e5; 1.1e6; 1.3e6; 1.5e6; 1.7e6; 1.9e6; 2.1e6; 2.3e6; 2.5e6; 2.7e6; and 2.9e6. A thorough check of the bottom tub girder bend regions was performed after each static test.

4.8.2 Procedure for Test to Ultimate Failure

Once the fatigue data was collected, a static test to failure was performed on both specimens. Each specimen was loaded in stroke control for increased safety and improved accuracy of the data. The load was increased in steps where the displacement of the actuator increased between 0.05 and 0.10 inches. Figure 4.18 shows the failure mode for a typical composite section. The specimen failed under ductility where the concrete deck was crushed.

Figure 4.18: Typical Failure Mode for Composite Specimens

4.9 SUMMARY

This chapter described the assembly of the 38 foot modular specimens. The 38 foot specimens were simply supported under their bearing plates creating a 37.5 foot simple span. The strain gages were placed at a distance twice the depth of the steel tub girder away from the loading location. A reinforced concrete deck poured over the girder connected by shear studs created the composite modular unit. After the concrete deck cured for 28 days, fatigue loading commenced on the specimen. Strains and deflections at predetermined cycle implements were recorded.

CHAPTER 5: EXPERIMENTAL TESTING RESULTS

5.1 INTRODUCTION

This chapter describes the results obtained during testing and the methods used to analyze the collected data. Results of the compressive testing of the concrete used in the concrete deck of each testing specimen are reported. A description of procedures used to calculate stresses and the moment induced by the applied load is included here. The testing summaries and comparison of experimental versus theoretical loads at each static test is provided. The deflections of each girder at the Service II loading are compared in the last section of this chapter.

5.2 CONCRETE STRENGTH

As noted in Chapter 4: Experimental Testing, concrete samples were tested after 28 days to calculate their compressive strength. The concrete compressive strength testing results of the deck for each test specimen are summarized in Table 5.1.

Table 5.1: Concrete Compressive Strength Results

Uncoated Steel Specimen	
Sample	Strength (psi)
1	3961
2	3991
3	4067
Average	4006

Galvized Steel Specimen	
Sample	Strength (psi)
1	2504
2	2574
3	2452
Average	2510

The concrete used for the deck of the uncoated steel girder met the desired compressive strength of 4000 psi. The concrete used in conjunction with the galvanized girder fell below the desired 4000 psi strength at 28 days. While it was crucial the compressive strength of the concrete not be significantly higher than 4000 psi to be able to ultimately fail the girder when testing concluded, the significantly weaker concrete was less than ideal. The weaker concrete led to more significant deck cracking throughout fatigue testing which was not as prevalent as in the testing

with the uncoated steel girder. The weaker concrete altered the composite properties of the testing specimen, so higher deflections and strains are expected to be present in the experimental results. Additional concrete properties are shown in Table 5.2.

Table 5.2: Concrete Section Properties

Uncoated Steel Specimen	
Thickness (in)	6
Width (in)	60
I_{slab} (in^4)	1080
E_{slab} (ksi)	3642.729

Galvized Steel Specimen	
Thickness (in)	6
Width (in)	60
I_{slab} (in^4)	1080
E_{slab} (ksi)	2883.422

5.3 MOMENT CALCULATION

5.3.1 Gage Configuration

The stresses in the system were obtained from the strain data collected using a method adopted by Hewlig and Fan (2000). Longitudinal stresses caused by bending moments and axial stresses are linearly distributed across the cross section of the member. Only three stress readings from non-collinear points are needed to determine the distribution plane of the stresses. The distribution of the stress on the cross-section can be expressed using Equation 5.1:

$$f(x, y) = a + bx + cy \qquad \text{Eq. 5.1}$$

Where a, b, and c are constants and x and y are the coordinate system on the cross-section of the member. The strain gage location in terms of x and y coordinates is shown in Table 5.3 where the x-datum is the bottom face of the bottom flange and y-datum is the short-term non-composite section centroid.

Table 5.3: x, y Coordinates of Strain Gages

Gauge Coordinates		
Gauge	From Datum	
	x (in)	y (in)
G01	-15.79	5.89
G02	-14.61	1.16
G03	-13.42	-3.57
G04	-5.06	-9.96
G05	0.00	-9.96
G06	5.06	-9.96
G07	13.42	-3.57
G08	14.61	1.16
G09	15.79	5.89
G10	-16.21	5.78
G11	-15.03	1.05
G12	-13.85	-3.68
G13	-5.06	-10.39
G14	0.00	-10.39
G15	5.06	-10.39
G16	13.85	-3.68
G17	15.03	1.05
G18	16.21	5.78

5.3.2 Gage Data Selection

After the system was statically loaded to the Service II moment twice, the strain gage and LVDT data were collected and sorted to only include consistent results, discarding any irregular data. Due to some inconsistencies, a degree of uncertainty is present in the system. Typically, a gage that performed irregularly would consistently perform irregularly, while gages that performed well consistently performed well. There were only a few instances where the data from a properly performing gage had to be discarded for inconsistency. The data inclusion matrix can be seen in Table 5.4 and 5.5, where “0” denotes data which was kept and “1” indicates data which was discarded due to inconsistency. Once a gage performed irregularly, it was not included in any further stress calculations.

Table 5.4: Gage Inclusion Matrix for Uncoated Steel Test

	Cycle Count																
Gage	**Base Test**	**100,000**	**200,000**	**300,000**	**500,000**	**700,000**	**900,000**	**1,100,000**	**1,300,000**	**1,500,000**	**1,700,000**	**1,900,000**	**2,100,000**	**2,300,000**	**2,500,000**	**2,700,000**	**2,900,000**
G01	1	1	1	1	1	1	1	1	1	1	1	1	1	1	1	1	1
G02	0	0	0	0	0	0	0	1	1	1	1	1	1	1	1	1	1
G03	0	0	0	0	0	0	0	0	0	0	0	0	0	0	0	0	0
G04	0	0	0	0	0	0	0	0	0	0	0	0	0	0	0	0	0
G05	0	0	0	0	0	0	0	0	0	0	0	0	0	0	0	0	0
G06	0	0	0	0	0	0	0	0	0	0	0	0	0	0	0	0	0
G07	1	1	1	1	1	1	1	1	1	1	1	1	1	1	1	1	1
G08	1	1	1	1	1	1	1	1	1	1	1	1	1	1	1	1	1
G09	1	1	1	1	1	1	1	1	1	1	1	1	1	1	1	1	1
G10	1	1	1	1	1	1	1	1	1	1	1	1	1	1	1	1	1
G11	0	0	0	0	0	0	0	0	0	0	0	0	0	0	0	0	0
G12	0	0	0	0	0	0	0	0	0	0	0	0	0	0	0	0	0
G13	0	0	0	0	0	0	0	0	0	0	0	0	0	0	0	0	0
G14	0	0	0	0	0	0	0	0	0	0	0	0	0	0	0	0	0
G15	0	0	0	0	0	0	0	0	0	0	0	0	0	0	0	0	0
G16	0	0	0	0	0	0	0	0	0	0	0	0	0	0	0	0	0
G17	0	0	0	0	0	0	0	0	0	0	0	0	0	0	1	1	1
G18	0	0	0	0	0	0	0	1	1	1	1	1	1	1	1	1	1

Table 5.5: Gage Inclusion Matrix for Galvanized Steel Test

	Cycle Count																
Gage	**Base Test**	**100,000**	**200,000**	**300,000**	**500,000**	**700,000**	**900,000**	**1,100,000**	**1,300,000**	**1,500,000**	**1,700,000**	**1,900,000**	**2,100,000**	**2,300,000**	**2,500,000**	**2,700,000**	**2,900,000**
G01	1	1	1	1	1	1	1	1	1	1	1	1	1	1	1	1	1
G02	0	0	0	0	0	0	0	0	0	0	0	0	0	1	1	1	1
G03	0	0	0	0	0	0	0	0	0	0	0	0	0	0	0	0	0
G04	0	0	0	0	0	0	0	0	0	0	0	0	0	0	0	0	0
G05	0	0	0	0	0	0	0	0	0	0	0	0	0	0	0	0	0
G06	0	0	0	0	0	0	0	0	0	0	0	0	0	0	0	0	0
G07	0	0	0	0	0	0	0	0	0	0	0	0	0	0	0	0	0
G08	0	0	0	0	0	0	0	1	1	1	1	1	1	1	1	1	1
G09	1	1	1	1	1	1	1	1	1	1	1	1	1	1	1	1	1
G10	1	1	1	1	1	1	1	1	1	1	1	1	1	1	1	1	1
G11	0	0	0	0	0	0	0	0	0	0	0	1	1	1	1	1	1
G12	0	0	0	1	1	1	1	1	1	1	1	1	1	1	1	1	1
G13	0	0	0	0	0	0	0	0	0	0	0	0	0	0	0	0	0
G14	0	0	0	0	0	0	0	0	0	0	0	0	0	1	1	1	1
G15	0	0	0	0	0	0	0	0	0	0	0	0	0	0	0	0	0
G16	0	0	0	0	0	0	0	0	0	0	0	0	0	0	0	0	0
G17	0	0	0	0	0	0	1	1	1	1	1	1	1	1	1	0	0
G18	0	1	1	1	1	1	1	1	1	1	1	1	1	1	1	1	1

5.3.3 Linear Regression

To further reduce the error caused by physical measurements, due to erroneous readings, a three-dimensional linear regression algorithm was employed. The error between data points and the representative plane is at its least when using the regression method based on least square criteria. The regression method is a statistical tool and does not rely on physical assumptions. Constants *b* and *c* from Equation 5.1 can be solved using Equations 5.2 through 5.10. The constant *a* can be solved using constants *b* and *c* in Equation 5.11.

$$\begin{bmatrix} L_{11} & L_{12} \\ L_{21} & L_{22} \end{bmatrix} \begin{Bmatrix} b \\ c \end{Bmatrix} = \begin{Bmatrix} L_{10} \\ L_{20} \end{Bmatrix} \quad \text{Eq. 5.2}$$

$$L_{11} = \sum_{i=1}^{n} (x_i - \bar{x})^2 \quad \text{Eq. 5.3}$$

$$L_{22} = \sum_{i=1}^{n} (y_i - \bar{y})^2 \quad \text{Eq. 5.4}$$

$$L_{12} = L_{21} = \sum_{i=1}^{n} (x_i - \bar{x})\,(y_i - \bar{y}) \quad \text{Eq. 5.5}$$

$$L_{10} = \sum_{i=1}^{n} (x_i - \bar{x})\left(f_i - \bar{f}\right) \quad \text{Eq. 5.6}$$

$$L_{20} = \sum_{i=1}^{n} (y_i - \bar{y})\left(f_i - \bar{f}\right) \quad \text{Eq. 5.7}$$

$$\bar{x} = \frac{1}{n}\sum_{i=1}^{n} x_i \quad \text{Eq. 5.8}$$

$$\bar{y} = \frac{1}{n}\sum_{i=1}^{n} y_i \quad \text{Eq. 5.9}$$

$$\bar{f} = \frac{1}{n}\sum_{i=1}^{n} f_i \quad \text{Eq. 5.10}$$

$$a = \bar{f} - b\bar{x} - c\bar{y} \quad \text{Eq. 5.11}$$

5.3.4 Calculation of Induced Moment

The induced moments were calculated using a procedure developed from Imhoff (1998). The total moment the system carries can be broken down into three individual pieces: the steel girder bending about its own neutral axis (M_L), concrete bending about its own neutral axis (M_u), and the couple induced by the composite action of the deck and girder (M_A) (Bertoldi 2009). Steel girder properties are summarized in Table 4.1 and concrete properties are summarized in Tables 5.1 and 5.2. These values were used in Equations 5.12 through 5.15 to calculate the total moment.

$$\mathrm{M}_L = (\sigma_O - \sigma_{CG})S_{steel} \quad \text{Eq. 5.12}$$

$$\mathrm{M}_u = \left(\frac{E_{slab}I_{slab}}{E_{steel}I_{steel}}\right)M_L \quad \text{Eq. 5.13}$$

$$\mathrm{M}_A = \sigma_{CG}A_{steel}\left(d_{steel} - CG + haunch + \frac{t_{slab}}{2}\right) \quad \text{Eq. 5.14}$$

$$\mathrm{M}_{total} = M_L + M_u + M_A \quad \text{Eq. 5.15}$$

Where:

S_{steel} = section modulus of the steel girder

E_{slab} = modulus of elasticity of concrete

I_{steel} = moment of inertia of the steel girder

A_{steel} = steel cross-sectional area

d_{steel} = depth of steel girder section

haunch = distance between the steel girder and concrete deck

The gage locations were 2*d* (46 inches) away from midspan during testing; therefore, the moments calculated were adjusted to calculate the moments at midspan. The moment calculations for the uncoated steel specimen used centerline to centerline bearing distance of 37 feet, while the galvanized steel specimen used a centerline to centerline bearing distance of 37.5 feet. These values were used to back calculate the applied load using the equation for moment induced by a point load at midspan. The difference in distances between centerline to centerline bearing distances was due to an error in measurement of the specimens. The percent error values between the theoretical and back calculated loads at 92.5 and 93 kip are shown in Tables 5.1 and 5.2 along with the R^2 values for the uncoated steel specimen and the galvanized steel specimen, respectively.

Table 5.1: Least Squares and Percent Error for Uncoated Steel Specimen

Cycle Count	Least Square, R^2	Percent Error, %
0	0.9992	4.056
100,000	0.9992	4.426
200,000	0.9991	2.609
300,000	0.9990	4.643
500,000	0.9990	3.074
700,000	0.9990	3.871
900,000	0.9989	4.226
1,100,000	0.9989	3.988
1,300,000	0.9985	1.530
1,500,000	0.9988	7.052
1,700,000	0.9989	3.781
1,900,000	0.9986	2.524
2,100,000	0.9984	1.630
2,300,000	0.9988	3.688
2,500,000	0.9987	-0.839
2,700,000	0.9982	0.770
2,900,000	0.9988	3.377

Table 5.2: Least Squares and Percent Error for Galvanized Steel Specimen

Cycle Count	Least Square, R^2	Percent Error, %
0	0.9988	7.124
100,000	0.9989	7.301
200,000	0.9988	6.487
300,000	0.9986	4.952
500,000	0.9985	5.417
700,000	0.9987	6.895
900,000	0.9987	7.256
1,100,000	0.9986	7.161
1,300,000	0.9986	6.176
1,500,000	0.9988	6.323
1,700,000	0.9987	5.872
1,900,000	0.9987	6.260
2,100,000	0.9987	5.601
2,300,000	0.9989	5.105
2,500,000	0.9987	6.471
2,700,000	0.9989	5.645
2,900,000	0.9984	6.011

Tables 5.3 through 5.19 summarize the moments induced into the uncoated steel specimen during each static test. In addition, Figures 5.1 through 5.17 show the plots of the theoretical load versus the experimentally calculated values. Tables 5.20 through 5.36 and Figures 5.18 through 5.34 summarize the same information for the galvanized steel specimen. Figures 5.1 through 5.36 show the theoretical load applied and the actual load induced in the system are very close and linear in nature. The theoretical load is the load the actuator applied into the entire structural system, including the girder and frame. The experimental loads are calculated using strains obtained in the tub girder systems. A small portion of the load deflected the structural frame, which explains the discrepancies between the experimental and theoretical loads.

Table 5.3: Load Test Summary at 0 Cycles

Load Test Summary (N = 0)			
Applied Load, P (kip)	Moment @ Gage Loc. (ft-kip)	Moment @ Midspan (ft-kip)	Back-Calc. Appl. Load (kip)
0	0	0	0
9.25	85.15	107.41	11.61
18.50	148.72	187.59	20.28
27.75	211.03	266.18	28.78
37.00	273.46	344.93	37.29
46.25	336.16	424.01	45.84
55.50	398.49	502.64	54.34
64.75	460.94	581.41	62.86
74.00	523.88	660.80	71.44
83.25	586.44	739.72	79.97
92.50	650.82	820.92	88.75

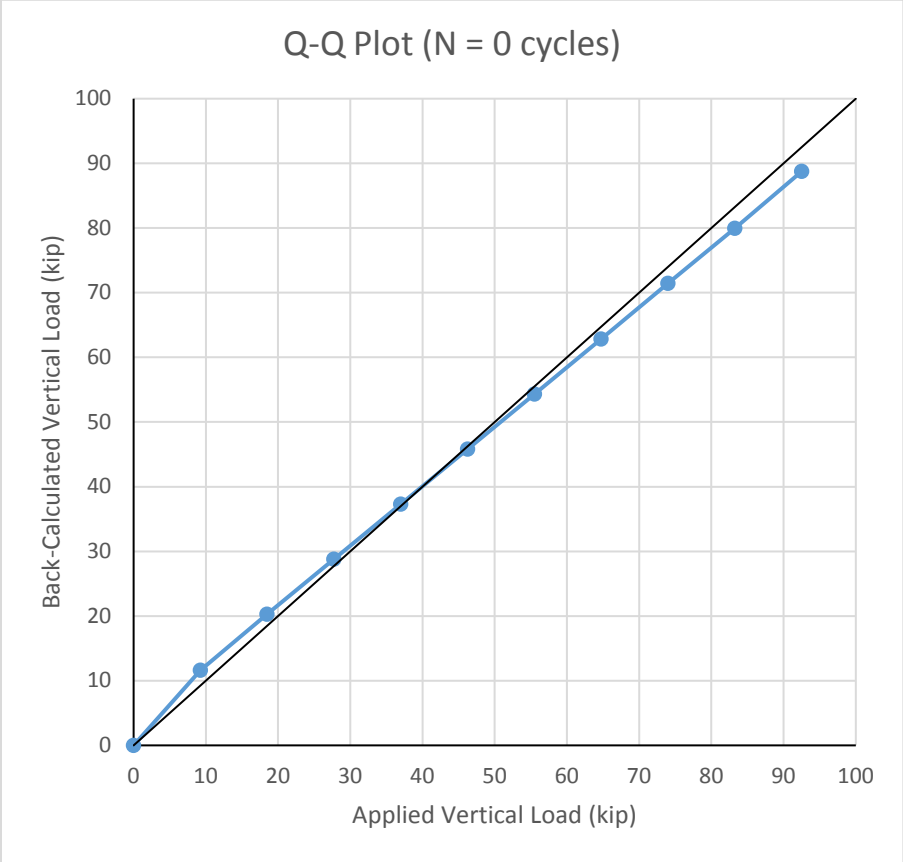

Figure 5.1: Experimental vs. Theoretical Loads at 0 Cycles

Table 5.4: Load Test Summary at 100,000 Cycles

Load Test Summary (N = 100,000)			
Applied Load, P (kip)	Moment @ Gage Loc. (ft-kip)	Moment @ Midspan (ft-kip)	Back-Calc. Appl. Load (kip)
0	0	0	0
9.25	84.65	106.77	11.54
18.50	147.93	186.60	20.17
27.75	210.77	265.86	28.74
37.00	273.41	344.87	37.28
46.25	335.71	423.45	45.78
55.50	398.04	502.07	54.28
64.75	460.80	581.24	62.84
74.00	522.75	659.38	71.28
83.25	585.27	738.23	79.81
92.50	648.31	817.76	88.41

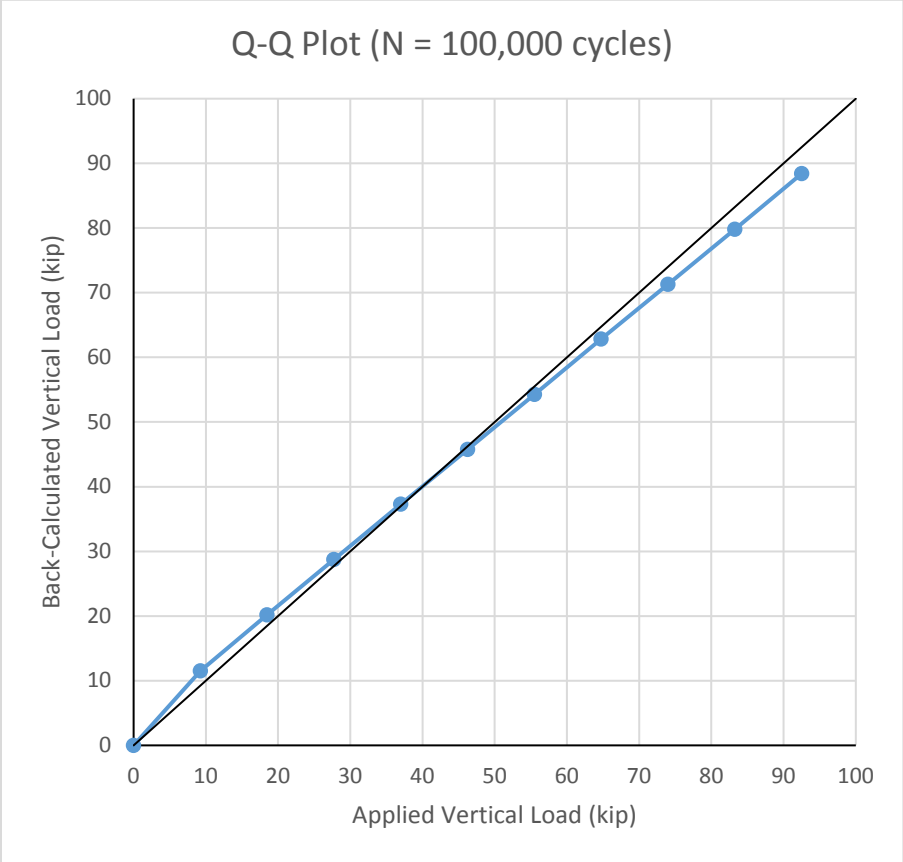

Figure 5.2: Experimental vs. Theoretical Loads at 100,000 Cycles

Table 5.5: Load Test Summary at 200,000 Cycles

Load Test Summary (N =200,000)			
Applied Load, P (kip)	Moment @ Gage Loc. (ft-kip)	Moment @ Midspan (ft-kip)	Back-Calc. Appl. Load (kip)
0	0	0	0
9.25	88.04	111.05	12.01
18.50	151.81	191.48	20.70
27.75	214.97	271.15	29.31
37.00	278.98	351.89	38.04
46.25	344.18	434.14	46.93
55.50	407.67	514.22	55.59
64.75	470.81	593.86	64.20
74.00	534.18	673.80	72.84
83.25	597.24	753.34	81.44
92.50	660.63	833.30	90.09

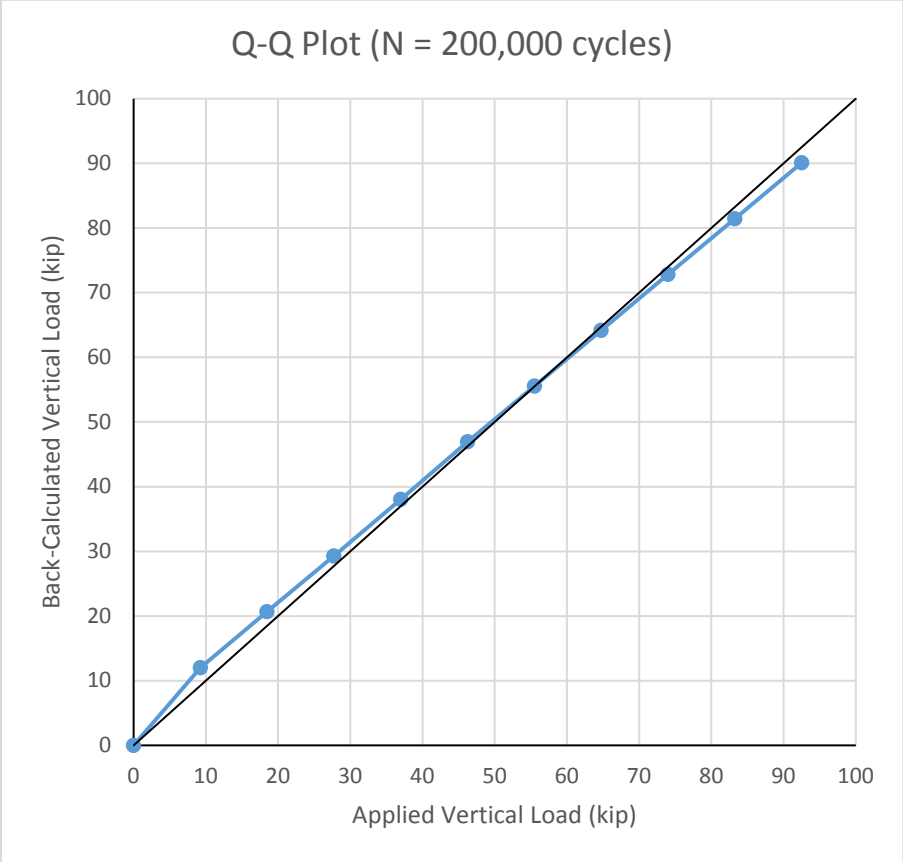

Figure 5.3: Experimental vs. Theoretical Loads at 200,000 Cycles

Table 5.6: Load Test Summary at 300,000 Cycles

Load Test Summary (N = 300,000 Cycles)			
Applied Load, P (kip)	Moment @ Gage Loc. (ft-kip)	Moment @ Midspan (ft-kip)	Back-Calc. Appl. Load (kip)
0	0	0	0
9.25	87.32	110.14	11.91
18.50	150.75	190.15	20.56
27.75	214.20	270.18	29.21
37.00	277.76	350.36	37.88
46.25	339.96	428.82	46.36
55.50	402.84	508.13	54.93
64.75	465.56	587.24	63.48
74.00	527.73	665.66	71.96
83.25	590.44	744.76	80.51
92.50	652.99	823.66	89.04

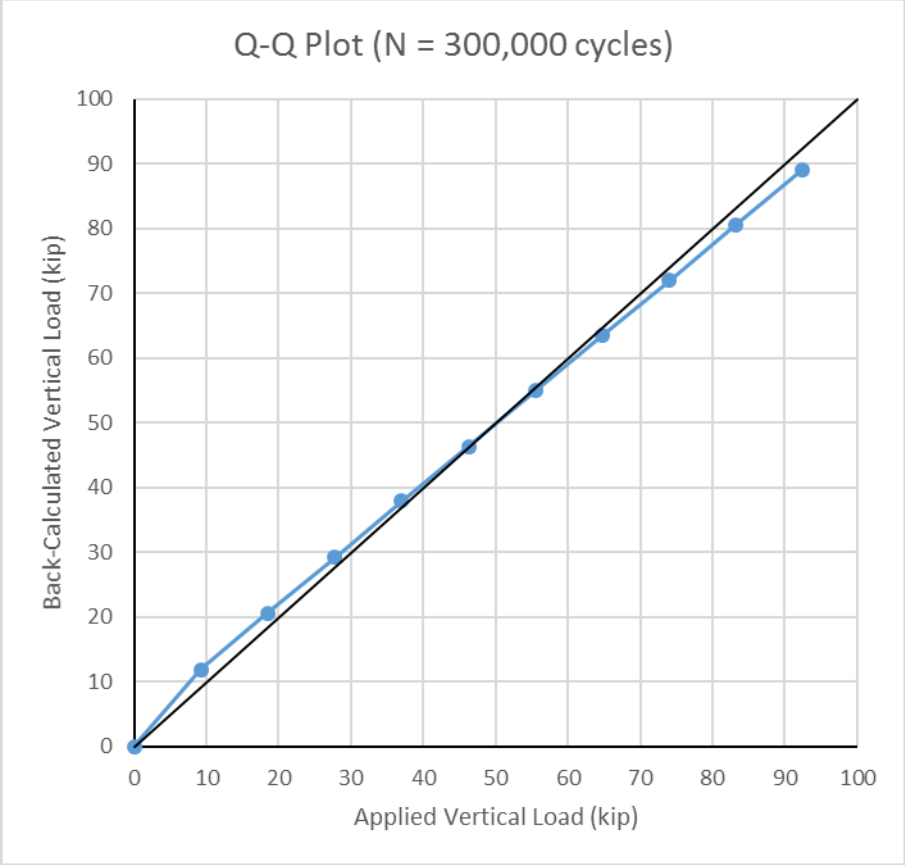

Figure 5.4: Experimental vs. Theoretical Loads at 300,000 Cycles

Table 5.7: Load Test Summary at 500,000 Cycles

Load Test Summary (N = 500,000)			
Applied Load, P (kip)	Moment @ Gage Loc. (ft-kip)	Moment @ Midspan (ft-kip)	Back-Calc. Appl. Load (kip)
0	0	0	0
9.25	87.59	110.48	11.94
18.50	151.76	191.43	20.69
27.75	216.09	272.57	29.47
37.00	279.25	352.23	38.08
46.25	342.43	431.93	46.70
55.50	405.45	511.42	55.29
64.75	468.14	590.50	63.84
74.00	531.68	670.64	72.50
83.25	594.02	749.28	81.00
92.50	657.48	829.32	89.66

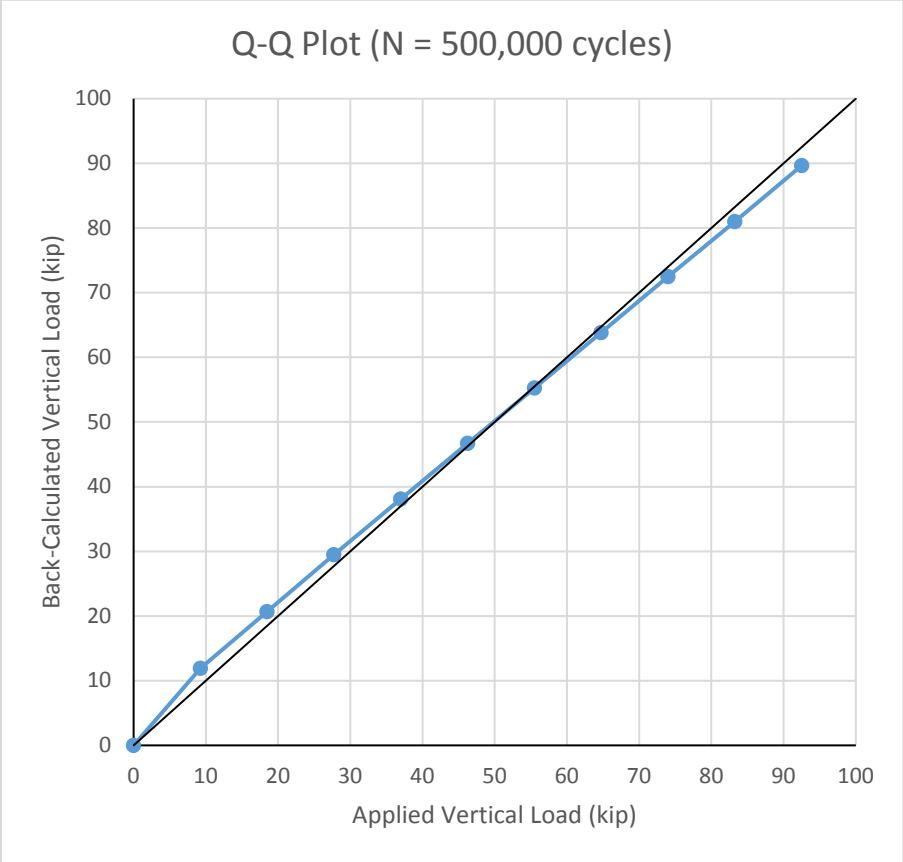

Figure 5.5: Experimental vs. Theoretical Loads at 500,000 Cycles

Table 5.8: Load Test Summary at 700,000 Cycles

Load Test Summary (N = 700,000)			
Applied Load, P (kip)	Moment @ Gage Loc. (ft-kip)	Moment @ Midspan (ft-kip)	Back-Calc. Appl. Load (kip)
0	0	0	0
9.25	87.92	110.90	11.99
18.50	152.70	192.61	20.82
27.75	217.19	273.96	29.62
37.00	280.44	353.74	38.24
46.25	343.62	433.43	46.86
55.50	406.18	512.34	55.39
64.75	468.99	591.56	63.95
74.00	531.32	670.19	72.45
83.25	594.36	749.70	81.05
92.50	657.22	828.99	89.62

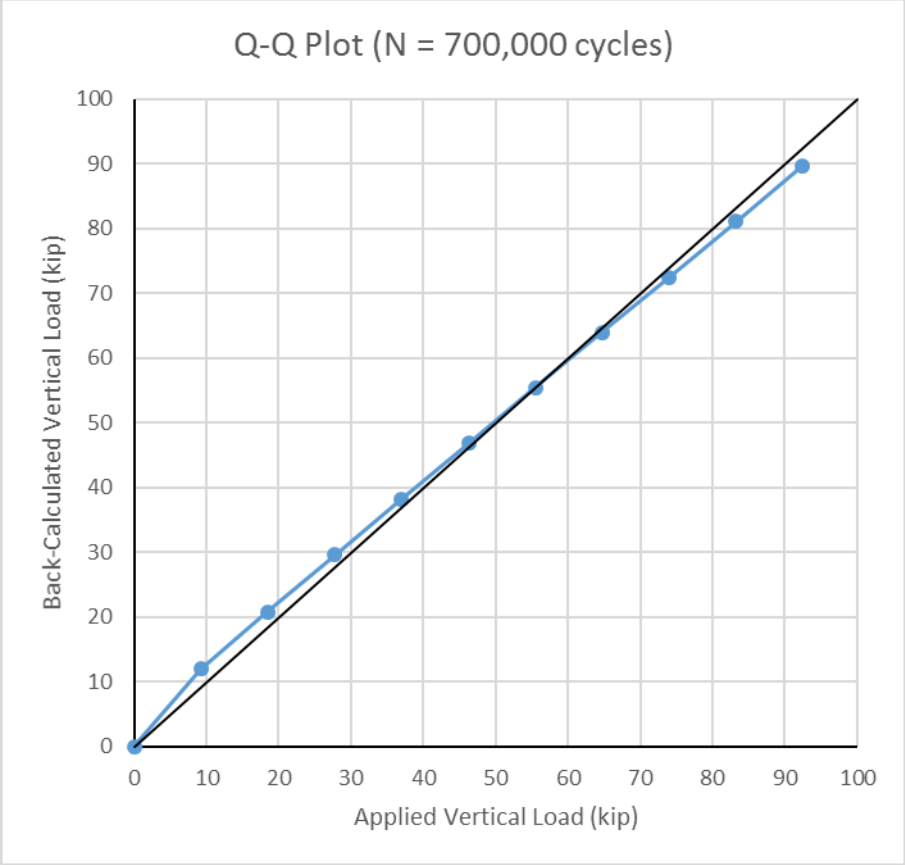

Figure 5.6: Experimental vs. Theoretical Loads at 700,000 Cycles

Table 5.9: Load Test Summary at 900,000 Cycles

Load Test Summary (N = 900,000)			
Applied Load, P (kip)	Moment @ Gage Loc. (ft-kip)	Moment @ Midspan (ft-kip)	Back-Calc. Appl. Load (kip)
0	0	0	0
9.25	88.65	111.82	12.09
18.50	153.48	193.60	20.93
27.75	217.25	274.04	29.63
37.00	280.34	353.61	38.23
46.25	342.89	432.51	46.76
55.50	405.61	511.62	55.31
64.75	467.93	590.23	63.81
74.00	529.75	668.21	72.24
83.25	592.73	747.64	80.83
92.50	654.89	826.05	89.30

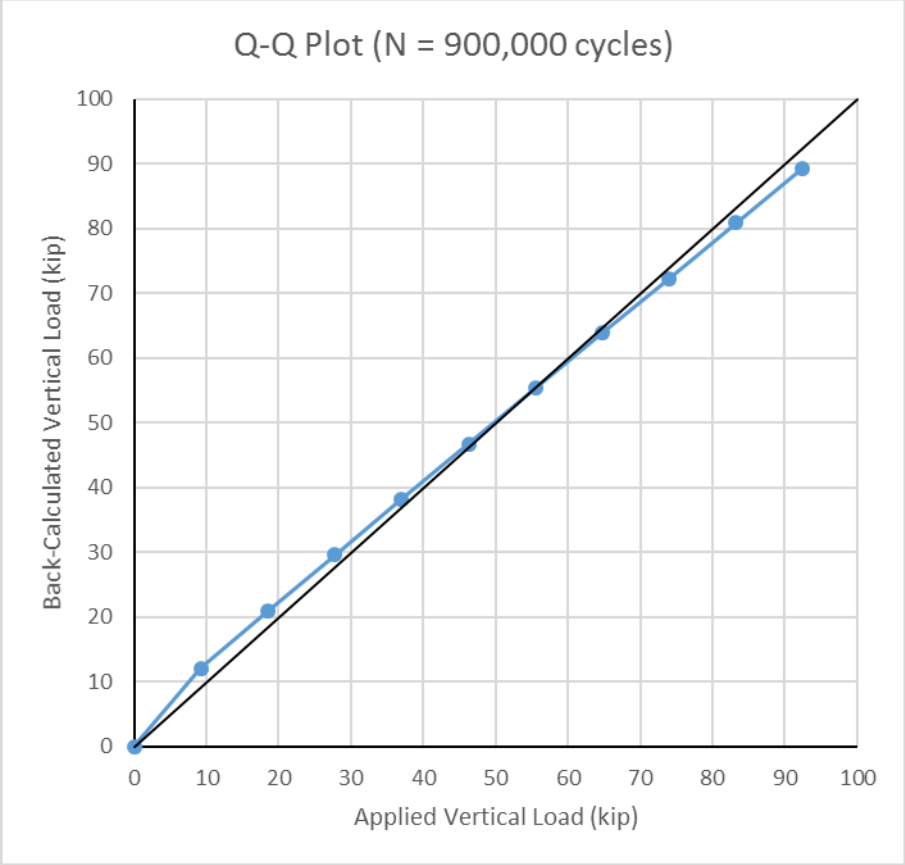

Figure 5.7: Experimental vs. Theoretical Loads at 900,000 Cycles

Table 5.10: Load Test Summary at 1,100,000 Cycles

Load Test Summary (N = 1,100,000)			
Applied Load, P (kip)	Moment @ Gage Loc. (ft-kip)	Moment @ Midspan (ft-kip)	Back-Calc. Appl. Load (kip)
0	0	0	0
9.25	89.36	112.71	12.19
18.50	154.06	194.32	21.01
27.75	218.54	275.66	29.80
37.00	282.12	355.85	38.47
46.25	345.33	435.59	47.09
55.50	408.33	515.05	55.68
64.75	471.42	594.63	64.28
74.00	534.63	674.36	72.90
83.25	597.53	753.70	81.48
92.50	660.70	833.38	90.10

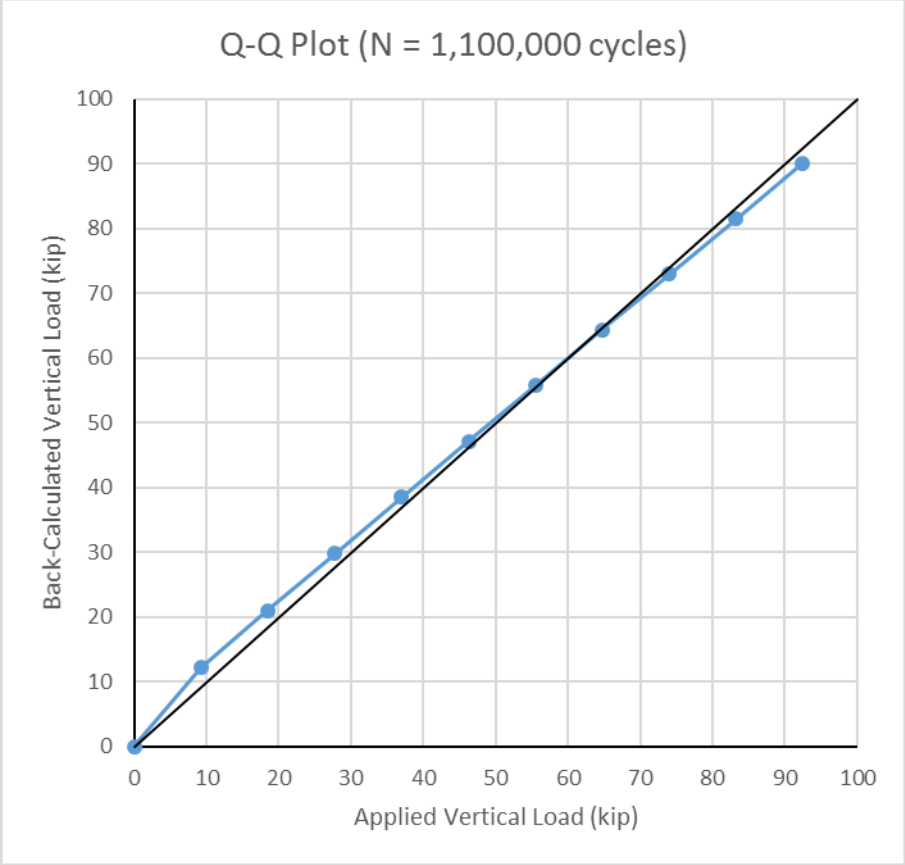

Figure 5.8: Experimental vs. Theoretical Loads at 1,100,000 Cycles

Table 5.11: Load Test Summary at 1,300,000 Cycles

Load Test Summary (N = 1,300,000)			
Applied Load, P (kip)	Moment @ Gage Loc. (ft-kip)	Moment @ Midspan (ft-kip)	Back-Calc. Appl. Load (kip)
0	0	0	0
9.25	91.94	115.97	12.54
18.50	156.91	197.92	21.40
27.75	221.41	279.28	30.19
37.00	286.05	360.82	39.01
46.25	350.02	441.50	47.73
55.50	413.01	520.95	56.32
64.75	476.38	600.88	64.96
74.00	540.05	681.20	73.64
83.25	605.15	763.31	82.52
92.50	668.45	843.16	91.15

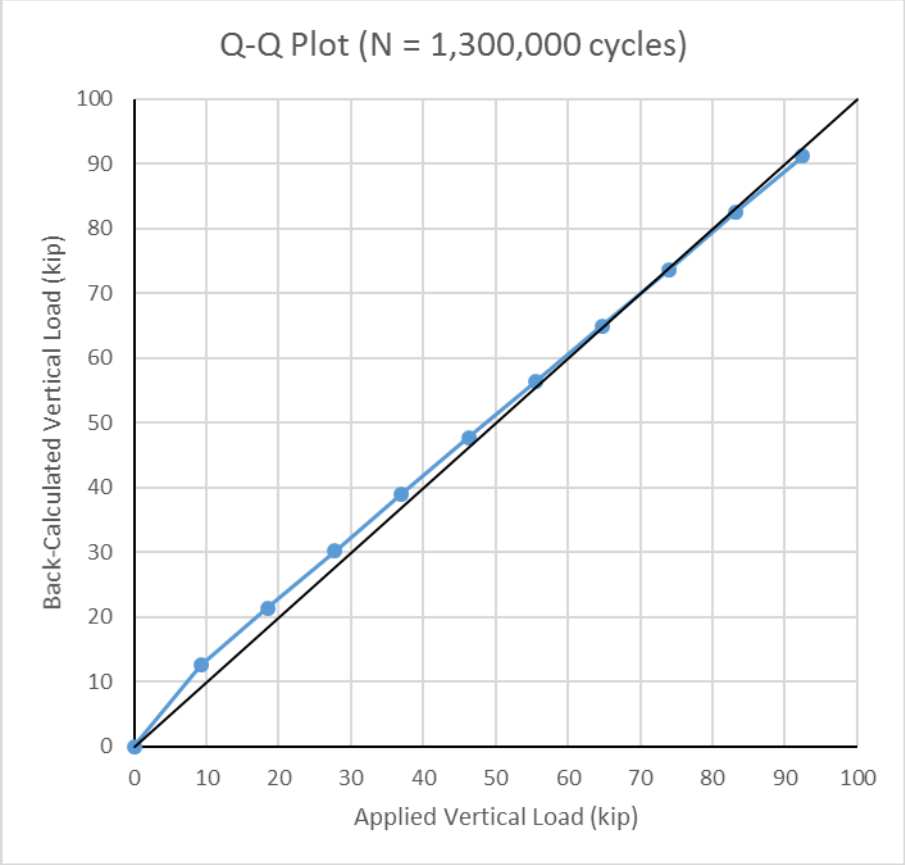

Figure 5.9: Experimental vs. Theoretical Loads at 1,300,000 Cycles

Table 5.12: Load Test Summary at 1,500,000 Cycles

Load Test Summary (N = 1,500,000)			
Applied Load, P (kip)	Moment @ Gage Loc. (ft-kip)	Moment @ Midspan (ft-kip)	Back-Calc. Appl. Load (kip)
0	0	0	0
9.25	87.65	110.56	11.95
18.50	152.23	192.02	20.76
27.75	216.82	273.49	29.57
37.00	280.70	354.07	38.28
46.25	344.09	434.02	46.92
55.50	406.97	513.34	55.50
64.75	469.76	592.54	64.06
74.00	532.75	671.99	72.65
83.25	595.79	751.51	81.24
92.50	658.52	830.64	89.80

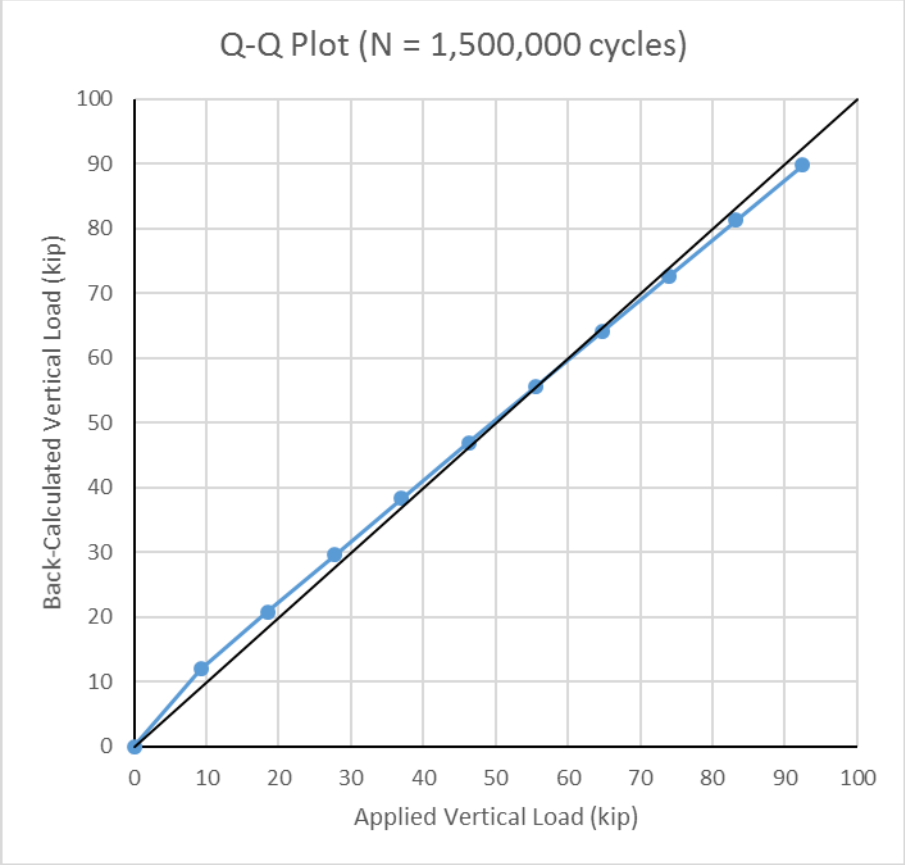

Figure 5.10: Experimental vs. Theoretical Loads at 1,500,000 Cycles

Table 5.13: Load Test Summary at 1,700,000 Cycles

Load Test Summary (N = 1,700,000)			
Applied Load, P (kip)	Moment @ Gage Loc. (ft-kip)	Moment @ Midspan (ft-kip)	Back-Calc. Appl. Load (kip)
0	0	0	0
9.25	86.70	109.36	11.82
18.50	152.14	191.90	20.75
27.75	216.26	272.79	29.49
37.00	280.20	353.43	38.21
46.25	343.37	433.11	46.82
55.50	406.80	513.12	55.47
64.75	469.34	592.01	64.00
74.00	532.62	671.83	72.63
83.25	596.57	752.49	81.35
92.50	659.78	832.23	89.97

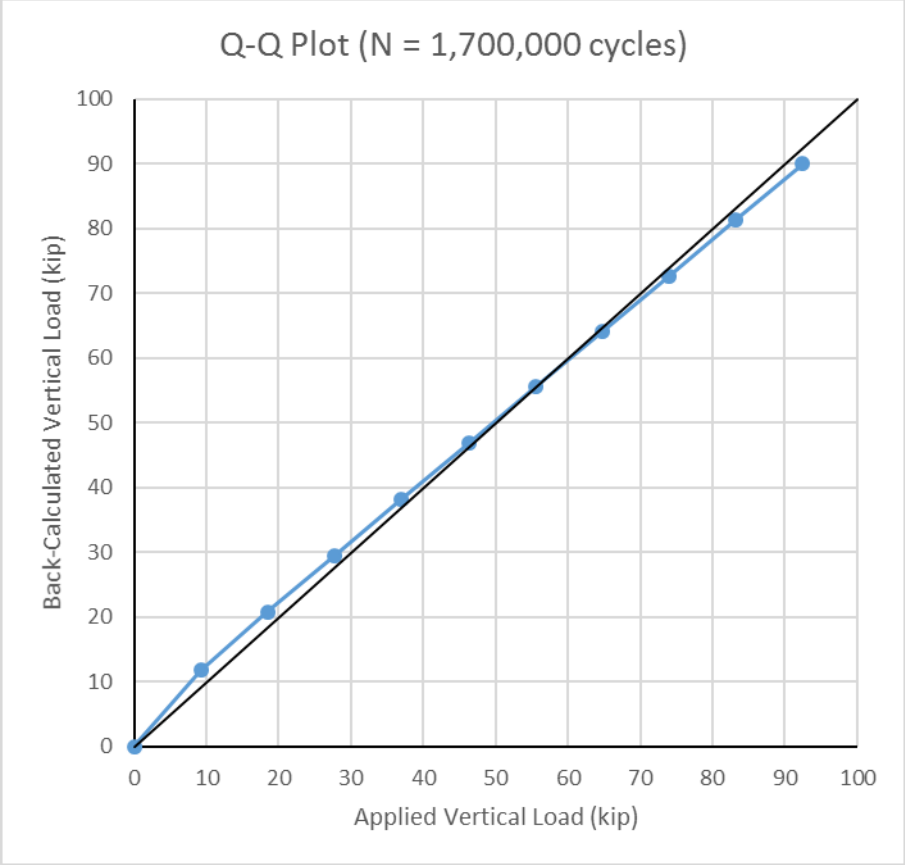

Figure 5.11: Experimental vs. Theoretical Loads at 1,700,000 Cycles

Table 5.14: Load Test Summary at 1,900,000 Cycles

Load Test Summary (N = 1,900,000)			
Applied Load, P (kip)	Moment @ Gage Loc. (ft-kip)	Moment @ Midspan (ft-kip)	Back-Calc. Appl. Load (kip)
0	0	0	0
9.25	91.87	115.89	12.53
18.50	157.12	198.19	21.43
27.75	221.73	279.68	30.24
37.00	286.02	360.77	39.00
46.25	349.88	441.32	47.71
55.50	413.29	521.31	56.36
64.75	476.88	601.52	65.03
74.00	540.35	681.58	73.68
83.25	603.87	761.70	82.35
92.50	667.48	841.93	91.02

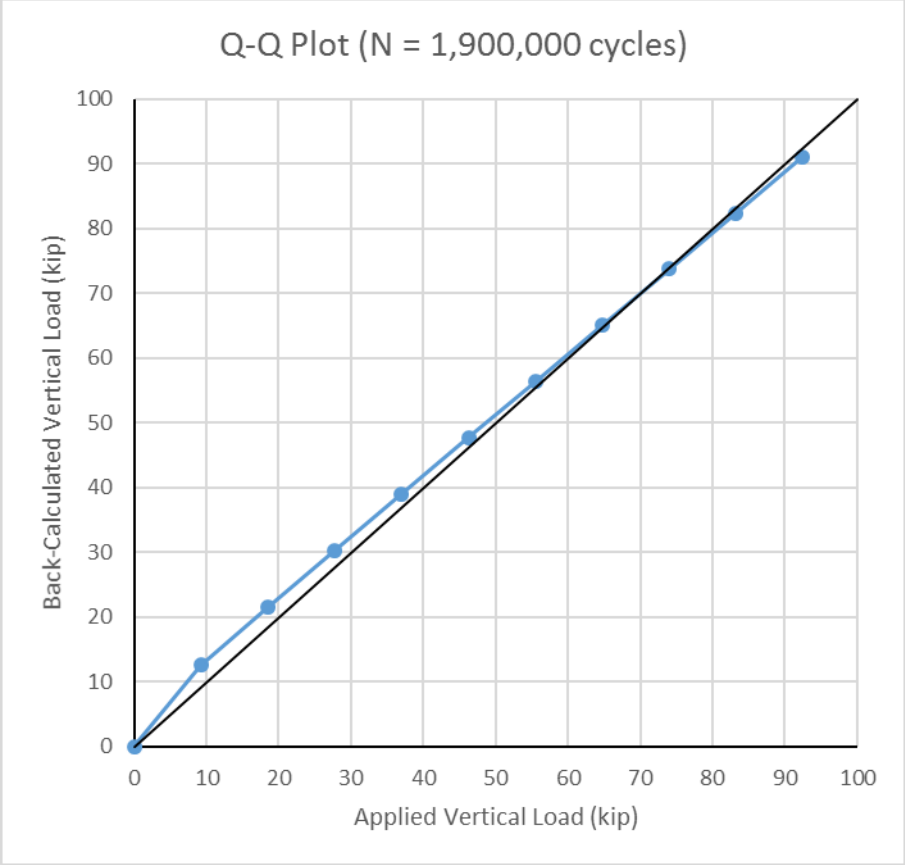

Figure 5.12: Experimental vs. Theoretical Loads at 1,900,000 Cycles

Table 5.15: Load Test Summary at 2,100,000 Cycles

Load Test Summary (N = 2,100,000)			
Applied Load, P (kip)	Moment @ Gage Loc. (ft-kip)	Moment @ Midspan (ft-kip)	Back-Calc. Appl. Load (kip)
0	0	0	0
9.25	91.47	115.38	12.47
18.50	157.18	198.26	21.43
27.75	221.54	279.45	30.21
37.00	285.78	360.48	38.97
46.25	349.65	441.04	47.68
55.50	413.19	521.18	56.34
64.75	477.01	601.68	65.05
74.00	540.38	681.62	73.69
83.25	604.29	762.23	82.40
92.50	667.28	841.68	90.99

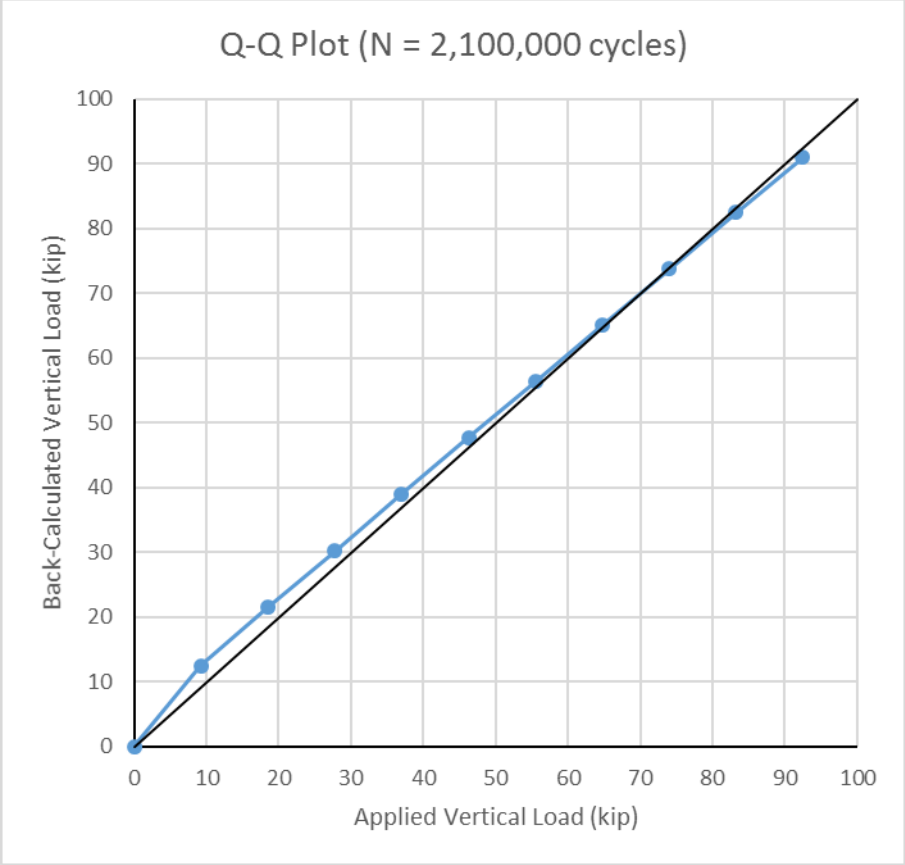

Figure 5.13: Experimental vs. Theoretical Loads at 2,100,000 Cycles

Table 5.16: Load Test Summary at 2,300,000 Cycles

Load Test Summary (N = 2,300,000)			
Applied Load, P (kip)	Moment @ Gage Loc. (ft-kip)	Moment @ Midspan (ft-kip)	Back-Calc. Appl. Load (kip)
0	0	0	0
9.25	88.44	111.56	12.06
18.50	153.01	193.00	20.86
27.75	216.79	273.45	29.56
37.00	280.25	353.49	38.22
46.25	342.97	432.61	46.77
55.50	404.78	510.58	55.20
64.75	466.95	588.99	63.67
74.00	529.13	667.42	72.15
83.25	591.70	746.35	80.69
92.50	653.31	824.07	89.09

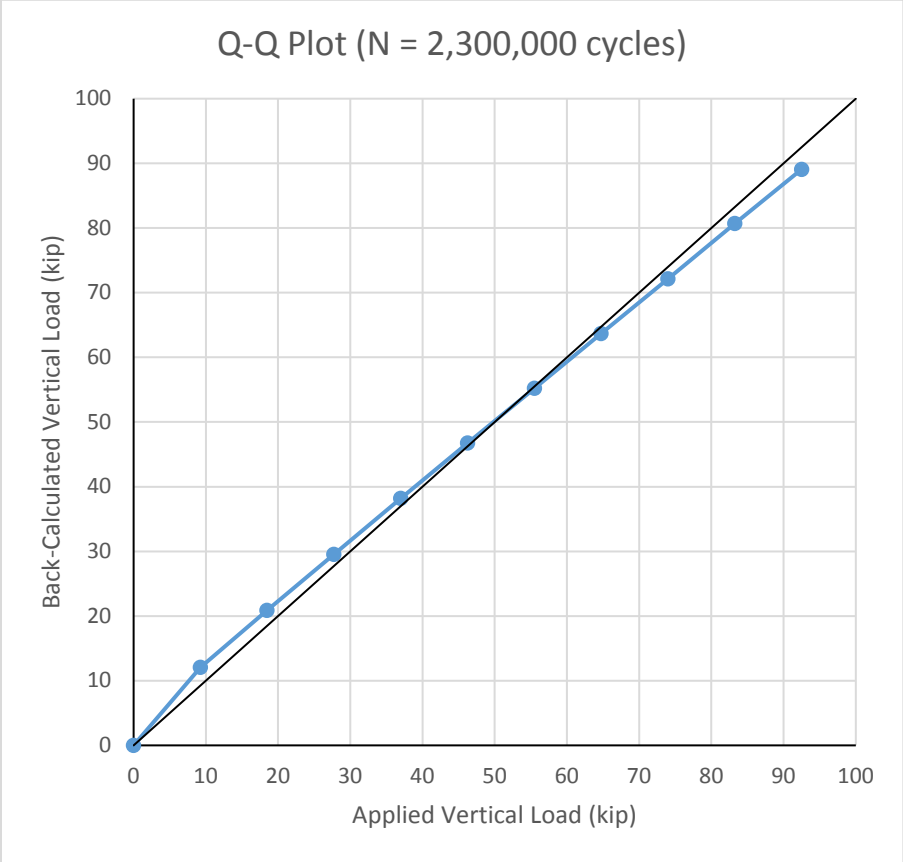

Figure 5.14: Experimental vs. Theoretical Loads at 2,300,000 Cycles

Table 5.17: Load Test Summary at 2,500,000 Cycles

Load Test Summary (N = 2,500,000)			
Applied Load, P (kip)	Moment @ Gage Loc. (ft-kip)	Moment @ Midspan (ft-kip)	Back-Calc. Appl. Load (kip)
0	0	0	0
9.25	93.79	118.30	12.79
18.50	161.37	203.54	22.00
27.75	227.65	287.15	31.04
37.00	293.69	370.45	40.05
46.25	359.17	453.04	48.98
55.50	424.46	535.40	57.88
64.75	489.26	617.14	66.72
74.00	554.15	698.99	75.57
83.25	619.19	781.02	84.44
92.50	684.03	862.81	93.28

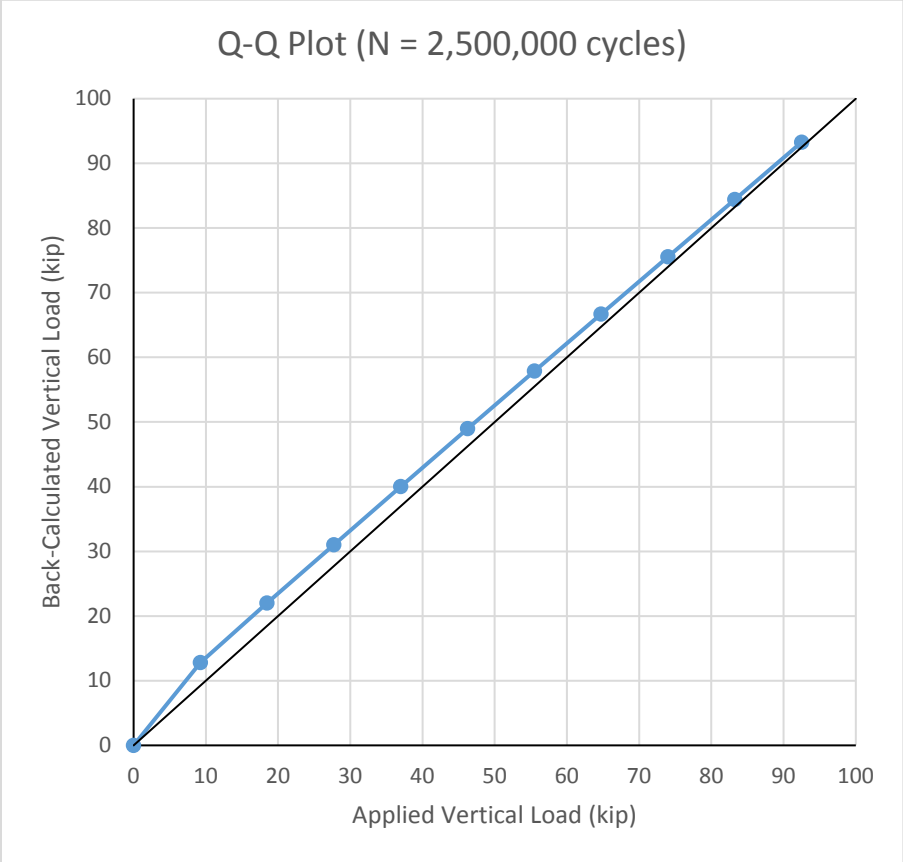

Figure 5.15: Experimental vs. Theoretical Loads at 2,500,000 Cycles

Table 5.18: Load Test Summary at 2,700,000 Cycles

Load Test Summary (N = 2,700,000)			
Applied Load, P (kip)	Moment @ Gage Loc. (ft-kip)	Moment @ Midspan (ft-kip)	Back-Calc. Appl. Load (kip)
0	0	0	0
9.25	94.29	118.94	12.86
18.50	161.68	203.93	22.05
27.75	228.04	287.65	31.10
37.00	294.22	371.12	40.12
46.25	359.32	453.24	49.00
55.50	424.78	535.81	57.93
64.75	489.87	617.90	66.80
74.00	555.12	700.21	75.70
83.25	620.19	782.28	84.57
92.50	685.36	864.48	93.46

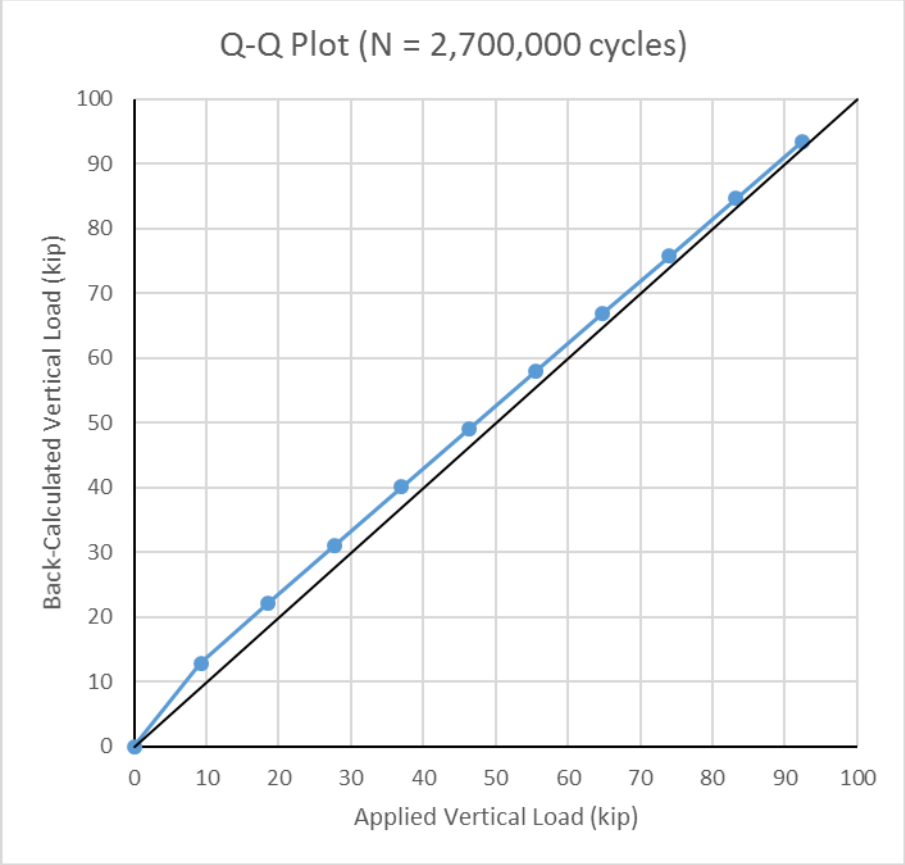

Figure 5.16: Experimental vs. Theoretical Loads at 2,700,000 Cycles

Table 5.19: Load Test Summary at 2,900,000 Cycles

Load Test Summary (N = 2,900,000)			
Applied Load, P (kip)	Moment @ Gage Loc. (ft-kip)	Moment @ Midspan (ft-kip)	Back-Calc. Appl. Load (kip)
0	0	0	0
9.25	95.57	120.55	13.03
18.50	163.33	206.02	22.27
27.75	229.89	289.98	31.35
37.00	295.84	373.17	40.34
46.25	361.70	456.23	49.32
55.50	426.29	537.71	58.13
64.75	491.33	619.75	67.00
74.00	556.22	701.60	75.85
83.25	621.27	783.65	84.72
92.50	686.50	865.93	93.61

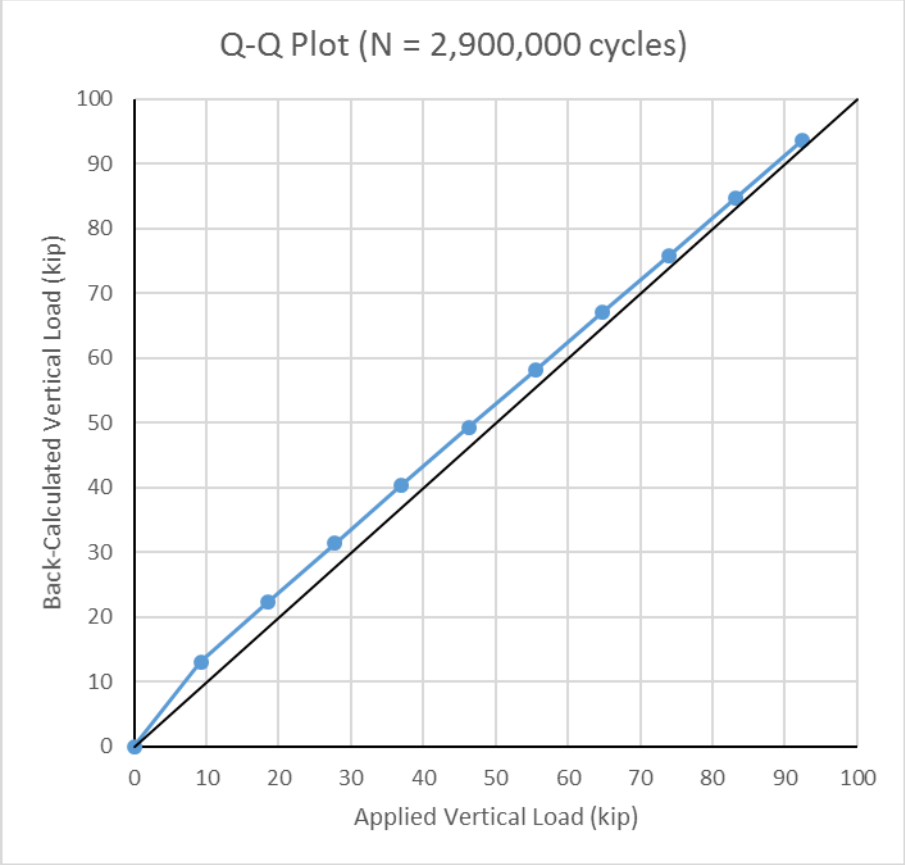

Figure 5.17: Experimental vs. Theoretical Loads at 2,900,000 Cycles

Table 5.20: Load Test Summary at 0 Cycles

Load Test Summary (N = 0)			
Applied Load, P (kip)	Moment @ Gage Loc. (ft-kip)	Moment @ Midspan (ft-kip)	Back-Calc. Appl. Load (kip)
0	0	0	0
9.30	87.09	109.46	11.68
18.60	150.41	189.07	20.17
27.90	213.07	267.83	28.57
37.20	275.23	345.96	36.90
46.50	337.87	424.70	45.30
55.80	399.56	502.24	53.57
65.10	460.86	579.30	61.79
74.40	521.94	656.07	69.98
83.70	583.02	732.85	78.17
93.00	644.21	809.76	86.37

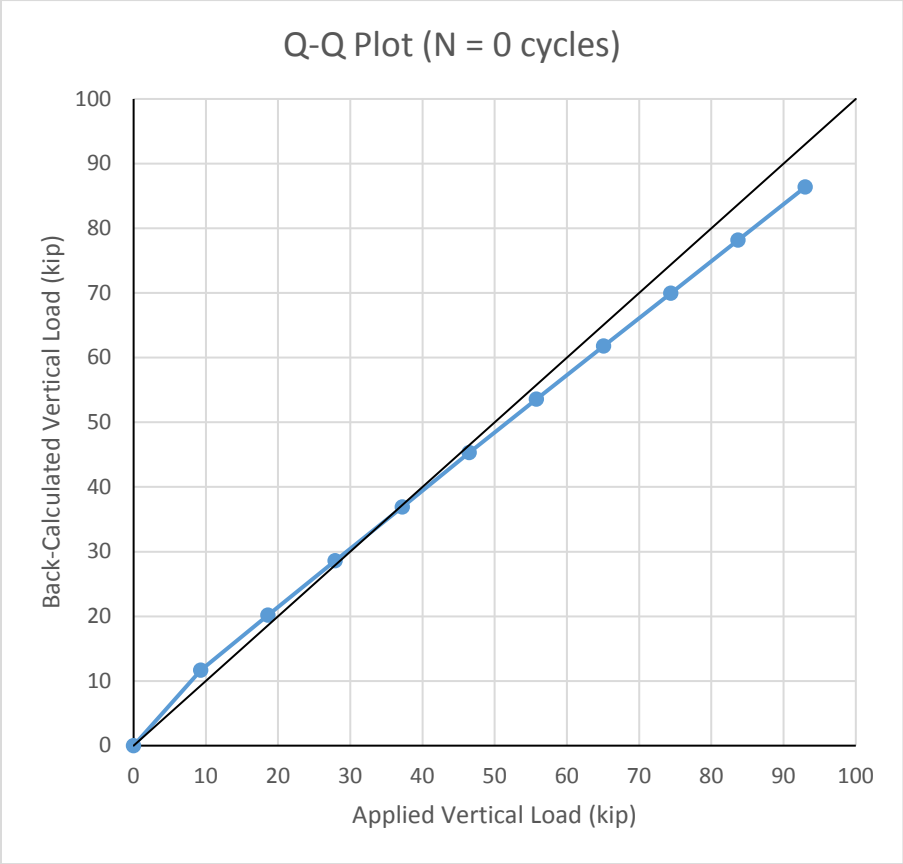

Figure 5.18: Experimental vs. Theoretical Loads at 0 Cycles

Table 5.21: Load Test Summary at 100,000 Cycles

Load Test Summary (N = 100,000)			
Applied Load, P (kip)	Moment @ Gage Loc. (ft-kip)	Moment @ Midspan (ft-kip)	Back-Calc. Appl. Load (kip)
0	0	0	0
9.30	86.41	108.62	11.59
18.60	149.13	187.45	20.00
27.90	211.95	266.42	28.42
37.20	274.23	344.70	36.77
46.50	336.41	422.86	45.11
55.80	398.24	500.58	53.39
65.10	459.17	577.17	61.56
74.40	520.52	654.29	69.79
83.70	581.87	731.40	78.02
93.00	642.98	808.22	86.21

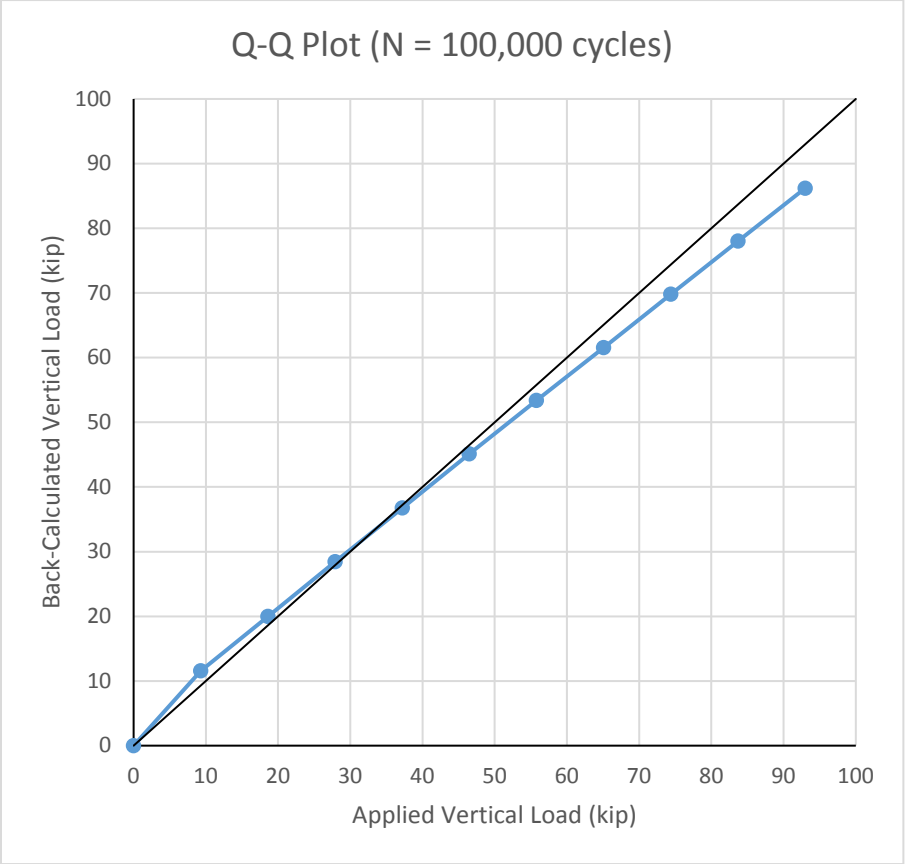

Figure 5.19: Experimental vs. Theoretical Loads at 100,000 Cycles

Table 5.22: Load Test Summary at 200,000 Cycles

Load Test Summary (N = 200,000)			
Applied Load, P (kip)	Moment @ Gage Loc. (ft-kip)	Moment @ Midspan (ft-kip)	Back-Calc. Appl. Load (kip)
0	0	0	0
9.30	86.58	108.83	11.61
18.60	149.37	187.76	20.03
27.90	211.49	265.83	28.36
37.20	273.37	343.62	36.65
46.50	335.00	421.08	44.92
55.80	396.87	498.86	53.21
65.10	458.42	576.23	61.46
74.40	520.19	653.86	69.75
83.70	581.49	730.92	77.97
93.00	643.31	808.62	86.25

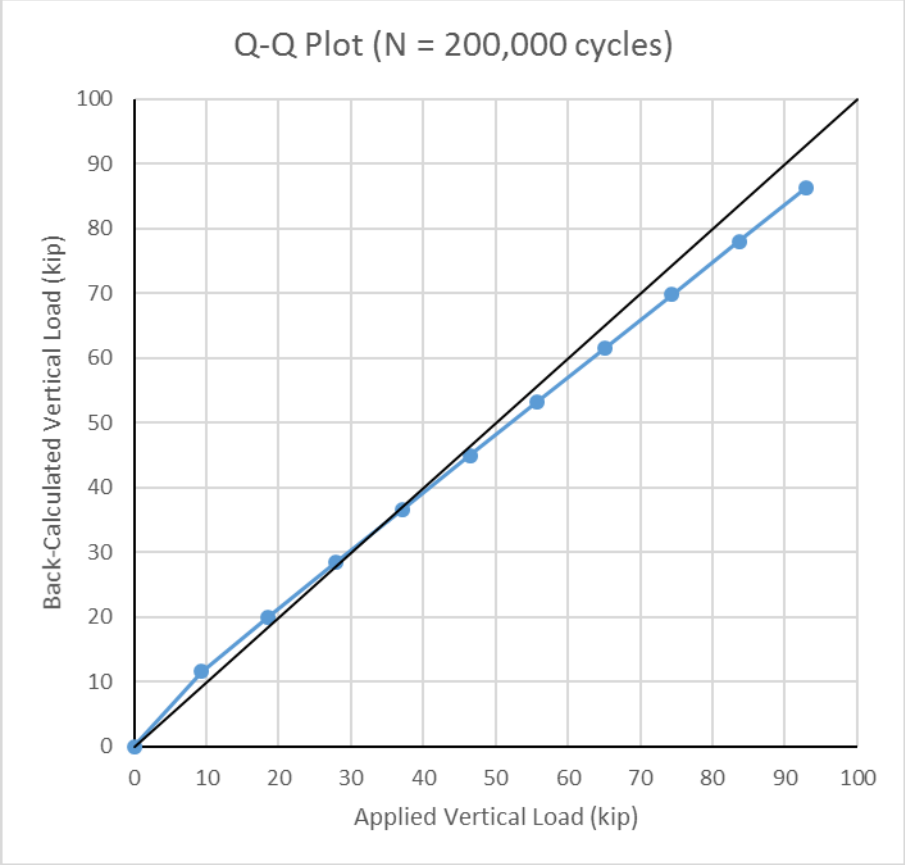

Figure 5.20: Experimental vs. Theoretical Loads at 200,000 Cycles

Table 5.23: Load Test Summary at 300,000 Cycles

Load Test Summary (N = 300,000)			
Applied Load, P (kip)	Moment @ Gage Loc. (ft-kip)	Moment @ Midspan (ft-kip)	Back-Calc. Appl. Load (kip)
0	0	0	0
9.30	88.21	110.88	11.83
18.60	152.69	191.93	20.47
27.90	216.56	272.22	29.04
37.20	279.89	351.82	37.53
46.50	342.88	431.00	45.97
55.80	405.42	509.60	54.36
65.10	467.87	588.11	62.73
74.40	529.73	665.86	71.03
83.70	591.76	743.83	79.34
93.00	653.30	821.19	87.59

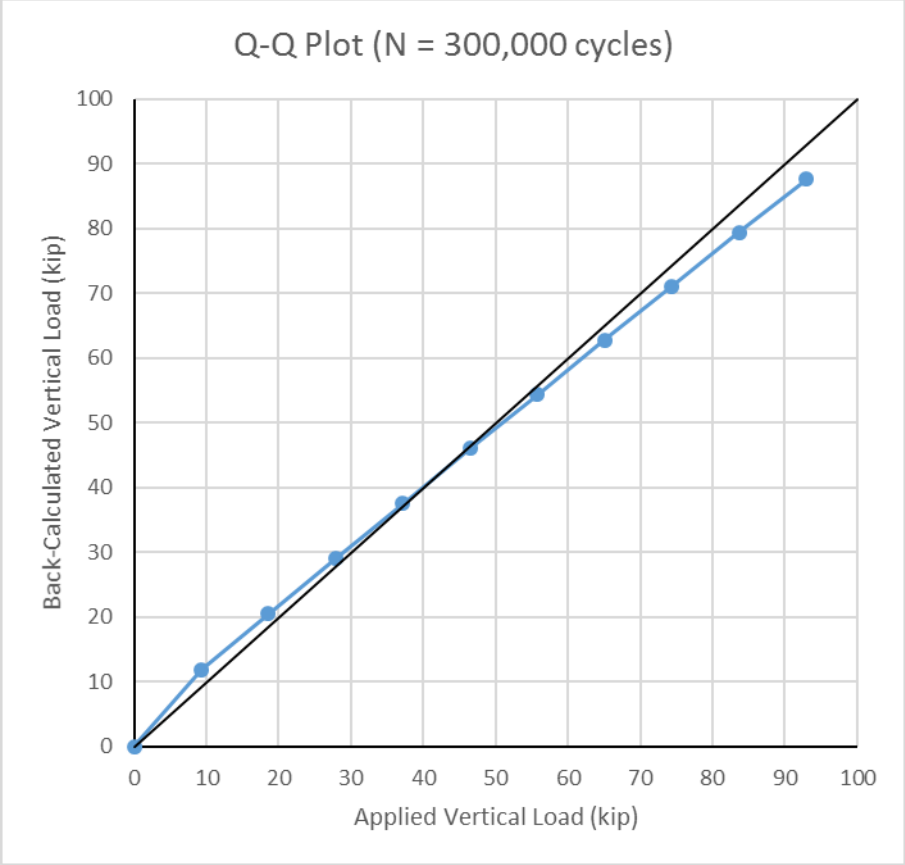

Figure 5.21: Experimental vs. Theoretical Loads at 300,000 Cycles

Table 5.24: Load Test Summary at 500,000 Cycles

Load Test Summary (N = 500,000)			
Applied Load, P (kip)	Moment @ Gage Loc. (ft-kip)	Moment @ Midspan (ft-kip)	Back-Calc. Appl. Load (kip)
0	0	0	0
9.30	88.71	111.51	11.89
18.60	154.18	193.81	20.67
27.90	218.58	274.75	29.31
37.20	281.96	354.42	37.80
46.50	344.61	433.17	46.21
55.80	407.49	512.20	54.64
65.10	469.47	590.11	62.95
74.40	531.78	668.44	71.30
83.70	593.95	746.59	79.64
93.00	655.85	824.39	87.93

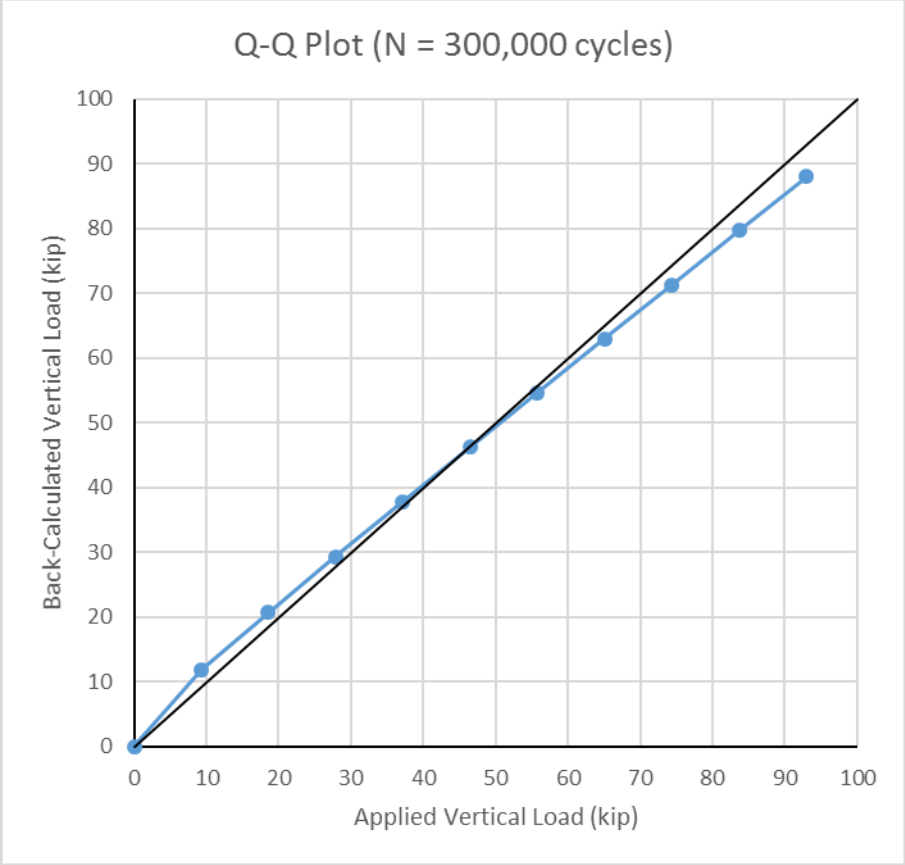

Figure 5.22: Experimental vs. Theoretical Loads at 500,000 Cycles

Table 5.25: Load Test Summary at 700,000 Cycles

Load Test Summary (N = 700,000)			
Applied Load, P (kip)	Moment @ Gage Loc. (ft-kip)	Moment @ Midspan (ft-kip)	Back-Calc. Appl. Load (kip)
0	0	0	0
9.30	88.86	111.70	11.91
18.60	153.27	192.66	20.55
27.90	217.58	273.49	29.17
37.20	281.37	353.67	37.73
46.50	344.20	432.65	46.15
55.80	406.46	510.92	54.50
65.10	468.25	588.59	62.78
74.40	529.60	665.70	71.01
83.70	591.28	743.23	79.28
93.00	652.80	820.56	87.53

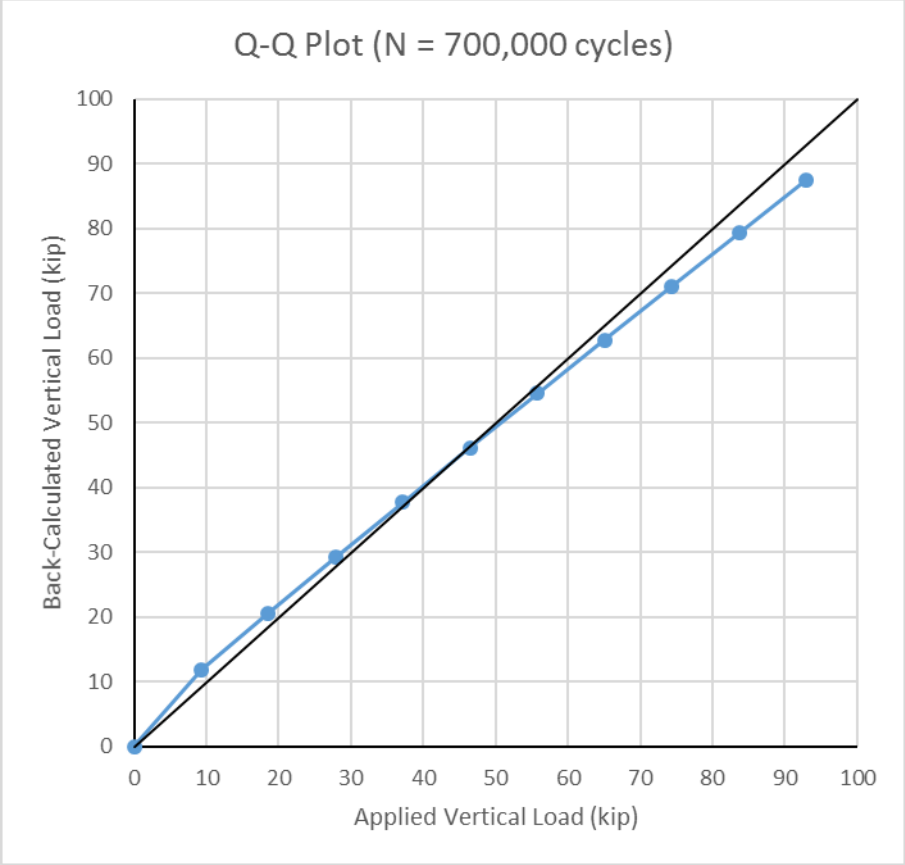

Figure 5.23: Experimental vs. Theoretical Loads at 700,000 Cycles

Table 5.26: Load Test Summary at 900,000 Cycles

Load Test Summary (N = 900,000)			
Applied Load, P (kip)	Moment @ Gage Loc. (ft-kip)	Moment @ Midspan (ft-kip)	Back-Calc. Appl. Load (kip)
0	0	0	0
9.30	88.46	111.19	11.86
18.60	152.89	192.18	20.50
27.90	217.72	273.67	29.19
37.20	280.76	352.92	37.64
46.50	343.24	431.45	46.02
55.80	404.93	508.99	54.29
65.10	466.64	586.55	62.57
74.40	528.36	664.15	70.84
83.70	589.57	741.08	79.05
93.00	650.19	817.28	87.18

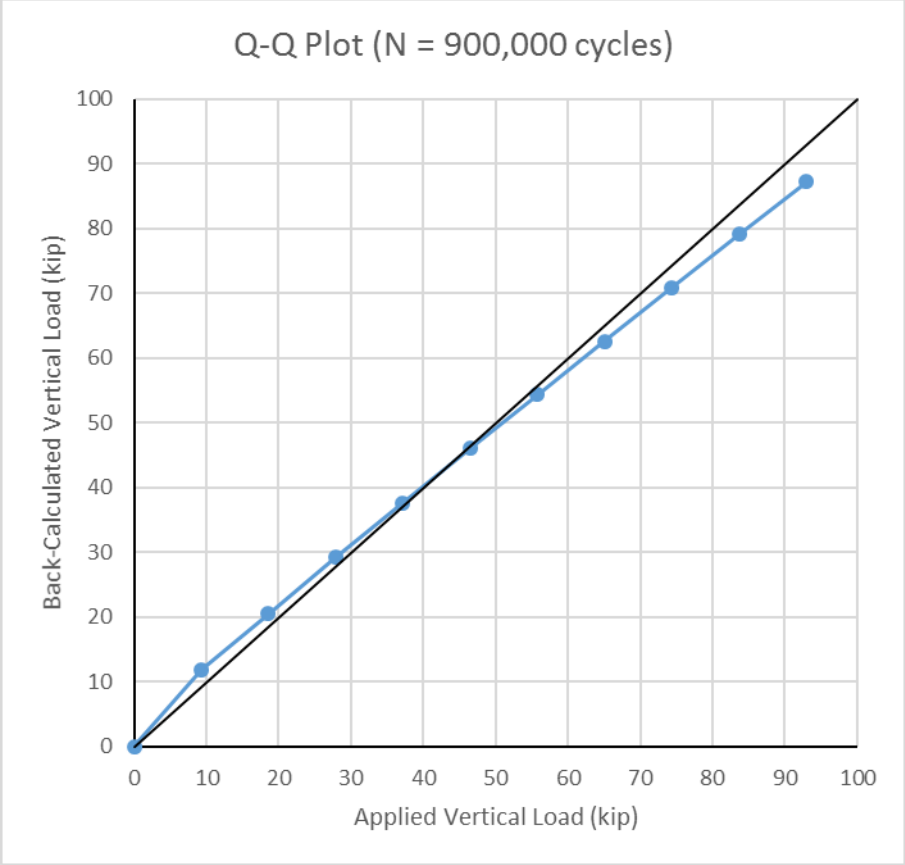

Figure 5.24: Experimental vs. Theoretical Loads at 900,000 Cycles

Table 5.27: Load Test Summary at 1,100,000 Cycles

Load Test Summary (N = 1,100,000)			
Applied Load, P (kip)	Moment @ Gage Loc. (ft-kip)	Moment @ Midspan (ft-kip)	Back-Calc. Appl. Load (kip)
0	0	0	0
9.30	88.88	111.73	11.92
18.60	153.57	193.03	20.59
27.90	218.65	274.84	29.32
37.20	282.11	354.61	37.82
46.50	344.63	433.20	46.21
55.80	406.59	511.08	54.52
65.10	467.93	588.18	62.74
74.40	529.07	665.03	70.94
83.70	589.94	741.54	79.10
93.00	650.74	817.97	87.25

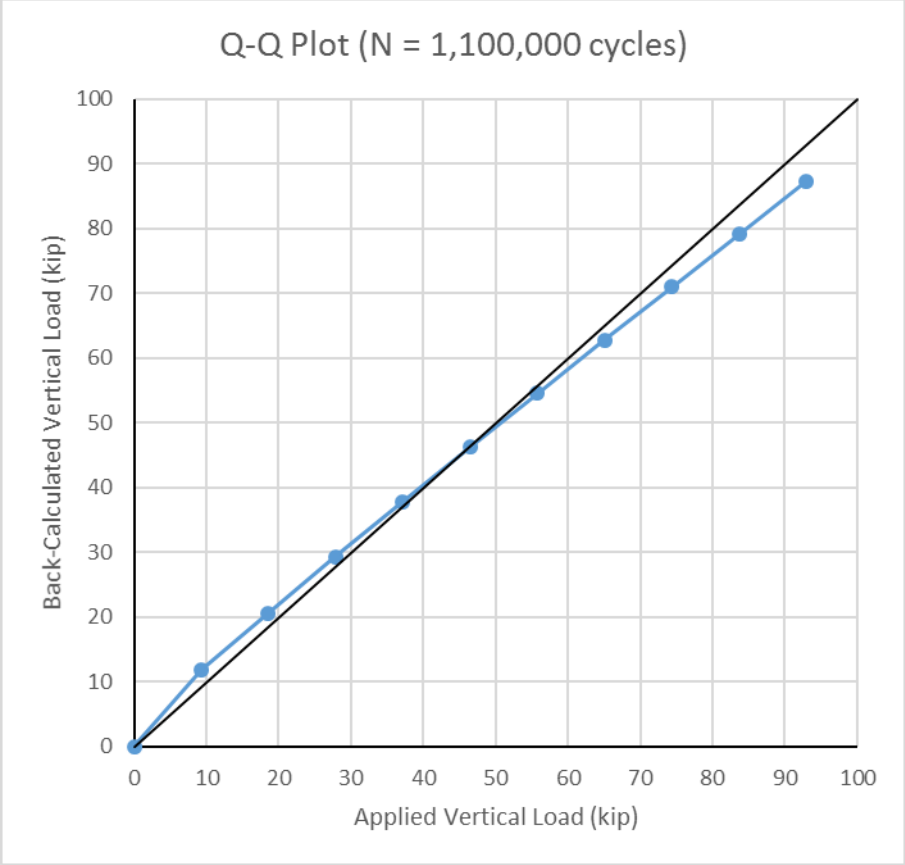

Figure 5.25: Experimental vs. Theoretical Loads at 1,100,000 Cycles

Table 5.28: Load Test Summary at 1,300,000 Cycles

Load Test Summary (N = 1,300,000)			
Applied Load, P (kip)	Moment @ Gage Loc. (ft-kip)	Moment @ Midspan (ft-kip)	Back-Calc. Appl. Load (kip)
0	0	0	0
9.30	89.51	112.52	12.00
18.60	154.91	194.72	20.77
27.90	220.36	276.99	29.55
37.20	284.60	357.73	38.16
46.50	347.74	437.11	46.62
55.80	410.14	515.54	54.99
65.10	472.48	593.90	63.35
74.40	533.99	671.22	71.60
83.70	595.74	748.84	79.88
93.00	656.89	825.70	88.08

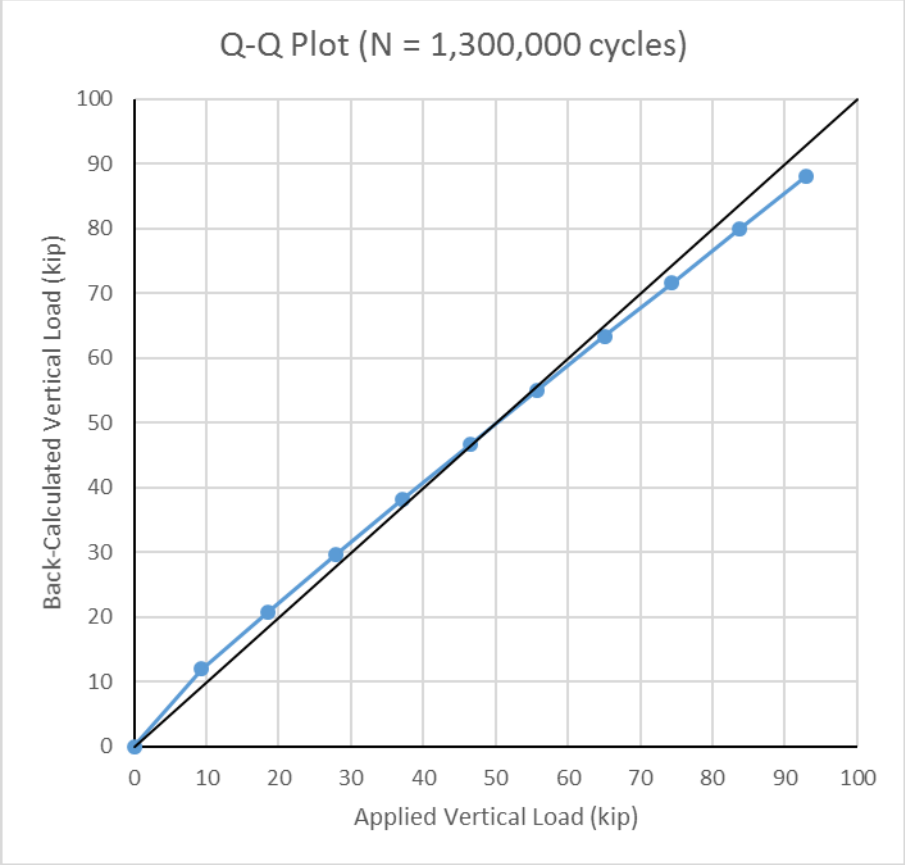

Figure 5.26: Experimental vs. Theoretical Loads at 1,300,000 Cycles

Table 5.29: Load Test Summary at 1,500,000 Cycles

Load Test Summary (N = 1,500,000)			
Applied Load, P (kip)	Moment @ Gage Loc. (ft-kip)	Moment @ Midspan (ft-kip)	Back-Calc. Appl. Load (kip)
0	0	0	0
9.30	89.10	112.00	11.95
18.60	154.73	194.50	20.75
27.90	220.30	276.92	29.54
37.20	284.71	357.88	38.17
46.50	347.74	437.11	46.62
55.80	410.38	515.85	55.02
65.10	472.73	594.21	63.38
74.40	534.72	672.14	71.69
83.70	596.44	749.71	79.97
93.00	658.21	827.36	88.25

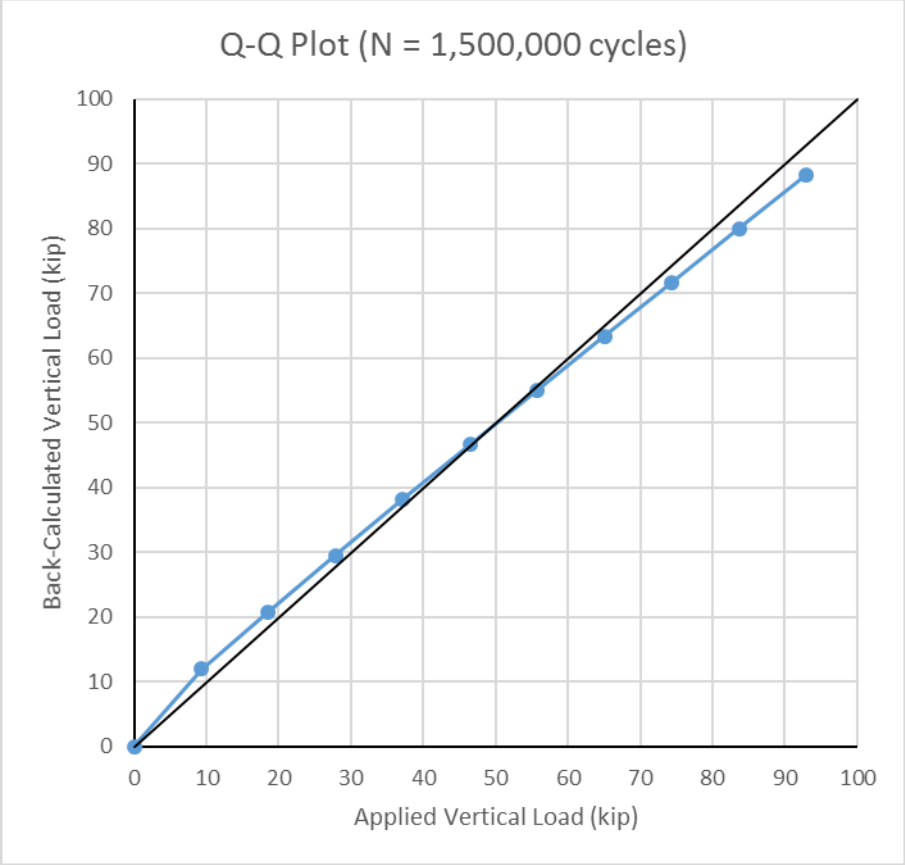

Figure 5.27: Experimental vs. Theoretical Loads at 1,500,000 Cycles

Table 5.30: Load Test Summary at 1,700,000 Cycles

Load Test Summary (N = 1,700,000)			
Applied Load, P (kip)	Moment @ Gage Loc. (ft-kip)	Moment @ Midspan (ft-kip)	Back-Calc. Appl. Load (kip)
0	0	0	0
9.30	89.39	112.36	11.99
18.60	154.79	194.57	20.75
27.90	220.80	277.54	29.60
37.20	285.32	358.64	38.25
46.50	348.69	438.29	46.75
55.80	411.38	517.10	55.16
65.10	473.94	595.74	63.55
74.40	535.58	673.22	71.81
83.70	597.41	750.94	80.10
93.00	659.03	828.39	88.36

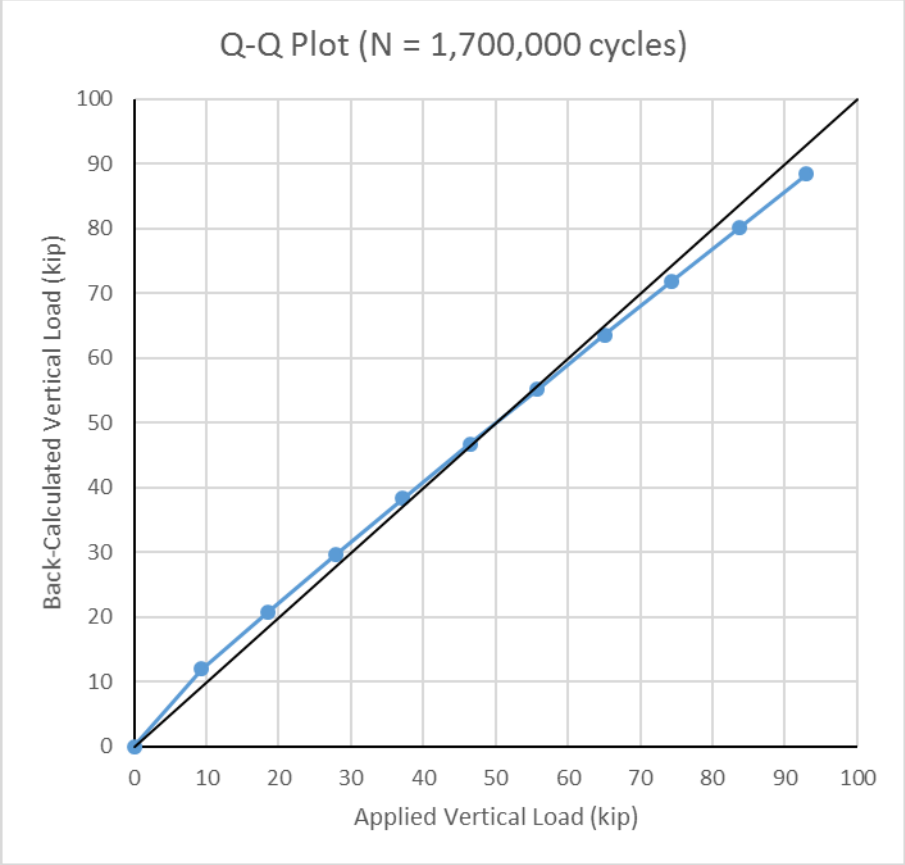

Figure 5.28: Experimental vs. Theoretical Loads at 1,700,000 Cycles

Table 5.31: Load Test Summary at 1,900,000 Cycles

Load Test Summary (N = 1,900,000)			
Applied Load, P (kip)	Moment @ Gage Loc. (ft-kip)	Moment @ Midspan (ft-kip)	Back-Calc. Appl. Load (kip)
0	0	0	0
9.30	90.36	113.58	12.12
18.60	157.05	197.41	21.06
27.90	224.09	281.68	30.05
37.20	289.27	363.61	38.79
46.50	352.96	443.67	47.32
55.80	415.76	522.61	55.74
65.10	477.99	600.82	64.09
74.40	539.70	678.39	72.36
83.70	601.53	756.11	80.65
93.00	662.87	833.21	88.88

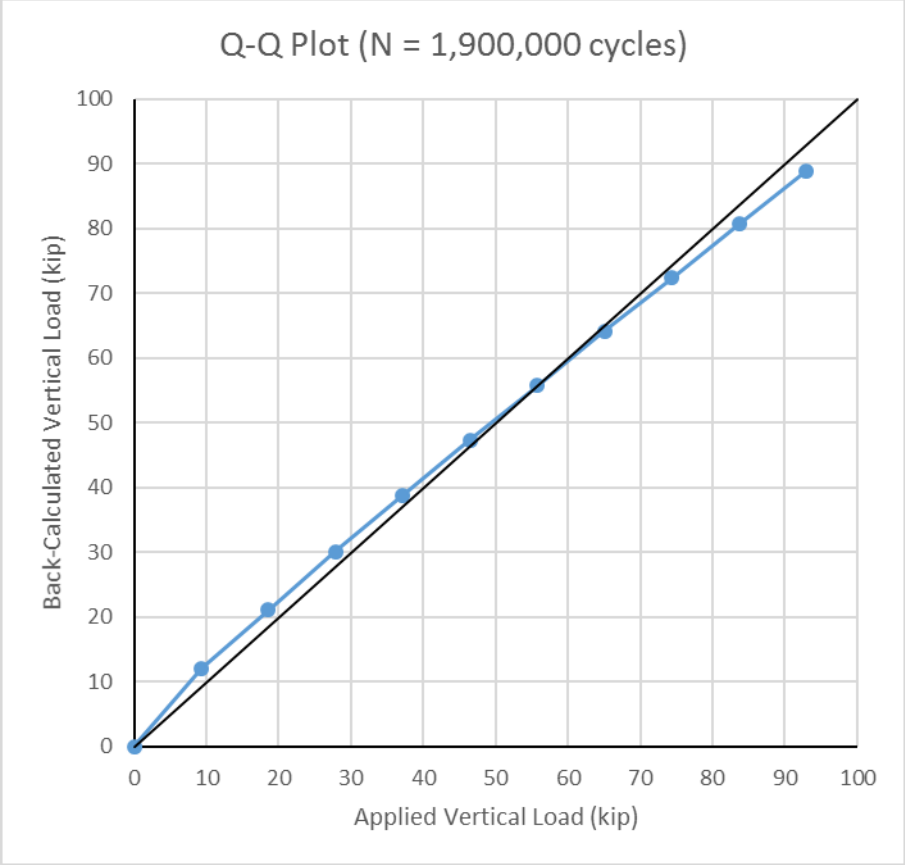

Figure 5.29: Experimental vs. Theoretical Loads at 1,900,000 Cycles

Table 5.32: Load Test Summary at 2,100,000 Cycles

Load Test Summary (N = 2,100,000)			
Applied Load, P (kip)	Moment @ Gage Loc. (ft-kip)	Moment @ Midspan (ft-kip)	Back-Calc. Appl. Load (kip)
0	0	0	0
9.30	89.91	113.01	12.05
18.60	156.43	196.63	20.97
27.90	223.66	281.14	29.99
37.20	289.34	363.69	38.79
46.50	353.11	443.85	47.34
55.80	415.88	522.76	55.76
65.10	478.20	601.09	64.12
74.40	539.67	678.36	72.36
83.70	601.45	756.01	80.64
93.00	662.83	833.17	88.87

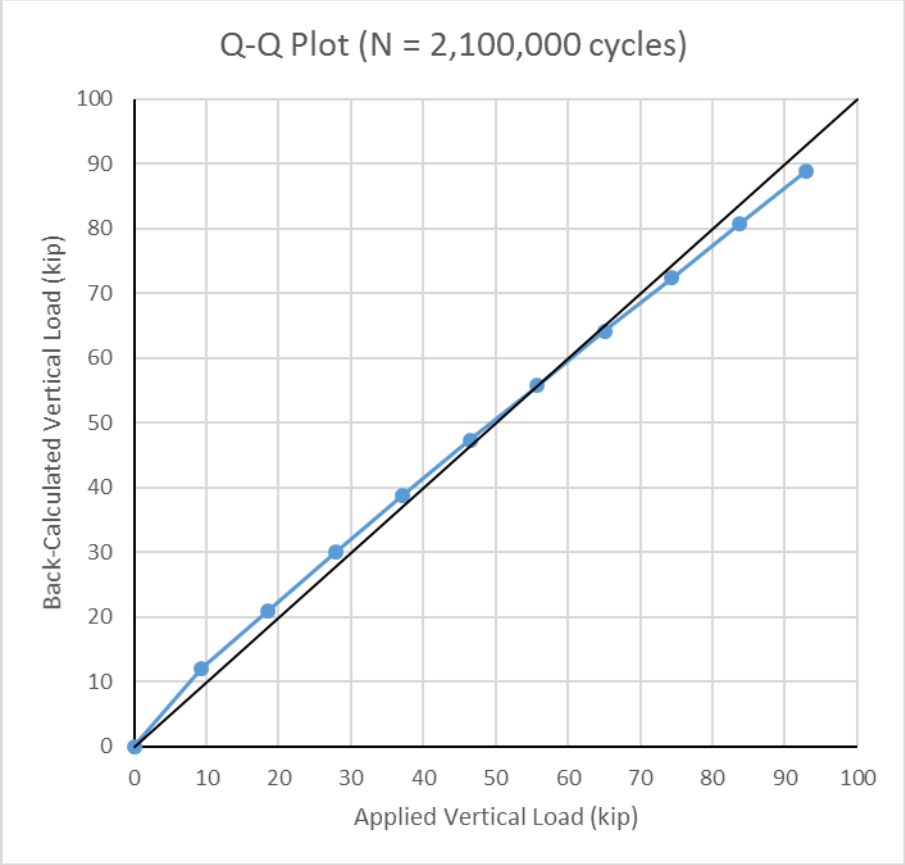

Figure 5.30: Experimental vs. Theoretical Loads at 2,100,000 Cycles

Table 5.33: Load Test Summary at 2,300,000 Cycles

Load Test Summary (N = 2,300,000)			
Applied Load, P (kip)	Moment @ Gage Loc. (ft-kip)	Moment @ Midspan (ft-kip)	Back-Calc. Appl. Load (kip)
0	0	0	0
9.30	89.22	112.15	11.96
18.60	154.16	193.77	20.67
27.90	219.39	275.77	29.42
37.20	284.76	357.93	38.18
46.50	349.43	439.22	46.85
55.80	413.60	519.88	55.45
65.10	477.85	600.65	64.07
74.40	541.84	681.08	72.65
83.70	605.58	761.21	81.20
93.00	669.66	841.76	89.79

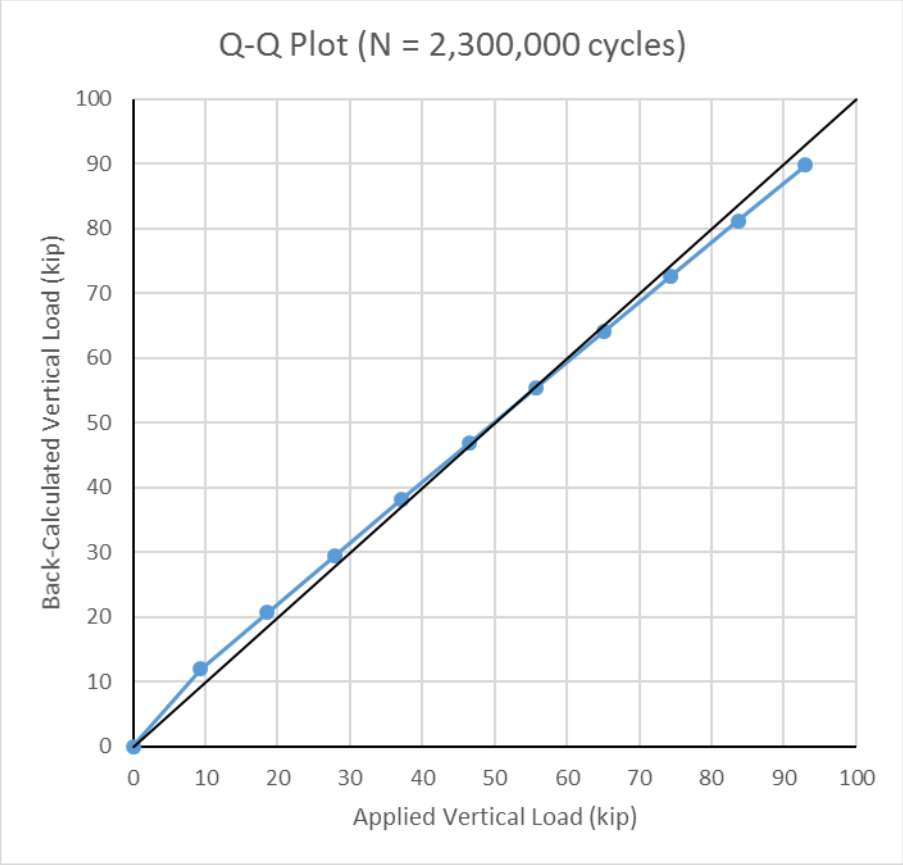

Figure 5.31: Experimental vs. Theoretical Loads at 2,300,000 Cycles

Table 5.34: Load Test Summary at 2,500,000 Cycles

Load Test Summary (N = 2,500,000)			
Applied Load, P (kip)	Moment @ Gage Loc. (ft-kip)	Moment @ Midspan (ft-kip)	Back-Calc. Appl. Load (kip)
0	0	0	0
9.30	89.19	112.11	11.96
18.60	154.14	193.75	20.67
27.90	220.17	276.75	29.52
37.20	285.47	358.83	38.27
46.50	350.26	440.27	46.96
55.80	418.23	525.71	56.08
65.10	479.58	602.83	64.30
74.40	543.49	683.16	72.87
83.70	607.83	764.04	81.50
93.00	671.84	844.49	90.08

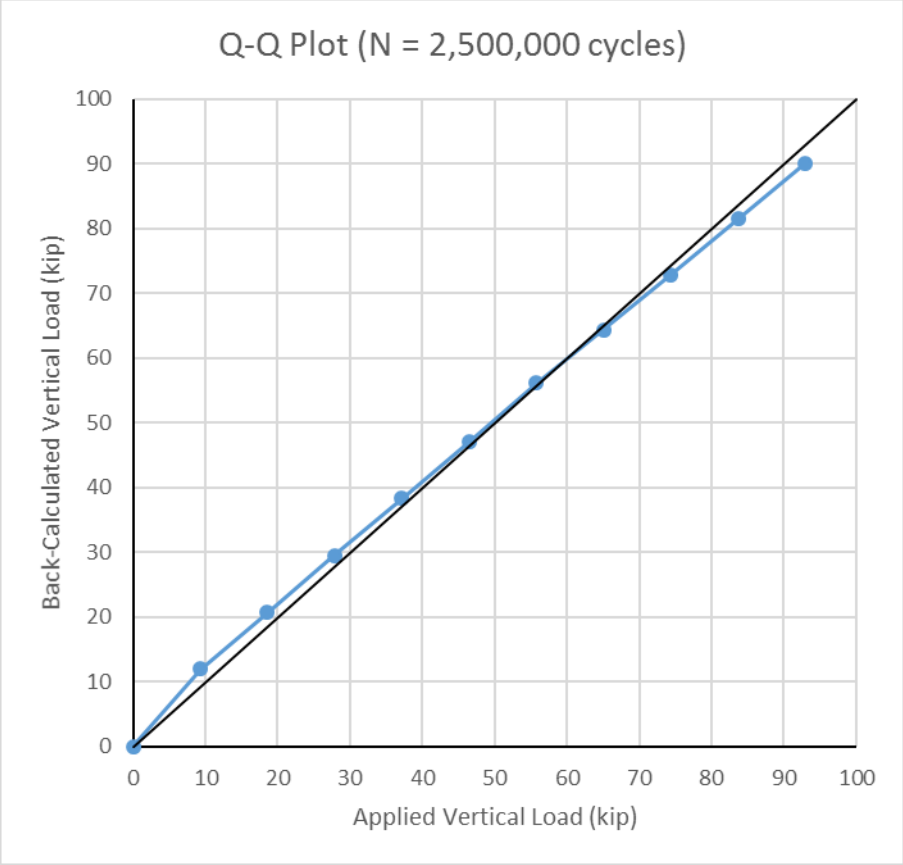

Figure 5.32: Experimental vs. Theoretical Loads at 2,500,000 Cycles

Table 5.35: Load Test Summary at 2,700,000 Cycles

Load Test Summary (N = 2,700,000)			
Applied Load, P (kip)	Moment @ Gage Loc. (ft-kip)	Moment @ Midspan (ft-kip)	Back-Calc. Appl. Load (kip)
0	0	0	0
9.30	89.10	112.00	11.95
18.60	153.71	193.21	20.61
27.90	219.40	275.78	29.42
37.20	284.52	357.64	38.15
46.50	349.50	439.31	46.86
55.80	414.05	520.46	55.52
65.10	478.40	601.34	64.14
74.40	542.47	681.88	72.73
83.70	606.70	762.61	81.35
93.00	670.03	842.22	89.84

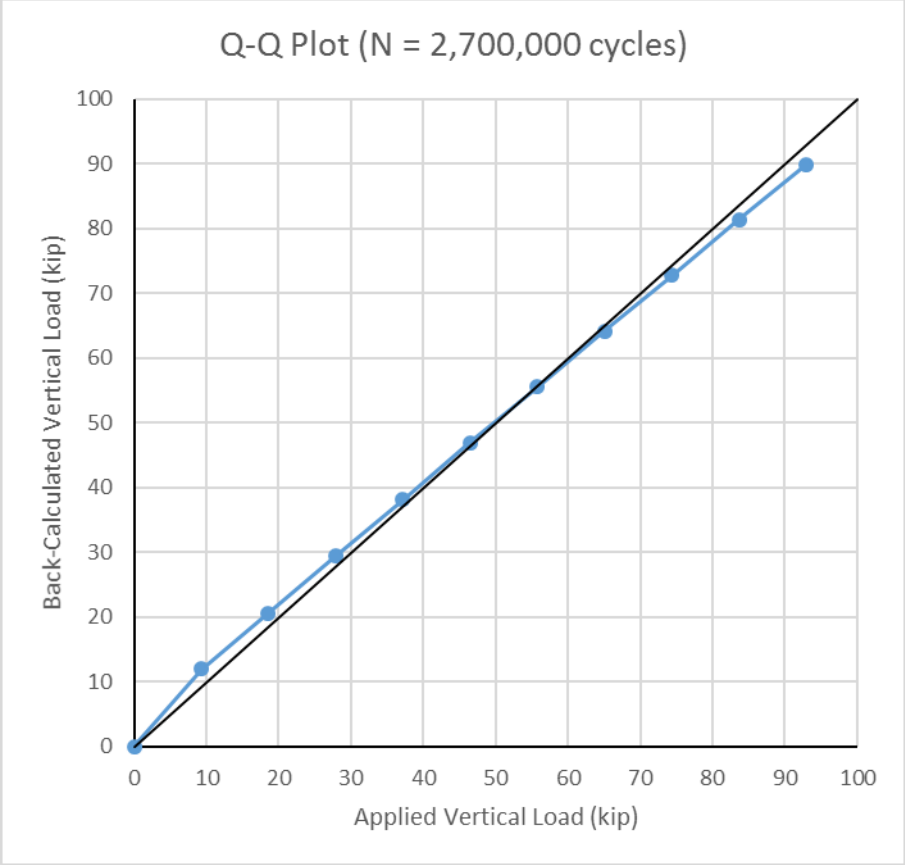

Figure 5.33: Experimental vs. Theoretical Loads at 2,700,000 Cycles

Table 5.36: Load Test Summary at 2,900,000 Cycles

Load Test Summary (N = 2,900,000)			
Applied Load, P (kip)	Moment @ Gage Loc. (ft-kip)	Moment @ Midspan (ft-kip)	Back-Calc. Appl. Load (kip)
0	0	0	0
9.30	88.81	111.63	11.91
18.60	154.19	193.82	20.67
27.90	219.55	275.97	29.44
37.20	284.78	357.96	38.18
46.50	349.61	439.45	46.87
55.80	414.12	520.54	55.52
65.10	478.35	601.28	64.14
74.40	542.66	682.11	72.76
83.70	606.66	762.56	81.34
93.00	670.68	843.03	89.92

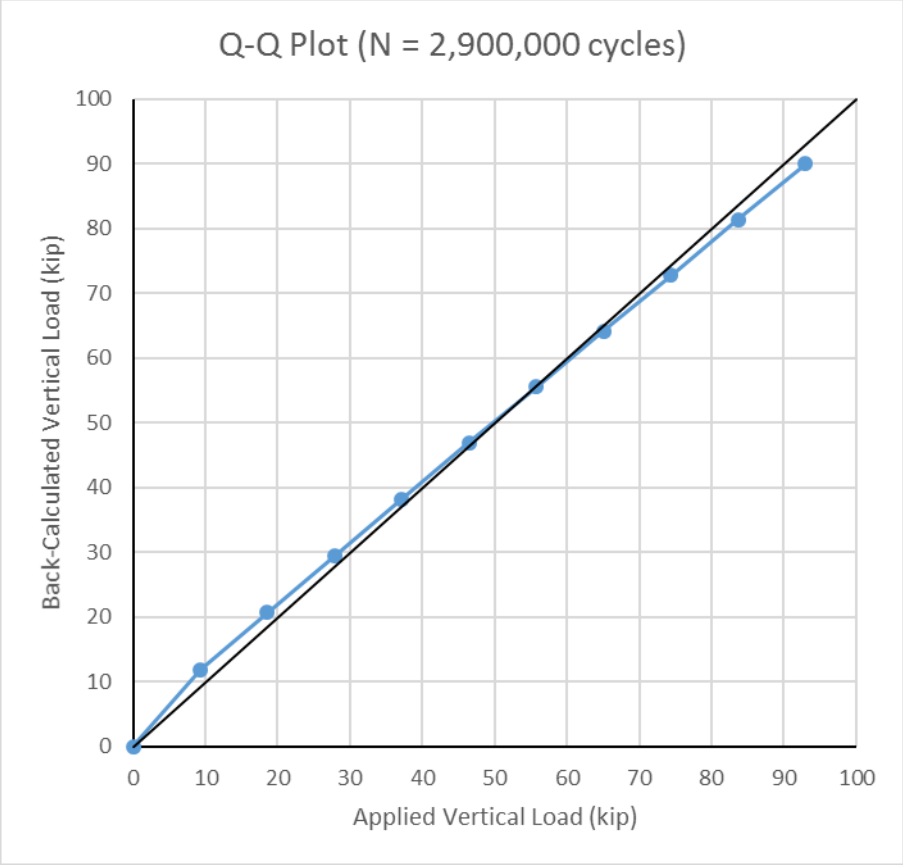

Figure 5.34: Experimental vs. Theoretical Loads at 2,900,000 Cycles

5.4 DEFLECTIONS

LVDTs measured vertical deflections at 92.50 kip for the uncoated steel specimen and 93.00 kip for the galvanized steel specimen. The LVDTs were placed at quarter points of each of the specimens. As seen in Tables 5.37 and 5.38, the deflection values remained nearly uniform throughout the entirety of the testing. The deflections of the galvanized steel specimen are larger than the those of the uncoated steel specimen, which can be attributed to weaker concrete in the deck of the galvanized specimen.

Table 5.37: Summary of Uncoated Steel Specimen Deflections

Cycle Count	Deflection at 92.50 kip (in)		
	Q1	Q2	Q3
0	0.536	0.809	0.568
100,000	0.549	0.828	0.581
200,000	0.556	0.837	0.586
300,000	0.555	0.836	0.587
500,000	0.565	0.850	0.596
700,000	0.591	0.877	0.611
900,000	0.596	0.885	0.615
1,100,000	0.609	0.903	0.629
1,300,000	0.617	0.917	0.637
1,500,000	0.615	0.913	0.635
1,700,000	0.619	0.918	0.637
1,900,000	0.633	0.939	0.650
2,100,000	0.637	0.945	0.655
2,300,000	0.637	0.945	0.652
2,500,000	0.642	0.951	0.655
2,700,000	0.649	0.962	0.663
2,900,000	0.658	0.974	0.674

Table 5.38: Summary of Galvanized Steel Specimen Deflections

Cycle Count	Deflection at 93.00 kip (in)		
	Q1	Q2	Q3
0	0.621	0.920	0.619
100,000	0.639	0.951	0.637
200,000	0.657	0.973	0.651
300,000	0.672	0.994	
500,000	0.692	0.994	0.685
700,000	0.714	1.053	0.711
900,000	0.730	1.074	0.729
1,100,000	0.743	1.095	0.744
1,300,000	0.759	1.116	0.760
1,500,000	0.760	1.127	0.767
1,700,000	0.779	1.144	0.775
1,900,000	0.793	1.164	0.789
2,100,000	0.799	1.171	0.793
2,300,000	0.803	1.178	0.797
2,500,000	0.811	1.188	0.804
2,700,000		1.201	0.814
2,900,000	0.824	1.208	0.820

5.5 TEST TO FAILURE RESULTS

The midspan load-deflection results for the uncoated steel specimen are shown in Figure 5.35. The LVDTs were removed from the testing after the specimen had deflected approximately 3.5 inches as the range the LVDTs could accurately measure had been exceeded. The strain-load relationship is shown in Figure 5.36 for the uncoated specimen. The load-deflection and strain-load relationships are shown in Figures 5.37 and 5.38, respectively. The load strain results show the ultimate load the specimen can hold before composite action is lost. After the loss of composite action, any additional load introduced into the system will cause increased deflection without increased load resistance. If the loading of the specimen had been in load control instead of stroke control, there would have been a sudden and catastrophic failure of the system.

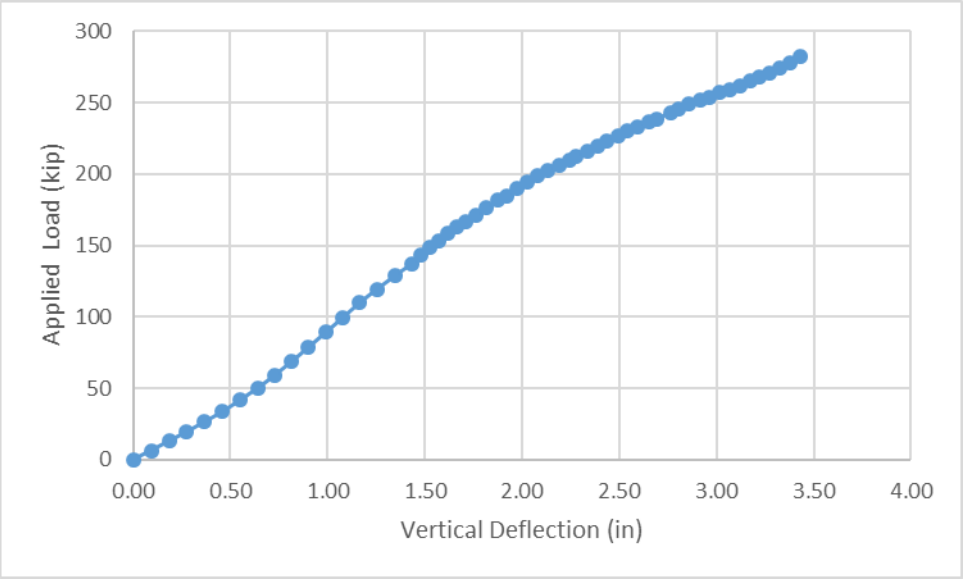

Figure 5.35: Load-Deflection Data from Flexural Testing of Uncoated Steel Specimen

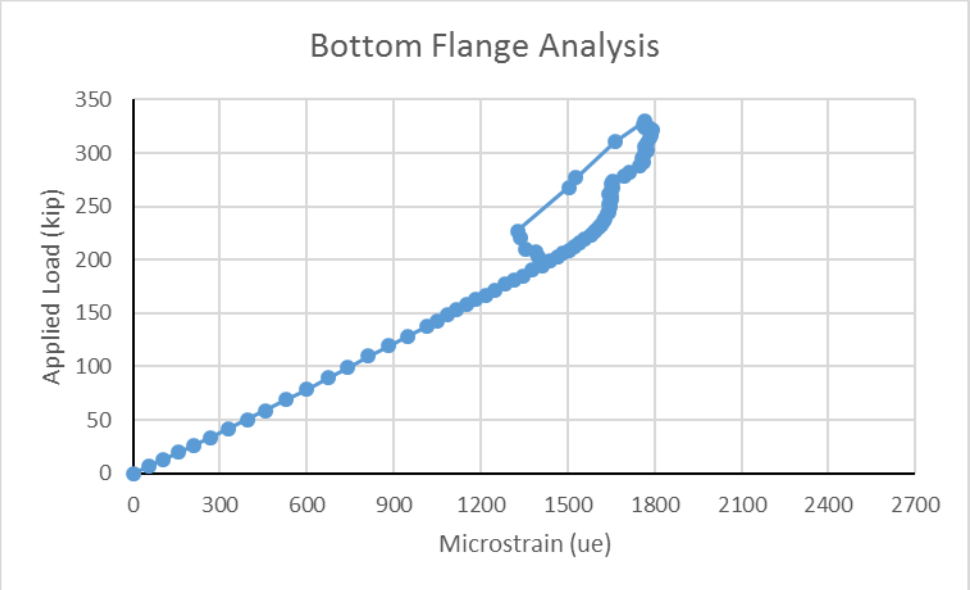

Figure 5.36: Bottom Flange Load-Strain Data from Flexural Testing Uncoated Steel Specimen

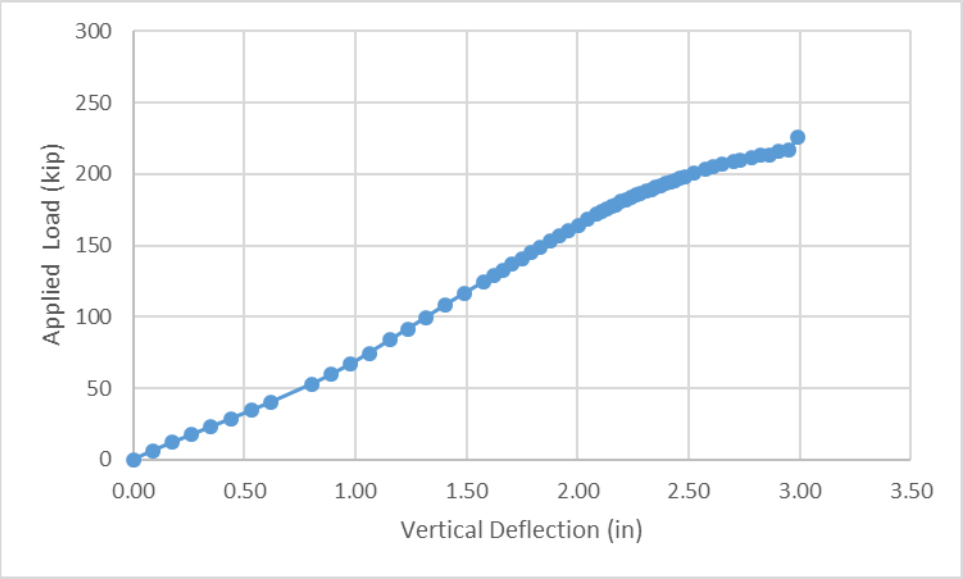

Figure 5.37: Load-Deflection Data from Flexural Testing of the Galvanized Specimen

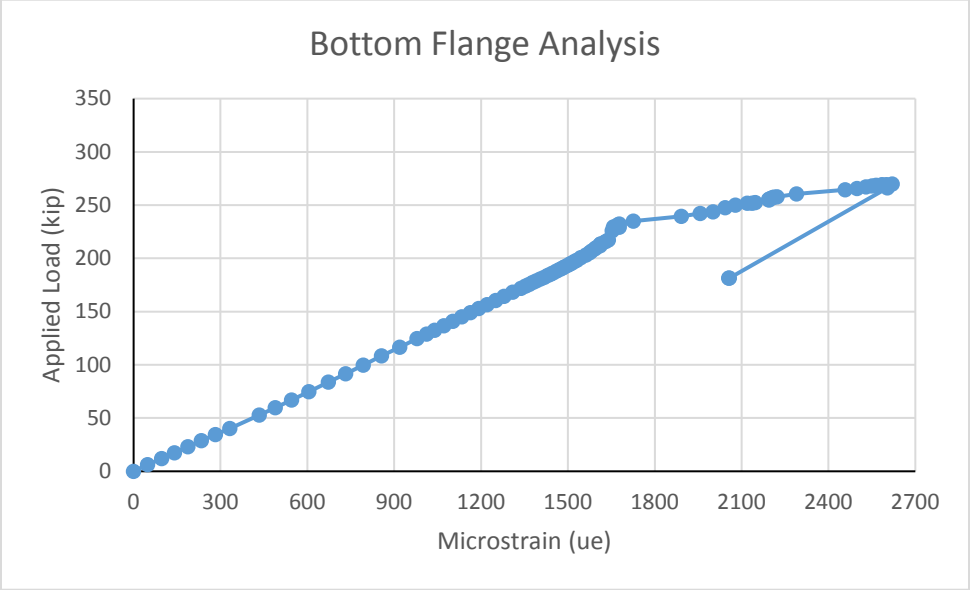

Figure 5.38: Bottom Flange Load-Strain Data from Flexural Testing Galvanized Steel Specimen

5.6 SUMMARY

This chapter summarized the results obtained throughout the testing of the different specimens. Hewlig and Fan's method to determine the longitudinal stresses from the strains obtained from the gages, in conjunction with Imhoff's procedure to calculate the induced moment from the stresses found, proved to be effective tools in the analysis of the obtained data. After some of the gages were removed for behaving inconsistently, a linear regression algorithm was also used to further reduce the error. Each girder behaved consistently for the entirety of the testing on each specimen, not varying significantly within its loading cycle. A difference in the magnitude of deflections and stresses is present between the two specimens, but the difference is constant through the test, so neither specimen behaved worse than the other through the testing. Overall, both steel specimens exhibited satisfactory performance through the fatigue analysis.

CHAPTER 6: PROJECT SUMMARY AND RECOMMENDATIONS FOR FUTURE WORK

6.1 PROJECT SUMMARY

The scope of this project was to evaluate the fatigue performance of modular press-brake-formed tub girders with differing steel types. This was accomplished by testing full-scale 38 foot composite girders inside a laboratory. The composite units consisted of a press-brake-formed tub girder with a six inch concrete deck cast on top of the upper flanges of the girder. The first girder consisted of ASTM A709 Grade 50 uncoated steel and the other consisted of ASTM A709 Grade 50 steel hot-dipped galvanized prior to arrival at the laboratory. Each specimen was fatigue tested to simulate a 75 year period in a non-interstate rural environment with an ADT of 800 vehicles, 15% of which were assumed to be truck traffic. A Service II moment was induced into each specimen at a predetermined number of cycles to evaluate the performance of each specimen. Based on the collected and analyzed strain gage and LVDT data, performance of each specimen behaved consistently throughout the entirety of the test. While the low strength of the concrete used in the galvanized steel specimen lead to overall higher strains and deflections, the specimens behaved similarly at every stage of testing, with the stresses increasing at approximately the same rate for each specimen. The data collected show the heat of the galvanization process does not have an adverse effect on the fatigue performance of cold bent press-brake-formed steel tub girders.

6.2 RECOMMENDATIONS FOR CONTINUED RESEARCH

Based on this study, the following recommendations for future work are given:

- Research could be conducted into the viability of longer span bridges using spliced tub girders. Performance of the composite system in negative flexure could lead to feasibility of press-brake-formed tub girders over longer spans and continuous span applications.

- The casting of the concrete deck in controlled conditions could benefit from improved detailing of the SIP metal formwork in the interior of the tub girder. Research into the effectiveness of crimping versus pour stop angles could improve the cost-effectiveness of the system.
- Once the press-brake-formed steel tub girder has been implemented for mainstream use, long-term monitoring may provide valuable information regarding fatigue performance.
- Research on improved live load distribution factors for steel box girders with a concrete deck could be conducted. For other types of superstructures, there are different distribution factors for whether shear or moment are being distributed to either interior or exterior beams and there is only one distribution factor for all beams in all cases for steel box girders with concrete decks.

REFERENCES

(2014). *AASHTO LRFD bridge design specifications*. Washington, DC: American Association of State Highway and Transportation Officials.

(4 Jul 2016). *Weathering steel: A guide to Corten and the A/B equivalents, origins & standards*. Retrieved from www.azom.com/article.aspx?ArticleID=12974.

Adams, M., Nicks, J., Stabile, T., Wu, J., Schlatter, W., & Hartmann, J. (2011). *Geosynthetic reinforced soil integrated bridge system, synthesis report* (Report No. FHWA-HRT-11-027). U. S. Department of Transportation, Federal Highway Administration.

Barth, K. E., Barth, A. S., Michaelson, G. K., Gibbs, C. L., & Tennant, R. M. (2017). *Evaluation of SMDI short span steel bridge design standards.*

Barth, K., Albrecht, P., & Righman, J. (2005). *Performance of weathering steel bridges in West Virginia*.

Bentley Systems, Inc. (2008). LEAP CONSYS™ AASHTO standard and LRFD live and static load analysis user manual (Version 01.03.02.00) [Computer Software].

Bertoldi, A. G. (2009). *A strength and serviceability assessement of high performance steel bridge 10462* (Master's thesis). Available from ProQuest.

Burgueño, R., & Pavlich, B. S. (2008). *Evaluation of prefabricated composite steel box girder systems for rapid bridge construction*. (Report No. RC-1507).

Burner, K. A. (2010). *Experimental investigation of folded plate girders and slap joints used in modular construction* (Master's Thesis). Available from University of Nebraska-Lincoln Database.

Chandar, G., Hyzak, M. D., & Wolf, L. M. (2010). *Rapid, economical bridge replacement*. Available from Modern Steel Construction.

Chen, B. S., Yura, J. A., Williamson, E. B., & Frank, K. H. (2005). *Top-lateral bracing systems for trapezoidal steel box-girder bridges*. (Report No. FHWA/TX-07/0-1898-4).

Corus Construction & Industrial. (2004). *The prevention of corrosion on structural steelwork*. Scunthorpe, Lincolnshire: Corus Construction & Industrial.

Culmo, M. P. (2011). *Accelerated bridge construction: Experience in design, fabrication and erection of prefabricated bridge elements and systems* (Report No. FHWA-HIF-12-013). U. S. Department of Transportation, Federal Highway Administration.

Ghavamian, A., Maghami, M. R., & Gomes, C. (2015). Concerns of corrosive effects with respect to lightning protection systems. *Engineering Failure Analysis, November 2015.* doi:101016/j.engfailanal.2015008.019

Gibbs, C. L. (2017). *Field performance assessment of press-brake-formed steel tub girder superstructures* (Master's thesis). Available from ProQuest.

Gilchrist, C. L., Yura, J. A., & Frank, K. H. (1997). *Buckling behavior of U-shaped girders*. (Report No. FHWA/TX-97/0-1395-1).

Glaser, L. A. (2010). *Constructability testing of folded plate girders* (Master's Thesis). Available from University of Nebraska-Lincoln Database.

Helwig, T. A., & Fan, Z. (2000). *Field and computational studies of steel trapezoidal box girder bridges* (Report No. 1395-3). Austin, Texas: Texas Department of Transportation.

Hudson, R. (2004). The prevention of corrosion on structural steelwork. *Corus Construction and Industrial*. Corus: North Lincolnshire.

Imhoff, C. M. (1998). *Testing and modeling of Bridge R-289*. (Master's Thesis). Available from University of Missouri.

Kassimali, A. (2015). *Structural analysis* (5th ed.). Stamford, CT: Cengage Learning.

Kelly, L. T. (2014). *Experimental evaluation of non-composite shallow press-brake-formed steel tub girders* (Master's thesis). Available from ProQuest.

Kline, E. (2009). Durable bridge coatings. *Modern Steel Construction*, 46-50.

Kozhokin, P. (2016). *Evaluation of modular press-brake-formed tub girders with UHPC joints* (Master's thesis). Available from ProQuest.

Masteel UK, Ltd. (2016). *Weathering steel: A guide to Corten and the A/B equivalents, origins and standards*. Retrieved from https://www.azom.com/.

Michaelson, G. K. (2014). *Development and feasibility assessment of shallow press-brake-formed steel tub girders for short-span bridge applications* (Doctoral dissertation). Available from ProQuest.

Micro-Measurements, Inc. (2010). StrainSmart [Data Collection]. Raleigh, North Carolina: Micro-Measurements, Inc.

Nakamura, S. (2002). Bending behavior of composite girders with cold formed steel U section. *ASCE Journal of Structural Engineering*, *128*(9), 1169-1176. Doi: 10.1061-(ASCE)0733-9455(2002)128:9(1169).

National Physical Laboratory. (2000). *Coating for the protection of structural steelwork*. Teddington, Middlesex: Crown.

Olson, A., Williams, T., Hudson, M., & Fleming, D. W. (3 Mar 2017). *Steel bridges protected with two-coat polyaspartic urethane coatings*. Retrieved from www.materialsperformance.com/articles/cathodic-protection/2017/01/steel-bridges-protected-with-two-coat-polyaspartic-urethane-coatings.

Phares, B., Deng, Y., & Steffens, O. (2017). *Evaluation of a folded plate girder bridge system*. (Report No. InTrans Project 13-458).

Taly, N. B., & GangaRao, H. V. S. (1976). *Development and design of standardized short span bridge superstructural.* (Report No. FHWA-WV-76-5).

Tricon Engineering Group, Ltd. (2008). *Standard design and details of press-brake-formed steel tub girder*. Tricon Engineering Group: Michigan.

U. S. Department of Transportation, Federal Highway Administration. (2013). *Slide-in bridge construction implementation guide: Planning and executing projects with the lateral slide method* (Project No. F-ST99(232)).

U. S. Department of Transportation, Federal Highway Administration. (2014). *Every day counts: Accelerated bridge construction.*

APPENDIX A: LOADING CALCULATIONS

Influence Line analysis was used to determine the moments at the midspan of a simply supported beam. Equation A1.1 displays the set of functions for the moment at midspan:

$$f(x) = \begin{cases} x/2 & [0\,, L/2] \\ (L-x)/2 & [L/2\,, L] \end{cases} \qquad \text{Eq. A1.1}$$

The AASHTO fatigue load model consists of a single HL-93 truck with a rear axle spacing fixed at 30 feet. Using a load factor of 1.75 for an infinite life fatigue, an impact factor of 1.15 and a live load distribution factor of 1.00, the Fatigue I moment was determined according to Equation A1.2:

$$M_{Fatigue\ I} = (1.75)(1.15)(1.00)M_{Fatigue\ Truck} \qquad \text{Eq. A1.2}$$

Since the fatigue truck is longer than the bridge span, only the front and middle axles were used to determine the highest moment induced at midspan. Figure A1.1 shows the AASHTO fatigue truck placement.

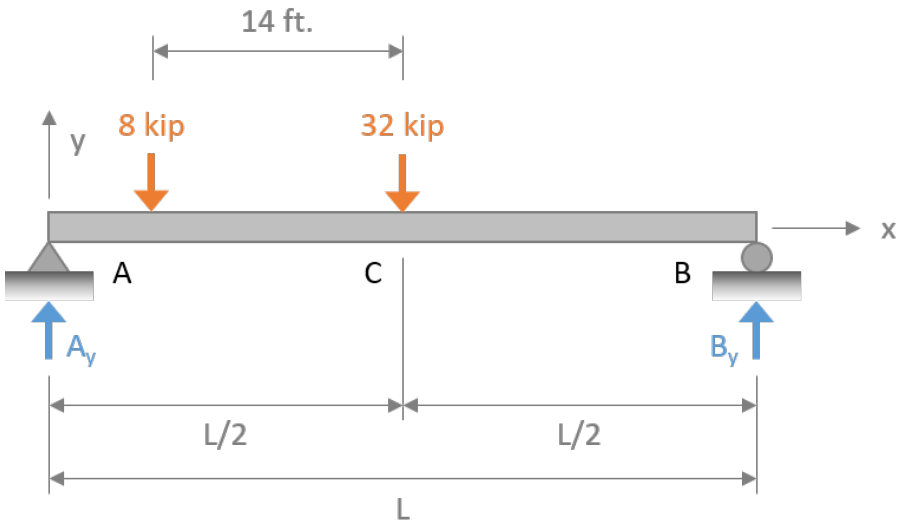

Figure A.1: HL-93 Fatigue Truck Placement

Using the influence line method, the fatigue-induced moment was determined as follows:

$$
\begin{aligned}
M_{Fatigue\ Truck} &= \sum_{i=1}^{n} P_i \times f(x_i) \\
&= 8 \times f(L/2 - 14) + 32 \times f(L/2) \\
&= 8 \times (L/4 - 7) + 32 \times f(L/4) \\
&= 2L - 56 + 8L \\
&\boxed{M_{Fatigue\ Truck} = 10L - 56}
\end{aligned}
$$

Therefore, the moment at midspan due to design fatigue loading for infinite life is as follows:

$$
\begin{aligned}
M_{Fatigue\ I} &= (1.75)(1.15)(1.00)(10L - 56) \\
\textit{*For } L = 37.00 ft \textit{ (Uncoated Steel)} \quad &= (1.75)(1.15)(1.00)(314) \\
&= 631.93\ kip - ft \\
\\
\textit{*For } L = 37.50 ft \textit{ (Galvanized Steel)} \quad &= (1.75)(1.15)(1.00)(319) \\
&= 641.99\ kip - ft
\end{aligned}
$$

To determine a point load to induce this moment, the equation for moment in a simply supported beam was rearranged:

$$
\begin{aligned}
P_{Fatigue\ I} &= \frac{4M_{Fatigue\ I}}{L} \\
\textit{*For } L = 37.00 ft \textit{ (Uncoated Steel)} \quad &= \frac{4 \times 631.93}{37.00} \\
&= 68.32\ kip \\
\textit{*For } L = 37.50 ft \textit{ (Galvanized Steel)} \quad &= \frac{4 \times 641.99}{37.50} \\
&= 68.48\ kip
\end{aligned}
$$

A similar procedure was used to determine the Service II moment. The AASHTO HL-93 load model consists of either the truck and the lane or the tandem and the lane. Using a load factor of 1.30 for Service II, an impact factor of 1.33 and a live load distribution factor of 1.00, the Service II moment was determined using Equation A1.3:

$$M_{Service\ II} = (1.30)(1.00)(1.33M_{Vehicle} + M_{Lane}) \qquad \text{Eq. A1.3}$$

Figure A1.2 shows the HL-93 Truck placement on the simple span bridge.

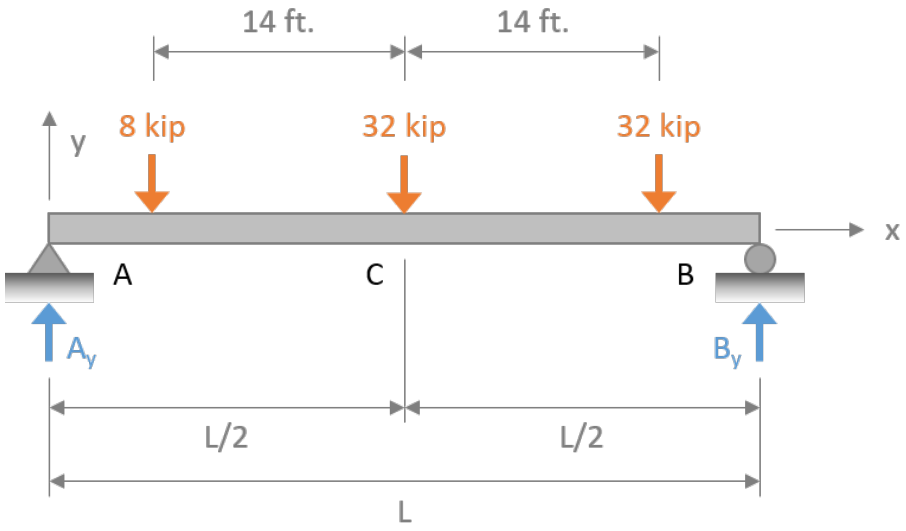

Figure A.2: HL-93 Truck Placement

Using the influence line method, the moment induced by the HL-93 Truck was determined as follows:

$$\begin{aligned} M_{Truck} &= \sum_{i=1}^{n} P_i \times f(x_i) \\ &= 8 \times f(L/2 - 14) + 32 \times f(L/2) + 32 \times f(L/2 + 14) \\ &= 8 \times (L/4 - 7) + 32 \times f(L/4) + 32 \times (L/4 - 7) \\ &= 2L - 56 + 8L + 8L - 224 \\ &\boxed{M_{Truck} = 18L - 280} \end{aligned}$$

Figure A1.3 shows the HL-93 Tandem placement on the simple span bridge.

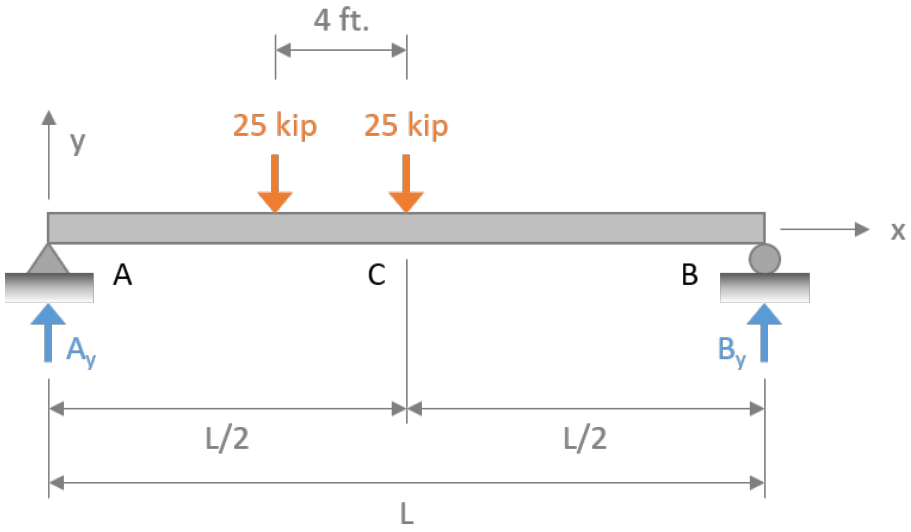

Figure A.3: HL-93 Tandem Placement

Using the influence line method, the moment induced by the HL-93 Tandem was determined as follows:

$$
\begin{aligned}
M_{Tandem} &= \sum_{i=1}^{n} P_i \times f(x_i) \\
&= 25 \times f(L/2 - 4) + 25 \times f(L/2) \\
&= 25 \times (L/4 - 2) + 25 \times f(L/4) \\
&= 6.25L - 50 + 6.25L \\
&\boxed{M_{Tandem} = 12.5L - 50}
\end{aligned}
$$

Figure A1.4 shows the HL-93 Lane model.

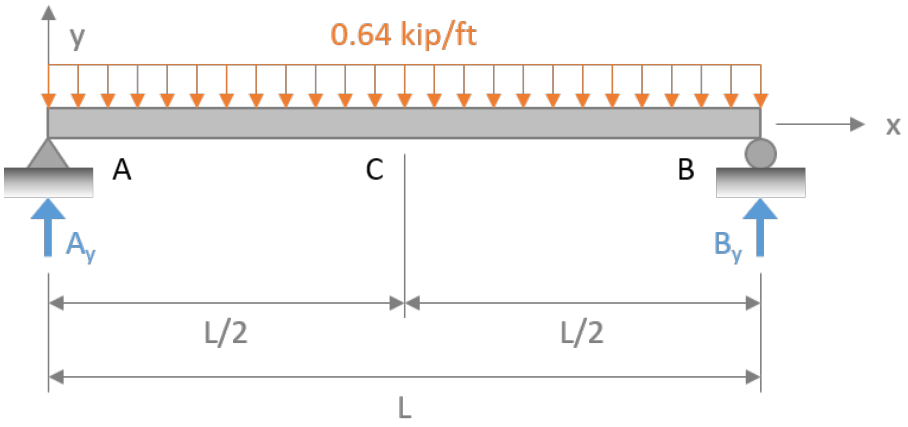

Figure A.4: HL-93 Lane Model

The moment at midspan is determined as follows:

$$M_{Lane} = \sum_{i=1}^{n} w_i \times A_i$$

$$= 0.64 \times (L^2/8)$$

$$\boxed{M_{Lane} = 0.08L^2}$$

Using a 37 foot clear span, for the uncoated steel specimen, moments due to the individual HL-93 Truck, Tandem, and Lane components were determined and are summarized in Table A1.1.

Table A.1: Summary of Moments for Uncoated Steel Specimen by Individual Components

Component	Moment (kip-ft)
HL-93 Truck	386
HL-93 Tandem	412.5
HL-93 Lane	109.52

The greater of the moments induced by either the truck or the tandem is used in Equation A1.3 as a vehicular load. Therefore, using the moments induced by the tandem and the lane components, the Service II moment was determined:

$$M_{Service\ II} = (1.30)(1.00)(1.33 \times 412.5 + 109.52) = 855.59kip - ft$$

To determine a point load to induce this moment, the equation for moment in a simply supported beam was rearranged:

$$P_{Service\ II} = \frac{4M_{Serivce\ II}}{L}$$

**For L=37.00ft (Uncoated Steel)*

$$= \frac{4 \times 855.59}{37.00}$$

$$= 92.50\ kip$$

Using a 37.5 foot clear span, for the galvanized steel specimen, moments due to the individual HL-93 Truck, Tandem, and Lane components were determined and are summarized in Table A1.2.

Table A.2: Summary of Moments for Galvanized Steel Specimen by Individual Components

Component	Moment (kip-ft)
HL-93 Truck	395
HL-93 Tandem	418.75
HL-93 Lane	112.5

The greater of the moments induced by either the truck or the tandem is used in Equation A1.3 as a vehicular load. Therefore, using the moments induced by the tandem and the lane components, the Service II moment was determined:

$$M_{Service\ II} = (1.30)(1.00)(1.33 \times 418.75 + 112.5) = 870.27kip - ft$$

To determine a point load to induce this moment, the equation for moment in a simply supported beam was rearranged:

$$P_{Service\ II} = \frac{4M_{Serivce\ II}}{L}$$

**For L=37.00ft (Uncoated Steel)*

$$= \frac{4 \times 870.27}{37.50}$$

$$= 92.83\ kip$$

APPENDIX B: GAGE DATA

B.1 ORIGINAL RAW DATA FROM UNCOATED STEEL SPECIMEN

Gage	Original Raw Data (N = 0)										
	P = 0.00k	P = 9.25k	P = 18.50k	P = 27.75k	P = 37.00k	P = 46.25k	P = 55.50k	P = 64.75k	P = 74.00k	P = 83.25k	P = 92.50k
G01	0	-15.224	-0.1663	55.814	39.2439	44.2175	52.0127	74.2791	73.9819	84.55	116.7128
G02	0	27.8766	49.7993	72.5814	96.351	119.5538	143.0262	167.0097	191.8139	216.0558	240.7927
G03	0	51.7089	90.2524	128.7178	166.8543	205.0399	243.5516	281.7342	320.2515	358.4259	397.3667
G04	0	85.4519	148.7265	209.5947	269.3096	328.8922	387.7847	446.3128	504.9409	563.808	621.1482
G05	0	87.9375	151.3364	214.5117	276.6729	339.0276	400.4615	462.4605	524.1416	585.2728	646.5511
G06	0	83.6526	143.4869	202.9065	262.0993	321.0648	379.3814	437.7046	496.1286	554.372	612.6219
G07	0	22.9263	35.0565	44.49	55.2284	65.7335	74.7015	84.9734	94.3118	105.703	113.5117
G08	0	14.2775	13.1899	28.6214	57.7037	83.4308	106.7507	144.3436	180.6332	211.7429	246.6887
G09	0	5.7433	9.9543	14.9137	20.5661	27.3762	34.5608	42.302	49.8108	58.2897	65.7988
G10	0	5.1218	8.8543	14.2082	19.5617	25.4679	31.8814	39.0325	46.4136	55.2727	65.6124
G11	0	29.9822	51.8642	73.4701	95.4042	116.9191	138.2947	159.5747	182.0612	204.5024	226.7617
G12	0	62.4231	108.1183	153.7263	199.1969	245.0884	290.4742	335.8124	381.1637	426.5641	472.0167
G13	0	53.7736	92.9952	131.9417	170.0101	208.6376	245.9699	284.4642	323.982	364.6165	402.0064
G14	0	88.1166	151.9623	215.2586	278.2842	341.3642	404.5456	467.0839	529.8623	592.4629	654.9785
G15	0	77.5802	143.8021	203.1633	264.7594	327.1993	389.4609	452.0091	514.5183	573.2268	651.5001
G16	0	57.7601	99.4894	140.894	182.7224	225.201	267.7752	310.2594	353.2595	396.8176	439.4068
G17	0	31.5189	55.1825	79.2186	103.6686	128.8622	154.009	179.4338	205.0908	231.2133	257.3377
G18	0	12.3004	22.75	33.0099	43.9709	54.7888	66.1231	77.2221	88.7421	100.2647	111.5069

Gage	Original Raw Data (N = 100,000)										
	P = 0.00k	P = 9.25k	P = 18.50k	P = 27.75k	P = 37.00k	P = 46.25k	P = 55.50k	P = 64.75k	P = 74.00k	P = 83.25k	P = 92.50k
G01	0	-1.3916	0.2603	3.2465	6.7378	10.9665	15.425	20.9883	26.5528	32.7688	38.8385
G02	0	26.1061	47.1532	69.1598	91.8728	114.5978	137.7329	161.7933	185.836	209.7515	234.1213
G03	0	50.3726	88.3118	126.3485	164.5726	202.5639	240.6064	279.2057	317.2519	355.5355	393.9561
G04	0	85.4492	149.3835	212.026	273.1917	333.5755	393.4096	452.6936	510.9166	566.4068	626.9654
G05	0	87.4591	151.485	214.9147	277.1459	339.198	400.7937	462.5368	523.7757	584.6973	645.812
G06	0	83.3322	144.3883	203.9538	262.9174	321.7003	380.0685	438.4908	496.5446	554.746	613.0009
G07	0	27.6365	42.8402	56.5075	70.2712	84.1276	97.3321	111.8376	127.5107	144.0669	217.9184
G08	0	80.7727	116.5919	169.9238	194.2392	237.3874	257.0743	283.0763	296.9662	329.2492	350.4917
G09	0	2.0285	4.572	9.9874	15.8672	22.1164	28.9197	36.8337	44.7491	52.7121	61.829
G10	0	3.964	8.013	16.5956	24.2988	30.802	37.7629	44.7238	51.5924	55.6865	62.7376
G11	0	27.0394	49.1794	70.9476	93.5072	115.6023	137.9755	160.4887	182.4033	206.4926	229.7024
G12	0	60.193	106.0897	151.4391	196.8394	242.6583	288.2037	333.9368	378.5232	424.3073	469.4551
G13	0	53.3929	93.7658	133.1221	172.9914	211.9831	251.6733	291.5987	331.6196	371.5979	412.9706
G14	0	87.7729	152.7192	216.7455	280.3615	343.3821	405.9464	469.4934	531.5158	593.964	656.6522
G15	0	83.3683	144.4089	204.9468	264.7967	324.4221	383.9616	443.508	503.0157	564.8033	624.5108
G16	0	57.2911	99.6231	142.2389	184.8101	227.3897	270.3393	313.4294	355.7372	399.1156	442.5401
G17	0	30.5083	53.2492	77.1001	101.7392	126.4704	151.4371	177.3738	202.4795	228.0949	254.3125
G18	0	11.8351	21.7243	32.0303	42.3322	52.6836	63.5479	74.5522	85.6558	97.0841	108.6073

Gage	Original Raw Data (N = 200,000)										
	P = 0.00k	P = 9.25k	P = 18.50k	P = 27.75k	P = 37.00k	P = 46.25k	P = 55.50k	P = 64.75k	P = 74.00k	P = 83.25k	P = 92.50k
G01	0	-0.2342	0.8145	3.9805	8.1141	13.1216	18.5891	24.38	31.1869	38.0826	44.746
G02	0	26.1383	45.8308	67.6393	90.0788	113.4274	136.6076	160.4773	184.5262	208.6743	233.0499
G03	0	51.5174	89.5026	127.7195	166.2643	204.6283	243.4107	282.0107	320.519	359.0312	397.5
G04	0	89.7971	155.4267	218.1868	283.0902	362.3036	424.1605	486.5361	547.9903	608.8943	669.4344
G05	0	89.4933	153.8385	217.1238	280.0921	342.3249	404.5655	465.8382	527.3044	588.6854	649.7019
G06	0	85.9915	147.6975	207.4908	267.3849	326.5369	385.6961	444.2999	502.8168	561.247	619.9183
G07	0	37.4341	73.4075	86.1268	97.6356	153.3023	161.4089	174.8818	190.5905	205.9299	214.5966
G08	0	26.2052	41.9803	54.9665	70.6722	86.2798	106.1815	124.1632	146.5473	166.7346	192.0807
G09	0	2.9519	4.7997	9.8445	16.0908	22.5706	30.6691	38.4914	46.9598	55.3848	64.5023
G10	0	3.7198	8.6894	15.3214	23.8905	31.0747	39.6901	48.6789	56.7889	65.6848	74.5805
G11	0	30.0773	52.5298	75.5873	98.8767	121.7947	145.3624	168.6567	192.0887	215.2007	238.775
G12	0	61.4769	106.7775	152.0787	198.027	243.4296	288.7882	334.3364	379.4285	424.2478	469.1628
G13	0	58.9763	101.5569	143.5385	185.5235	227.3271	269.4583	311.6859	354.0561	396.476	439.4099
G14	0	90.1455	155.3274	219.1714	283.2556	346.7907	410.0553	472.4449	534.8888	597.2012	659.986
G15	0	87.5103	150.5105	211.4784	273.2888	334.3643	395.1231	455.425	516.291	576.4683	637.0707
G16	0	58.9533	101.1476	143.2981	186.2862	228.5824	271.9944	314.6699	357.9005	400.6279	444.2823
G17	0	31.2565	52.9857	76.6149	101.0743	125.9985	151.3389	176.4978	202.302	228.4363	254.3371
G18	0	12.729	22.1531	31.9457	42.7669	53.4457	64.1222	74.7539	86.3239	97.3332	108.9028

Gage	Original Raw Data (N = 300,000)										
	P = 0.00k	P = 9.25k	P = 18.50k	P = 27.75k	P = 37.00k	P = 46.25k	P = 55.50k	P = 64.75k	P = 74.00k	P = 83.25k	P = 92.50k
G01	0	-2.4549	-1.8629	0.9397	5.4364	9.614	14.8481	20.4679	26.807	33.2782	40.1194
G02	0	26.5349	46.5598	68.648	91.0131	113.5851	137.2154	161.0398	184.0047	208.2103	232.772
G03	0	51.6012	89.4413	128.2115	166.7044	204.973	243.7511	281.8395	320.3409	359.125	397.4499
G04	0	89.552	153.7322	217.0397	279.3799	339.6852	400.1369	459.9458	519.0652	578.1453	636.8602
G05	0	89.2353	153.9195	217.4047	280.4336	342.2622	404.1453	465.5711	526.5862	587.6552	648.546
G06	0	85.9068	147.3385	207.3256	266.9454	324.8857	383.9104	441.6769	499.6373	557.7922	616.1412
G07	0	20.5825	34.2895	48.0455	61.2865	74.3485	87.5921	101.0808	114.6295	127.7768	141.2546
G08	0	21.3509	37.8991	56.6386	76.139	95.2825	116.9278	135.8675	156.7584	177.7937	200.0107
G09	0	2.4446	3.8304	8.7355	15.7218	22.0156	30.1144	38.2593	46.6845	55.8003	64.1768
G10	0	4.2002	8.8953	15.4381	22.8984	29.9008	38.1006	46.7145	55.0552	63.4821	72.2774
G11	0	29.3058	51.2115	74.0462	97.2918	119.9417	143.1929	166.7718	189.4701	213.2333	236.299
G12	0	61.3276	106.6623	152.3654	198.257	243.3269	288.6759	333.8432	378.5113	423.5962	468.1777
G13	0	56.2099	97.7339	138.4736	179.0774	219.221	259.507	299.9349	339.8564	380.4769	421.2394
G14	0	89.3537	154.8126	219.3047	283.3875	346.1775	408.9295	471.503	533.5736	596.1165	658.1091
G15	0	87.5717	150.781	212.7005	274.3961	334.662	395.1669	456.2356	515.8739	575.7052	635.5898
G16	0	58.4967	100.3207	143.0783	185.9257	228.4607	271.2261	313.8095	356.8137	399.6812	443.0166
G17	0	31.2639	52.9964	76.3488	101.5045	125.8325	150.805	176.6142	201.9151	227.9564	253.8139
G18	0	11.3772	20.4266	30.1256	40.8965	50.5441	61.4099	72.3227	83.518	94.712	105.9556

Gage	Original Raw Data (N = 500,000)										
	P = 0.00k	P = 9.25k	P = 18.50k	P = 27.75k	P = 37.00k	P = 46.25k	P = 55.50k	P = 64.75k	P = 74.00k	P = 83.25k	P = 92.50k
G01	0	-2.8609	-2.6766	-0.7489	2.102	6.103	10.6576	15.808	22.5703	28.2295	34.2106
G02	0	25.3709	45.1768	66.5426	88.6896	111.2588	134.4569	158.1947	182.7483	206.8172	231.1111
G03	0	51.565	89.9625	129.0576	167.3725	205.5986	243.7811	282.7072	321.3551	359.3633	397.9242
G04	0	91.4315	157.718	222.9916	285.9984	348.4563	410.1323	471.3973	532.8097	593.2538	653.5192
G05	0	90.0336	155.6666	220.008	282.7324	345.326	406.9517	467.6561	529.2968	590.1089	651.1607
G06	0	87.1382	149.5088	210.5873	270.1409	329.3773	387.6917	446.3381	504.9909	562.7221	620.7853
G07	0	83.595	133.5157	169.7949	186.9353	204.6324	220.0087	237.4771	255.0799	271.156	288.3936
G08	0	21.3022	37.4133	58.2245	79.1914	101.0613	122.3419	144.6186	167.4049	190.2917	219.0268
G09	0	-4.1291	-5.3828	-1.2659	4.6568	11.1371	19.0501	27.195	36.357	44.5029	54.2206
G10	0	2.0743	4.4228	9.3097	14.7506	21.1628	27.7106	35.7375	44.129	51.5591	59.4437
G11	0	28.9311	50.6528	73.0662	94.9745	117.3016	139.6275	162.0469	185.529	207.3967	230.4205
G12	0	62.4621	108.1966	154.7592	200.3615	245.9224	291.212	335.907	381.3844	425.6755	471.0712
G13	0	58.2241	100.5188	143.002	183.8674	225.3849	267.4616	308.43	350.977	393.0182	435.3873
G14	0	91.1982	157.7035	222.7313	286.6059	350.0238	413.0787	475.3045	537.7702	599.5002	662.4005
G15	0	88.3256	152.1463	214.492	276.3354	337.6302	398.0513	458.387	519.1011	579.0803	641.2005
G16	0	57.344	99.5414	142.4833	185.0158	227.6448	270.4125	313.3247	356.8407	399.2041	442.4934
G17	0	27.1891	47.7127	71.2897	95.1942	119.8393	145.412	170.7512	196.8344	222.3193	248.5411
G18	0	10.9158	20.3425	30.5093	40.5768	50.8801	61.789	72.3732	83.5657	94.3356	106.2785

Gage	Original Raw Data (N = 700,000)										
	P = 0.00k	P = 9.25k	P = 18.50k	P = 27.75k	P = 37.00k	P = 46.25k	P = 55.50k	P = 64.75k	P = 74.00k	P = 83.25k	P = 92.50k
G01	0	-8.7076	-17.6899	-19.3514	-16.963	-12.9651	-9.0132	-3.5414	2.1591	8.3176	14.5682
G02	0	20.1962	33.1142	51.6221	73.2215	95.7883	118.5416	141.586	164.2952	188.0151	212.2587
G03	0	50.6888	86.7345	124.8657	163.1388	201.506	239.8781	278.5719	317.1802	356.1115	394.5819
G04	0	94.0825	163.2055	227.8337	289.9165	351.4495	411.6896	472.4941	532.2841	591.8027	651.7925
G05	0	93.7171	162.8906	229.1019	292.9533	355.6519	417.3824	479.1677	539.845	601.2271	662.0587
G06	0	89.4401	154.6961	216.8017	276.4526	335.2744	393.4987	450.9864	508.6196	566.3533	624.0926
G07	0	-16.452	-2.0388	11.0255	23.8106	36.9693	49.1045	64.3192	154.1619	163.9197	173.6766
G08	0	17.2275	31.586	49.7402	70.1698	91.8599	113.7306	135.5349	158.9243	181.803	205.4167
G09	0	-11.0271	-16.9077	-14.9174	-9.6871	-2.6507	4.5691	12.6223	21.2342	29.7982	38.8713
G10	0	-3.3379	-8.5689	-6.7883	-1.3118	5.4585	12.6924	19.877	27.7105	35.9141	43.703
G11	0	25.596	42.4087	62.9189	85.1905	107.5086	129.9225	152.4766	175.8644	198.8368	221.9498
G12	0	61.2985	105.8587	152.0777	197.5658	243.4261	288.3707	333.4565	378.4112	423.6424	468.4644
G13	0	60.3699	105.5944	148.4133	190.1697	232.0222	272.9047	314.4396	355.5147	398.3082	439.9001
G14	0	93.9911	164.2171	231.4799	295.8247	359.7594	422.7268	485.7015	547.6618	610.0479	672.3023
G15	0	91.8151	159.4474	223.9364	285.8365	347.1414	407.4801	468.1972	527.9469	588.2145	648.8604
G16	0	56.5523	99.4463	142.5246	185.1016	227.8217	270.315	313.5492	356.232	399.6609	442.9059
G17	0	24.2322	42.8182	65.4264	89.1054	113.6643	139.1974	164.5451	189.7542	216.0298	241.9357
G18	0	9.142	17.6818	27.9391	37.5403	47.7972	58.2859	68.6363	79.8744	91.1179	102.5919

Gage	Original Raw Data (N = 900,000)										
	P = 0.00k	P = 9.25k	P = 18.50k	P = 27.75k	P = 37.00k	P = 46.25k	P = 55.50k	P = 64.75k	P = 74.00k	P = 83.25k	P = 92.50k
G01	0	-8.2002	-17.9192	-21.8368	-19.9545	-16.5978	-12.1839	-7.2155	-1.5107	4.3309	10.5033
G02	0	21.2251	34.1022	51.3627	72.4951	94.9675	118.0908	141.6267	165.3948	189.765	214.0896
G03	0	51.1867	86.9966	124.2909	162.4165	200.9166	239.0487	277.4168	315.509	354.2501	392.4403
G04	0	95.4125	165.3128	231.9268	294.6497	356.1264	417.0998	476.9194	536.5144	595.9301	654.8885
G05	0	94.4265	164.399	230.9449	294.3409	356.6766	417.9514	479.6057	540.0125	601.4028	662.1032
G06	0	91.3264	157.9477	220.5043	280.8673	339.7388	398.2892	456.3312	514.1924	572.2949	629.982
G07	0	24.3693	38.6441	52.5987	66.2271	79.0633	92.7375	106.4621	119.8651	134.0119	146.6683
G08	0	16.8255	30.6821	47.5584	67.738	89.0037	110.9285	133.5533	156.4659	179.3128	202.646
G09	0	-13.0642	-20.1948	-20.0991	-15.4709	-8.6207	-0.6622	6.7896	14.5662	23.4508	32.2479
G10	0	-8.3236	-19.2767	-23.7656	-20.7256	-15.5624	-9.6622	-3.9455	7.4102	17.4686	22.672
G11	0	25.517	41.5062	60.7845	82.1436	103.9667	126.3884	148.7698	170.7786	193.8503	216.3684
G12	0	61.9594	106.4186	151.7559	197.3755	242.7473	288.141	333.4122	378.0799	423.2275	467.6517
G13	0	59.4364	103.0803	145.2914	185.3281	224.8584	264.6694	304.7622	344.4873	385.2815	425.8012
G14	0	95.1508	165.8527	233.0354	297.952	361.2044	424.3261	486.3869	547.9911	610.7179	672.8481
G15	0	92.2061	160.7925	225.2628	286.8212	347.6913	407.9201	468.1562	527.3326	587.351	647.3765
G16	0	57.1927	99.7132	141.5427	184.0723	226.2325	269.6447	312.3235	354.5392	398.15	440.6981
G17	0	23.1155	41.3277	61.8999	85.8974	110.3136	135.8362	160.9476	185.9678	212.1442	237.5364
G18	0	9.4279	17.3646	26.2702	35.9198	46.0386	56.8098	67.0684	78.0309	89.7903	100.5189

Gage	Original Raw Data (N = 1,100,000)										
	P = 0.00k	P = 9.25k	P = 18.50k	P = 27.75k	P = 37.00k	P = 46.25k	P = 55.50k	P = 64.75k	P = 74.00k	P = 83.25k	P = 92.50k
G01	0	-11.2858	-21.6067	-25.8501	-24.802	-21.6358	-16.764	-11.8945	-5.7826	0.1473	6.6273
G02	0	19.3386	31.5235	47.8618	68.7673	90.5971	113.0715	136.4227	160.2344	184.5621	208.9747
G03	0	50.1257	86.1683	123.6472	161.4537	199.6312	238.0427	276.269	314.7767	353.4742	391.2927
G04	0	96.2615	165.9861	233.2129	296.2693	357.2909	417.576	477.5435	537.2393	596.2918	655.5837
G05	0	97.2503	167.9137	235.7076	299.5632	361.9869	423.7215	485.3708	546.5169	607.4843	668.6915
G06	0	93.724	160.9141	224.5076	285.1584	344.4112	402.7807	461.3915	519.6811	577.6962	635.7648
G07	0	21.6865	34.7653	48.231	61.4673	74.8851	88.5038	102.2829	116.7733	130.9508	145.9112
G08	0	15.486	28.7573	45.7734	65.4842	86.3887	108.7336	130.7918	153.8676	176.4746	199.5374
G09	0	-15.2399	-23.2972	-24.0371	-19.78	-13.4862	-6.2196	1.2304	9.7461	17.7523	26.5461
G10	0	-4.454	-12.1863	-12.7064	-7.2688	0.481	9.8461	19.8606	31.7712	44.193	59.7576
G11	0	25.3688	41.5868	60.579	82.0248	104.0759	126.6795	149.3325	172.7736	195.4748	218.4556
G12	0	62.6393	106.7	152.1843	197.4031	242.8076	287.633	332.4994	377.3106	422.5408	467.4061
G13	0	59.6267	102.5791	145.1646	185.0658	224.6919	263.8113	303.2582	343.0328	382.8105	422.7305
G14	0	97.4156	168.9928	237.5158	302.38	366.4166	429.2074	491.6806	554.3479	616.465	678.8692
G15	0	94.0155	163.1013	228.0691	290.1233	351.0258	411.0536	471.414	530.9462	590.6246	650.0787
G16	0	57.9348	100.6865	142.8367	185.3661	227.7586	270.2922	312.9676	355.9682	398.373	441.7078
G17	0	22.235	39.5694	60.0938	83.3033	107.3926	132.3626	157.5674	183.001	208.3904	234.4279
G18	0	10.1483	17.251	25.8858	35.4063	45.2537	55.5205	65.931	77.2812	87.9276	98.9938

Gage	Original Raw Data (N = 1,300,000)										
	P = 0.00k	P = 9.25k	P = 18.50k	P = 27.75k	P = 37.00k	P = 46.25k	P = 55.50k	P = 64.75k	P = 74.00k	P = 83.25k	P = 92.50k
G01	0	-14.8263	-25.2354	-31.5505	-30.823	-27.4707	-23.4286	-18.372	-13.3183	-7.0154	-0.719
G02	0	16.2471	27.6978	42.7887	62.9083	85.2406	107.1639	130.2837	153.6814	177.9445	201.8063
G03	0	49.9414	85.3851	121.9397	160.2531	198.661	236.1945	274.7026	313.0695	351.6243	389.9988
G04	0	100.447	171.5705	240.0109	304.6523	367.5838	428.8973	489.8463	550.3848	614.3229	674.1794
G05	0	99.5568	170.4754	238.5235	303.4685	366.4241	428.4579	489.8951	551.805	612.7926	674.0201
G06	0	95.7808	163.8122	227.919	289.3646	349.131	408.1553	466.8586	525.2407	583.5829	642.2127
G07	0	30.7773	47.2727	63.9085	80.6886	97.2359	112.5771	128.9422	144.7487	163.5629	179.2261
G08	0	15.7975	28.0971	44.3242	64.2673	86.178	107.6453	129.6079	152.4622	179.0152	201.9047
G09	0	-15.8855	-25.1915	-27.6894	-23.5253	-17.0478	-10.7989	-3.2544	4.6098	13.4992	22.1066
G10	0	-13.9922	2.8251	5.5391	30.1152	55.2004	69.2869	83.8794	96.5757	109.1346	118.9611
G11	0	25.5815	41.3288	59.5754	80.5058	102.8259	124.8726	147.5222	170.3559	193.7015	216.3969
G12	0	63.1332	106.8911	152.069	198.0837	243.6817	288.2289	333.6949	378.8862	423.562	468.4804
G13	0	63.0495	109.4726	154.1395	197.0032	238.7119	280.0065	321.2584	363.1627	404.9315	445.7303
G14	0	99.2763	171.3546	240.4238	306.6224	370.6455	433.6084	496.6256	559.3715	621.4283	684.4225
G15	0	97.1262	166.9575	233.1812	296.584	358.0465	418.2642	478.6745	539.2315	610.3773	670.1147
G16	0	60.437	102.821	144.6539	187.7396	230.3189	272.8126	315.3543	358.3585	402.0647	445.0778
G17	0	23.8501	40.538	60.2314	83.3963	107.8572	132.0428	156.7847	182.4987	208.0821	233.5665
G18	0	12.728	20.3494	28.9367	38.8308	48.6306	58.3812	68.6951	79.6676	90.4891	101.4166

Gage	Original Raw Data (N = 1,500,000)										
	P = 0.00k	P = 9.25k	P = 18.50k	P = 27.75k	P = 37.00k	P = 46.25k	P = 55.50k	P = 64.75k	P = 74.00k	P = 83.25k	P = 92.50k
G01	0	-13.9063	-24.6845	-32.061	-32.2175	-29.3421	-24.8867	-20.1567	-14.4592	-8.1609	-1.8155
G02	0	-6.5763	-104.766	-113.854	-160.684	-121.03	-108.388	-192.038	-201.304	-184.102	-128.754
G03	0	48.3479	84.0817	121.2014	160.8248	200.5867	238.8709	277.6676	315.9082	354.8457	392.3052
G04	0	94.7797	164.4019	234.173	297.2168	358.921	419.0527	478.1691	536.6416	595.1678	653.3751
G05	0	95.5257	166.6361	235.6196	300.5707	363.578	425.5708	487.3396	548.6041	609.783	670.6442
G06	0	91.564	159.3117	224.1186	285.2335	344.6231	403.7852	462.1582	520.3969	578.3617	636.6609
G07	0	26.4083	42.4546	57.0073	71.0015	86.2121	101.2368	115.0987	130.6373	146.1765	160.4105
G08	0	14.6261	26.8348	42.7807	62.0795	84.0363	104.9221	127.2069	149.8605	172.8015	195.8349
G09	0	-15.4259	-25.105	-27.9303	-24.2744	-18.2124	-11.037	-3.6773	4.3296	12.5208	21.3173
G10	0	-10.0039	-18.7022	-24.0297	-22.1038	-17.0365	-10.6765	-4.0395	3.4751	10.5728	18.1309
G11	0	23.746	39.6388	56.878	77.4026	99.1317	121.2318	143.4707	167.0551	190.1287	213.2503
G12	0	60.4425	104.0743	149.6917	195.3154	240.5187	285.8236	330.6708	376.0306	421.1123	466.1066
G13	0	58.8954	102.5963	144.6329	184.3087	222.8289	260.8884	298.719	336.8305	374.9451	413.1088
G14	0	95.1608	166.9845	237.1465	302.9992	367.235	430.271	493.0825	555.6232	618.1718	680.5421
G15	0	93.1809	162.7305	229.2287	292.2573	353.392	413.5134	473.3175	533.4529	592.9931	652.4934
G16	0	57.6563	100.0803	142.283	184.6743	227.1594	269.3717	312.0945	354.8675	398.1086	441.0269
G17	0	22.6032	39.2912	58.3344	80.8965	104.709	129.4468	154.4658	179.7126	205.3794	231.0015
G18	0	11.4595	18.8955	26.9699	35.8806	45.4933	55.2433	65.4654	76.156	87.2705	98.3865

Gage	Original Raw Data (N = 1,700,000)										
	P = 0.00k	P = 9.25k	P = 18.50k	P = 27.75k	P = 37.00k	P = 46.25k	P = 55.50k	P = 64.75k	P = 74.00k	P = 83.25k	P = 92.50k
G01	0	-15.6069	-26.4283	-34.079	-34.1244	-31.141	-26.6854	-21.9989	-16.1948	-9.716	-3.4651
G02	0	14.3652	25.6281	39.6107	58.7183	80.2717	102.704	125.5504	149.0443	173.3246	197.3296
G03	0	46.8138	82.4494	118.7365	156.365	194.3673	232.7406	270.7002	309.3559	348.0582	386.6272
G04	0	95.7038	167.5985	236.623	301.8941	364.9897	427.1638	487.6263	548.0953	609.0368	669.1493
G05	0	95.2897	167.1864	235.8886	300.9759	363.3772	425.4602	486.9934	548.3019	609.8972	671.2207
G06	0	91.7982	160.2481	225.2886	286.7317	346.2152	405.6115	463.3285	521.9425	580.7038	638.8629
G07	0	27.821	46.664	77.6889	96.5442	113.1406	130.5854	156.9792	178.8961	195.4821	211.3693
G08	0	13.8693	26.5823	42.2399	61.9358	82.6759	104.3498	126.434	148.8016	171.9993	194.9764
G09	0	-16.7646	-27.1383	-30.1472	-26.8631	-20.8	-13.7207	-6.7305	1.1828	10.1115	18.6764
G10	0	-8.8872	-16.012	-21.1028	-19.7289	-14.6632	-7.566	-0.2803	8.0678	15.9473	24.1562
G11	0	23.1	39.0404	55.8622	76.3864	97.7896	120.3504	142.6358	165.1992	188.5038	211.3494
G12	0	60.7059	105.8584	151.1258	197.2371	242.2588	287.4328	332.0154	377.2922	423.1037	467.8435
G13	0	56.9775	100.9315	143.0352	183.4262	223.0784	261.945	300.8615	339.6415	378.3321	417.9532
G14	0	94.9311	167.8243	237.0596	303.1462	367.2442	430.2818	492.6767	555.5443	618.5589	681.21
G15	0	92.1409	163.1481	229.3873	292.6659	353.5397	414.0957	474.1952	534.7195	595.2512	654.8155
G16	0	57.1593	99.8662	141.7475	183.9103	226.4943	269.0769	311.1542	354.1597	397.9527	441.0146
G17	0	21.0337	37.5337	56.6273	78.8661	102.4476	127.4639	152.0192	177.3606	203.6275	229.3424
G18	0	10.8019	17.9993	25.6946	34.7909	44.35	54.5166	64.4041	74.8083	86.5717	97.2126

Gage	Original Raw Data (N = 1,900,000)										
	P = 0.00k	P = 9.25k	P = 18.50k	P = 27.75k	P = 37.00k	P = 46.25k	P = 55.50k	P = 64.75k	P = 74.00k	P = 83.25k	P = 92.50k
G01	0	-17.31	-29.1879	-38.4917	-40.5749	-38.1904	-34.3339	-29.5558	-24.1772	-18.1539	-12.0879
G02	0	14.6839	25.6284	38.4597	56.6431	77.8248	100.025	122.8219	146.3166	170.0862	194.3662
G03	0	49.6269	85.2116	121.5388	159.2552	197.6676	235.9898	274.1294	312.6412	351.5727	389.8114
G04	0	101.4754	174.6473	244.1611	310.6191	374.4849	437.058	499.1742	560.4615	621.3382	682.2688
G05	0	100.7152	173.2574	242.5587	308.8963	372.5012	434.6273	496.8076	558.2516	619.7034	680.9768
G06	0	96.4817	165.9163	232.0363	294.2774	354.8399	414.0043	473.2695	531.8855	590.649	648.7635
G07	0	33.0108	51.6747	69.8837	87.493	104.9642	122.0214	139.4074	157.0753	175.3514	193.1631
G08	0	14.458	25.0061	40.1884	58.9269	79.8054	101.1601	123.6665	146.0313	168.6348	191.6607
G09	0	-17.3189	-29.774	-34.1259	-32.0909	-26.4474	-19.369	-12.4295	-4.6997	3.4414	11.584
G10	0	-12.6264	-22.9673	-30.5735	-30.9504	-27.2538	-21.4245	-14.5759	-7.3571	2.4146	8.8433
G11	0	24.6651	39.9076	56.2655	75.4887	97.1677	119.029	141.6336	164.0534	186.7999	209.6831
G12	0	63.5251	107.3379	152.1782	197.7197	243.2553	288.4245	333.458	378.7708	423.4006	468.5458
G13	0	62.0737	107.4292	151.7694	193.7505	234.9936	275.4982	315.7747	357.0739	398.0524	439.7759
G14	0	99.92	173.2474	243.7526	310.7365	375.2674	438.9232	502.216	564.7722	627.8486	690.0951
G15	0	97.8367	168.7455	237.2523	301.5003	363.6228	424.6389	485.5227	546.2289	606.6637	667.1525
G16	0	59.8914	102.1869	144.3002	186.6041	228.7708	271.3584	314.1349	357.0979	399.786	443.1759
G17	0	23.1561	38.5453	56.6622	78.7127	102.1518	126.4701	151.4359	176.4958	201.9729	227.7297
G18	0	11.8365	18.1465	25.657	34.2367	43.1868	52.885	63.1922	73.6898	83.9069	95.481

Gage	Original Raw Data (N = 2,100,000)										
	P = 0.00k	P = 9.25k	P = 18.50k	P = 27.75k	P = 37.00k	P = 46.25k	P = 55.50k	P = 64.75k	P = 74.00k	P = 83.25k	P = 92.50k
G01	0	-17.7238	-30.6619	-40.709	-42.6953	-40.2213	-36.1361	-31.5896	-26.4451	-19.6421	-14.3121
G02	0	14.7244	25.5709	38.1238	56.6747	77.6214	100.0976	122.3376	145.4145	169.1347	193.0451
G03	0	49.3897	84.8779	120.7862	158.5002	196.7701	235.2277	273.5461	312.0556	350.6581	388.8024
G04	0	101.1278	174.7343	245.0537	311.6667	376.105	438.5532	501.0093	562.8225	624.5035	684.8908
G05	0	100.7215	173.3615	243.178	309.1017	372.6644	435.0728	496.9319	558.6124	620.3002	681.2987
G06	0	96.5054	165.7035	232.0092	294.299	354.2563	413.4245	472.1787	531.0336	589.7545	647.546
G07	0	28.7195	47.2737	64.5754	82.8415	100.683	116.988	135.441	153.9186	172.0078	187.873
G08	0	14.4276	24.8435	39.1497	57.8296	78.6986	100.1375	122.5379	144.6678	167.357	190.1854
G09	0	-18.0638	-30.706	-35.5675	-33.5328	-28.1215	-21.1336	-13.8708	-6.0487	2.0948	9.7284
G10	0	191.4719	140.8971	105.1777	178.2823	144.2137	95.0897	64.2476	-240.168	-244.814	-258.842
G11	0	24.4758	40.1752	56.5745	76.3495	97.8855	120.3439	142.8982	165.6853	189.1209	211.8193
G12	0	62.5798	107.1007	151.6136	197.0443	242.3066	287.5628	333.3644	378.0576	423.3377	468.1445
G13	0	61.7757	108.4023	151.742	194.0658	235.2342	275.71	316.9314	357.6921	399.1057	440.0588
G14	0	100.1222	173.8336	244.2106	311.1594	375.8402	439.5536	502.9025	565.6559	628.7884	690.6273
G15	0	97.562	169.0767	236.8436	301.141	363.6358	424.6548	486.0984	546.157	606.6405	666.9459
G16	0	59.6106	102.227	143.8762	185.9944	228.4383	270.7454	313.7499	356.4352	399.4458	442.091
G17	0	22.7436	38.1363	56.1186	77.7089	101.1983	125.612	150.4885	175.416	201.0348	226.1031
G18	0	11.2242	17.4426	24.3418	33.0116	42.2435	52.3589	62.5225	72.2663	83.3703	94.0553

Gage	Original Raw Data (N = 2,300,000)										
	P = 0.00k	P = 9.25k	P = 18.50k	P = 27.75k	P = 37.00k	P = 46.25k	P = 55.50k	P = 64.75k	P = 74.00k	P = 83.25k	P = 92.50k
G01	0	-17.6305	-30.3831	-40.3821	-43.291	-41.4118	-38.059	-33.462	-28.0371	-22.4756	-17.0959
G02	0	13.5325	23.8329	35.374	52.9569	73.8598	96.1084	118.9965	142.1684	166.0762	189.9825
G03	0	48.2974	83.4756	119.2542	156.794	195.0293	233.3141	271.1397	309.5688	347.9958	386.3387
G04	0	99.375	172.5724	243.2715	310.4032	374.0124	436.1891	497.63	558.5204	619.6044	679.1609
G05	0	98.9517	171.7267	241.7716	308.2954	371.7147	433.9344	495.6038	557.1878	618.5471	679.1236
G06	0	95.4494	165.1637	231.5629	294.4582	354.4104	413.105	471.9468	530.1401	588.7616	646.6866
G07	0	28.5138	44.9087	60.2725	76.2226	92.1148	107.5208	123.0118	138.8955	156.1472	172.1566
G08	0	13.3019	23.1122	36.5649	54.1703	75.612	96.277	118.2208	140.2624	163.1367	186.0545
G09	0	-18.5308	-33.447	-39.4229	-38.405	-33.4092	-27.3457	-20.4491	-12.9946	-5.1301	2.6478
G10	0	-13.0074	-24.0653	-33.0858	-33.5123	-29.0441	-22.172	-15.72	-8.7114	-0.1815	8.3979
G11	0	23.3702	38.7952	54.0861	73.1688	94.4262	116.2383	138.7	161.2079	184.3179	206.7836
G12	0	61.4305	105.9365	150.4037	196.0696	241.4241	286.2547	331.621	376.9151	422.1489	466.3594
G13	0	60.2476	105.5771	149.4737	191.8905	231.9002	271.4493	310.9551	350.6499	390.7186	431.0225
G14	0	98.7227	171.8722	243.7776	311.2798	376.3752	439.2942	502.7792	565.2962	628.4717	690.1205
G15	0	96.3327	167.7707	236.3883	301.0719	363.3497	423.7324	484.0295	544.5659	605.2028	664.4075
G16	0	58.8652	100.8284	142.7957	184.8145	227.3466	269.3748	311.8166	354.5886	397.5927	439.586
G17	0	21.8651	36.0998	53.5256	74.4667	97.8165	121.5836	146.0415	171.3827	196.7218	221.5569
G18	0	10.8105	16.8933	23.6586	32.0528	40.9125	50.1458	60.3625	70.8135	81.2655	91.9091

Gage	Original Raw Data (N = 2,500,000)										
	P = 0.00k	P = 9.25k	P = 18.50k	P = 27.75k	P = 37.00k	P = 46.25k	P = 55.50k	P = 64.75k	P = 74.00k	P = 83.25k	P = 92.50k
G01	0	-19.3352	-32.5024	-43.9322	-47.6671	-45.8783	-42.9867	-38.3421	-33.6998	-28.1341	-22.3881
G02	0	13.1261	22.8287	34.2826	52.1899	72.9549	95.2916	117.7645	141.2104	165.3023	141.8028
G03	0	47.9306	83.3839	119.0723	156.5629	194.612	232.7089	270.5784	309.0033	347.526	385.9554
G04	0	100.3945	173.219	243.6845	311.3258	375.1196	437.853	499.4318	560.4142	620.8461	680.3086
G05	0	99.8825	172.3807	242.7989	309.5102	373.3959	435.5703	497.7524	558.9662	620.2339	680.9046
G06	0	96.4376	166.1092	233.2144	295.5044	355.5068	414.9075	473.425	531.6682	590.2931	648.456
G07	0	28.6856	46.0731	61.2279	75.2183	92.0518	108.2817	124.8411	141.8201	158.427	187.578
G08	0	11.805	20.5585	33.4716	52.0278	72.9385	94.2697	116.6731	138.7594	161.4023	184.2802
G09	0	-20.2851	-35.6601	-43.5326	-43.3512	-37.9837	-31.2273	-23.9614	-17.1132	-9.152	-0.9602
G10	0	-14.704	-28.8979	-41.2801	-44.2463	-38.9022	-28.6615	-19.4392	-10.6333	11.9446	-12.8035
G11	0	23.0976	38.1097	53.0802	71.4278	92.6391	114.4994	136.8691	159.0533	181.7978	204.6323
G12	0	62.3867	106.6907	151.2043	196.941	242.4415	287.7522	332.7383	377.5204	422.4853	467.0559
G13	0	61.6679	106.661	150.4533	192.1174	233.1362	274.4366	314.6275	354.868	395.2974	436.1937
G14	0	99.8293	173.2516	244.7798	312.6949	377.7848	441.7217	504.6441	567.4815	630.0944	692.2034
G15	0	96.8318	167.8904	236.4541	301.5009	363.7719	424.9833	485.5987	545.6179	605.5052	665.8171
G16	0	58.2665	100.2296	141.7353	184.1697	226.5153	269.2337	311.4906	354.449	397.3145	440.0911
G17	0	20.666	34.4394	50.8975	71.9334	95.1906	119.6043	144.2506	169.0832	194.3351	219.9095
G18	0	10.111	16.2897	22.1663	30.7956	39.6076	48.9785	59.1474	69.0359	79.3952	90.5986

Gage	Original Raw Data (N = 2,700,000)										
	P = 0.00k	P = 9.25k	P = 18.50k	P = 27.75k	P = 37.00k	P = 46.25k	P = 55.50k	P = 64.75k	P = 74.00k	P = 83.25k	P = 92.50k
G01	0	9.25	18.5	27.75	37	46.25	55.5	64.75	74	83.25	92.5
G02	0	-19.3289	-33.9497	-45.8816	-50.355	-48.5208	-45.1246	-40.7134	-35.7967	-30.2347	-23.7517
G03	0	12.7862	-47.407	-34.5206	-17.9672	2.7879	25.4397	48.4966	78.204	103.0314	127.2137
G04	0	48.8929	84.2959	120.1199	157.4702	195.5158	233.8382	272.0746	310.4488	348.9666	387.4371
G05	0	102.2945	176.0318	247.457	315.8704	380.2029	443.7534	506.1959	568.2269	629.4754	690.8249
G06	0	100.5401	173.6943	244.3501	311.9495	375.3756	438.3919	500.5328	562.3558	623.3498	684.7693
G07	0	96.3826	166.3545	234.0437	297.5781	358.3593	417.9785	476.762	535.4118	594.0218	652.6387
G08	0	9.0083	28.0017	45.944	63.5638	82.065	100.9994	119.5804	139.0554	158.525	172.5233
G09	0	13.1533	20.4623	33.128	50.0234	70.1359	91.7807	113.5052	135.6674	158.2599	181.2725
G10	0	-19.1283	-35.2879	-43.9489	-44.8299	-40.5755	-33.9131	-27.5757	-20.1268	-12.3084	-3.8394
G11	0	595.893	54556.69	54610.42	13435.47	17705.62	54302.8	54345.29	54329.1	54316.82	54376.04
G12	0	23.3684	37.6848	52.4242	70.9991	91.4258	113.2872	135.4732	158.1679	181.0505	203.5622
G13	0	61.9591	105.7984	149.6426	195.0122	240.3977	285.4449	330.6657	375.6493	420.4542	465.4156
G14	0	62.4397	107.6065	152.7776	196.0993	237.5249	278.3051	319.5519	360.9415	402.4733	444.7039
G15	0	99.6369	173.3328	245.414	314.0676	379.0607	443.2721	506.2833	569.4884	631.9116	694.2029
G16	0	97.9281	169.717	238.9184	304.5112	366.7717	428.6229	489.6459	550.1198	610.8328	671.321
G17	0	58.501	100.0097	141.3366	183.0843	224.8827	267.4685	309.9664	352.8358	395.4762	438.4923
G18	0	21.6349	34.7158	50.9911	71.01	93.6673	117.8512	142.036	166.9595	192.1178	217.5079

Gage	Original Raw Data (N = 2,900,000)										
	P = 0.00k	P = 9.25k	P = 18.50k	P = 27.75k	P = 37.00k	P = 46.25k	P = 55.50k	P = 64.75k	P = 74.00k	P = 83.25k	P = 92.50k
G01	0	-20.2625	-35.2333	-47.4905	-52.2135	-50.9453	-47.8735	-42.8753	-37.785	-32.1839	-26.2145
G02	0	18.423	28.9301	40.0088	56.5964	77.3143	98.674	121.3398	144.2744	167.9136	191.6023
G03	0	49.4866	84.6093	120.4727	158.0029	196.413	234.2226	272.9134	311.2357	349.4252	388.1253
G04	0	103.2615	177.6896	249.9443	318.492	383.8881	446.6425	508.9866	570.6876	631.0476	692.2516
G05	0	102.3445	176.0978	247.3529	314.6694	379.0674	441.5218	503.984	565.4781	626.7471	688.0236
G06	0	97.9878	168.553	236.4584	299.7826	360.6321	419.755	478.9326	537.7416	596.6512	655.1463
G07	0	27.0286	44.0149	60.8637	77.3941	94.2041	110.2903	126.4545	143.1844	161.6578	180.085
G08	0	12.8603	21.3271	34.242	51.101	71.3463	92.188	114.0065	136.2995	158.7457	181.4738
G09	0	-19.9238	-36.5575	-44.5277	-45.458	-41.0165	-35.2319	-28.1505	-20.9309	-13.4791	-5.1469
G10	0	0	0	-44858.7	0	-51361	0	0	0	0	0
G11	0	22.7345	36.7318	50.6914	68.7212	89.2472	110.4696	132.0186	154.3996	176.8284	199.6724
G12	0	62.5725	106.1406	151.014	197.3039	242.9513	287.556	333.1366	377.6404	422.4217	467.3908
G13	0	60.3205	104.4178	147.2669	188.6819	228.0597	266.5588	305.4788	343.9841	383.6987	424.2049
G14	0	101.5179	175.8818	248.6767	317.0683	382.7271	446.3496	509.8409	572.8291	635.3131	697.9446
G15	0	99.3863	172.0257	241.7993	307.4523	370.0519	431.4985	492.6277	553.2073	613.8408	674.0634
G16	0	59.7471	101.7565	143.2166	184.6813	227.4944	269.4288	311.734	354.2749	397.2378	440.2948
G17	0	22.1951	35.046	51.2754	71.3916	94.3317	117.9645	142.5715	167.2233	191.9237	217.6892
G18	0	10.1026	15.4827	20.655	28.297	37.198	46.3306	55.9288	65.8104	76.1185	86.8927

B.2 ORIGINAL RAW DATA FROM GALVANIZED STEEL SPECIMEN

Gage	Original Raw Data (N = 0)										
	P = 0.00k	P = 9.30k	P = 18.60k	P = 27.90k	P = 37.20k	P = 46.50k	P = 55.80k	P = 65.10k	P = 74.40k	P = 83.70k	P = 93.00k
G01	0	0.1371	-1.4046	-1.6435	1.0125	3.9408	7.3326	9.608	14.3618	18.4155	29.5738
G02	0	19.9219	33.0148	45.8308	59.6152	73.6278	87.1786	100.6378	114.3709	127.7806	141.467
G03	0	54.4659	94.4533	133.8436	173.1931	212.4057	252.2256	291.4497	330.7661	370.3652	410.0116
G04	0	93.2085	162.4181	229.4067	294.7319	359.9261	424.5246	488.2482	551.4686	614.7436	678.3981
G05	0	89.8304	155.3361	218.2539	279.3245	339.7532	399.2615	457.9422	516.4903	574.3955	632.5861
G06	0	89.5685	156.198	220.9774	283.9059	346.7029	408.7639	470.2744	531.0489	592.2489	652.8054
G07	0	51.0482	87.7082	126.5897	165.5664	205.3777	245.1942	284.5059	324.4218	364.1567	404.3109
G08	0	19.9838	32.9832	50.6105	70.6424	92.0623	114.0857	135.9727	158.3679	181.1343	203.9472
G09	0	-8.2113	-16.8818	-18.8629	-16.5117	-12.7359	-8.2239	-3.014	2.8853	8.8288	15.0028
G10	0	-1.3309	-3.7298	-3.7279	-1.2296	2.282	6.4851	10.8287	16.3675	21.908	28.1386
G11	0	25.3921	43.2541	61.9059	80.6499	100.2719	119.85	139.9405	160.0737	180.2997	200.6195
G12	0	44.2846	74.9512	104.826	136.5674	170.9201	200.4278	231.7103	260.9882	290.5021	321.274
G13	0	90.3425	157.2284	219.7157	281.7939	342.5799	401.3777	460.2289	518.1126	575.1202	631.856
G14	0	91.9949	159.8548	225.9159	289.4356	353.5661	417.1484	479.9035	542.8523	606.5974	668.7734
G15	0	88.2067	153.861	217.2947	278.8327	340.3311	401.3265	461.818	521.945	581.7077	641.7095
G16	0	52.7642	90.7764	130.1363	169.1322	208.7322	248.6137	287.8504	327.2286	366.9791	406.7318
G17	0	25.5313	42.5337	62.5789	84.3356	106.6912	129.6948	152.1951	175.4776	198.8986	222.7359
G18	0	10.4083	16.4023	24.7995	33.387	42.3062	51.1327	59.7213	69.0671	78.2692	87.8961

Gage	Original Raw Data (N = 100,000)										
	P = 0.00k	P = 9.30k	P = 18.60k	P = 27.90k	P = 37.20k	P = 46.50k	P = 55.80k	P = 65.10k	P = 74.40k	P = 83.70k	P = 93.00k
G01	0	-5.2774	-10.9245	-14.5212	-13.4071	-11.6458	-7.6392	-3.7735	0.3708	5.9657	11.0914
G02	0	18.9645	31.5614	43.9676	57.7073	71.672	85.494	99.0416	112.5858	126.037	139.5363
G03	0	53.9216	92.8967	131.9257	171.3305	211.1983	251.1193	290.255	329.9948	369.2732	409.1131
G04	0	96.7219	168.2883	237.6356	304.205	369.3891	433.7453	497.0873	560.5772	623.7956	686.4181
G05	0	92.2497	160.5439	225.5089	287.6067	348.8307	408.8099	467.4041	526.0048	584.4274	642.3002
G06	0	92.5039	161.9274	228.7116	292.6224	355.7046	417.8186	478.7781	539.6977	600.5321	660.8619
G07	0	50.1665	86.1774	123.8063	163.2422	202.7261	242.3529	281.8469	321.6671	361.6763	401.5024
G08	0	16.4708	26.2322	40.5756	59.917	80.5964	102.2027	124.4607	147.3681	170.0907	192.861
G09	0	-16.4226	-31.2755	-38.8385	-39.2594	-35.6672	-31.8022	-26.1341	-21.5768	-14.9417	-9.9234
G10	0	-8.1041	-16.5855	-21.3307	-20.6312	-17.578	-13.1416	-8.3851	-2.382	4.1268	10.6342
G11	0	22.3884	37.3873	54.1423	72.5603	92.2738	112.494	132.3935	152.8012	173.7182	194.3112
G12	0	42.9834	73.9806	105.3953	136.4398	167.8561	199.2291	230.0006	261.9371	294.4804	325.5792
G13	0	93.5801	162.1764	228.9262	290.7674	352.0129	412.1059	470.9062	529.4351	587.414	644.842
G14	0	94.9169	165.9773	235.1467	300.6628	365.6772	429.4009	492.1129	554.832	617.2814	679.8306
G15	0	91.6025	159.8626	225.8559	289.4892	351.3652	413.2488	473.1882	533.5997	594.0184	655.6532
G16	0	52.3608	89.5023	128.3608	167.9203	207.2033	246.5367	285.78	325.1651	365.0134	404.5903
G17	0	22.0298	35.0247	52.7181	73.3666	95.3998	117.8496	140.8549	164.1809	187.7388	211.4341
G18	0	7.8725	11.7097	17.794	26.1004	34.5036	43.4707	52.485	61.9248	71.7386	81.6476

Gage	Original Raw Data (N = 200,000)										
	P = 0.00k	P = 9.30k	P = 18.60k	P = 27.90k	P = 37.20k	P = 46.50k	P = 55.80k	P = 65.10k	P = 74.40k	P = 83.70k	P = 93.00k
G01	0	-9.2429	-19.0439	-25.5325	-25.6796	-24.9432	-21.3595	-17.8224	-12.3718	-7.3847	-2.2133
G02	0	18.6486	31.4401	43.2517	56.9025	70.7309	84.6949	98.5178	112.5226	126.3434	140.213
G03	0	53.159	91.6838	129.8723	168.8511	208.2976	247.9772	287.7999	327.8073	367.4963	407.7451
G04	0	98.6156	171.661	241.9769	308.3075	373.5785	438.2538	501.7756	565.5843	628.8433	692.5291
G05	0	93.7322	163.1387	229.4014	291.684	352.444	412.5624	471.6196	531.288	590.0354	649.2072
G06	0	94.1371	164.0313	231.6113	295.2953	357.6855	419.8045	481.047	542.112	603.1835	664.1236
G07	0	49.9536	85.6081	122.4652	160.9906	200.5385	240.3207	280.2464	320.3109	360.5208	400.5484
G08	0	14.2497	22.9043	35.0734	53.627	74.4963	96.1496	118.9635	141.9161	164.6859	187.5949
G09	0	-18.4051	-35.0545	-45.2016	-45.8493	-43.2725	-39.2206	-33.2775	-28.1209	-21.993	-15.3569
G10	0	-11.5148	-22.713	-29.9888	-30.6246	-28.6293	-24.2413	-18.9752	-12.516	-5.5454	1.1008
G11	0	20.4959	33.742	48.8837	66.6603	85.4537	105.5401	125.7666	146.406	167.4203	188.4319
G12	0	44.0049	74.6271	105.8105	136.6212	167.0122	198.2441	229.8529	261.6438	292.8816	325.5187
G13	0	94.6634	164.1067	229.384	291.8858	352.8639	412.4102	471.825	530.1784	587.9816	646.0237
G14	0	96.5028	168.5441	237.8136	303.7542	368.1261	431.9499	494.8997	557.8585	620.2675	683.2877
G15	0	92.5339	162.0967	228.7429	291.9139	353.6529	415.0279	475.6201	535.8943	595.8043	656.6043
G16	0	51.7582	88.8557	126.7461	165.6116	204.7142	244.6512	284.0344	324.1602	363.8258	403.7716
G17	0	20.3284	31.9881	47.8912	68.3136	89.5232	112.4416	135.772	159.7041	183.3132	207.1528
G18	0	7.6374	10.3013	14.79	22.251	30.1864	38.7305	48.078	57.6129	67.2893	77.0101

Gage	Original Raw Data (N = 300,000)										
	P = 0.00k	P = 9.30k	P = 18.60k	P = 27.90k	P = 37.20k	P = 46.50k	P = 55.80k	P = 65.10k	P = 74.40k	P = 83.70k	P = 93.00k
G01	0	-10.1012	-18.5105	-25.7543	-25.8062	-25.023	-21.0106	-14.3309	-7.7461	-1.2526	4.6767
G02	0	18.8405	31.9162	44.1082	57.3469	71.4088	85.191	99.0616	112.6541	126.1986	139.7951
G03	0	53.5445	92.4618	130.6536	169.9185	209.6943	249.4273	289.0229	328.8084	368.7837	408.2056
G04	0	99.6576	174.1586	246.7657	314.6906	380.7195	445.6419	509.9679	573.0471	636.3669	699.6949
G05	0	95.4434	166.0993	234.4002	298.1649	359.9436	420.3844	479.9984	538.7368	597.8534	656.3738
G06	0	95.1079	166.4856	235.7351	300.6716	363.8026	426.0588	487.8576	549.0121	609.8026	670.1351
G07	0	49.4322	85.4029	121.6494	160.3492	199.9341	239.8007	279.808	319.5886	359.837	399.6698
G08	0	13.5121	21.4246	32.1146	50.114	70.7957	92.4978	114.9411	137.4781	160.3863	182.7396
G09	0	-20.5704	-37.0768	-51.6982	-54.2854	-52.0325	-48.9523	-44.0262	-38.2679	-32.2806	-26.3831
G10	0	-13.4978	-26.7696	-36.8586	-39.9833	-38.5444	-34.6138	-29.6754	-23.4425	-17.1184	-10.8878
G11	0	20.2207	33.0045	47.3128	64.7662	83.8354	103.6417	123.7244	144.5501	165.3739	186.0599
G12	0	43.0122	73.2476	104.6468	135.302	146.8568	169.0752	194.4015	220.2656	247.9969	278.1975
G13	0	96.9064	168.9262	238.7297	303.3007	365.2822	426.0644	485.7872	544.3101	602.6541	660.2157
G14	0	97.5293	171.1989	242.5607	309.4803	374.7391	439.0319	502.637	565.276	628.0158	690.1602
G15	0	93.8778	164.5067	233.4271	297.8049	360.5647	421.9385	483.7381	544.151	604.525	664.5344
G16	0	51.4286	88.3341	125.942	165.2202	204.5496	244.1114	284.085	323.6509	363.5418	403.3925
G17	0	19.9567	30.6928	45.1181	65.2172	86.702	108.9251	132.2033	156.0365	179.9683	203.992
G18	0	8.3927	10.8174	15.2599	21.9635	30.4124	39.1451	48.3474	57.9257	67.7416	77.5553

Gage	Original Raw Data (N = 500,000)										
	P = 0.00k	P = 9.30k	P = 18.60k	P = 27.90k	P = 37.20k	P = 46.50k	P = 55.80k	P = 65.10k	P = 74.40k	P = 83.70k	P = 93.00k
G01	0	-12.3476	-26.6612	-37.5593	-41.7307	-40.9921	-37.6438	-35.0345	-30.1818	-25.3322	-21.5102
G02	0	19.3098	32.7607	45.466	59.077	73.0481	87.4282	100.8392	114.7529	128.7611	142.5378
G03	0	53.5878	92.3243	131.3921	170.1874	209.8648	249.8148	288.9458	329.1419	368.7855	408.4342
G04	0	101.3544	178.1154	252.5653	321.4985	387.5604	452.9343	516.5039	580.1282	643.8071	707.1689
G05	0	96.5111	169.0228	239.5972	304.3381	365.9792	427.0251	487.0111	546.4946	606.0308	665.7596
G06	0	96.0851	168.8116	239.7356	305.2311	368.5036	430.8072	491.8631	553.2521	613.9971	674.9359
G07	0	49.4823	85.2236	121.2435	159.7171	199.1667	238.8982	278.2648	318.7431	358.9015	398.6934
G08	0	12.955	19.3861	28.5923	45.1514	65.3684	86.9267	108.9051	132.0866	154.8985	177.6191
G09	0	-20.7945	-40.7211	-57.2341	-60.6036	-58.9511	-54.9932	-50.4794	-44.6766	-38.8272	-32.8367
G10	0	-15.9422	-32.5265	-45.655	-49.653	-48.3496	-44.699	-39.7524	-33.4291	-27.2446	-20.7827
G11	0	18.8777	30.1833	43.4791	60.0509	78.3792	98.3235	118.3152	139.0919	159.7761	180.5519
G12	0	43.7326	75.1177	106.0357	137.9807	168.906	200.7605	231.7382	263.6904	295.1325	327.2745
G13	0	96.7827	169.9736	240.5769	305.1123	366.6861	426.8285	486.0968	544.7224	603.7255	661.5749
G14	0	98.964	178.2418	250.7153	318.9792	384.0055	448.9007	513.9899	576.5359	639.4605	701.8366
G15	0	94.6694	166.6467	236.7767	301.9456	364.3824	426.1761	486.8625	547.2769	607.6991	667.9424
G16	0	51.9915	88.3465	125.2186	163.9916	203.1849	242.9347	282.3684	322.5392	362.3902	402.0122
G17	0	19.7271	29.7743	41.9448	61.0786	82.2475	105.0732	127.9023	151.6985	175.5412	199.5235
G18	0	8.8098	11.5679	14.0346	20.7387	28.8118	36.9767	45.5208	55.0513	65.0996	74.8662

Gage	Original Raw Data (N = 700,000)										
	P = 0.00k	P = 9.30k	P = 18.60k	P = 27.90k	P = 37.20k	P = 46.50k	P = 55.80k	P = 65.10k	P = 74.40k	P = 83.70k	P = 93.00k
G01	0	-17.5049	-32.8464	-48.5665	-55.0281	-54.6164	-52.5696	-49.2607	-45.4832	-39.9725	-35.3992
G02	0	18.5888	31.8681	44.7249	57.9786	71.5844	85.4148	99.0562	112.5119	126.2444	139.8398
G03	0	51.8772	89.6922	127.8818	166.5397	205.8945	245.6689	285.2606	324.9502	364.5011	404.2436
G04	0	102.3475	179.5394	255.5361	327.0371	393.7153	458.6832	522.6367	585.7617	648.7552	712.1287
G05	0	98.9472	171.9072	243.5332	310.3006	373.0426	433.8906	493.6327	552.2689	611.4683	670.4427
G06	0	98.287	171.7826	244.4528	312.3002	376.438	438.9575	500.5549	561.2295	622.1445	682.8804
G07	0	49.1888	83.9934	119.4484	157.4946	196.9339	236.6536	276.2389	316.3374	356.3923	396.4512
G08	0	10.0373	14.7563	20.9563	35.4359	55.192	76.4279	98.7307	121.0804	144.2188	166.8961
G09	0	-26.2931	-48.985	-69.835	-77.7233	-77.3148	-74.4196	-69.8609	-64.3784	-58.6664	-52.9071
G10	0	-21.6158	-42.5761	-61.1371	-70.2949	-71.0181	-68.1943	-62.9293	-57.6203	-51.1591	-44.6992
G11	0	15.8708	25.1937	35.8117	50.6316	68.872	88.4499	108.6764	129.1792	150.5627	170.9722
G12	0	42.5254	73.1808	101.6935	131.6504	161.2854	192.3142	222.6494	253.2676	284.6294	316.2275
G13	0	97.3931	169.7079	240.9199	306.2491	366.7136	424.7722	481.3057	536.8243	592.3026	648.3909
G14	0	101.738	177.8579	253.6185	324.0571	390.2387	454.7591	518.2673	580.9022	643.637	705.8699
G15	0	98.0574	171.056	243.6933	310.7205	374.3652	436.113	497.4035	557.4933	617.497	677.8335
G16	0	52.3509	88.3769	124.1298	162.5224	201.7067	241.2639	280.591	320.1055	359.9472	399.5596
G17	0	18.2846	26.4844	35.6555	52.2915	72.7588	94.7912	117.5176	141.2114	164.998	188.6465
G18	0	10.3213	13.318	14.85	20.5194	28.1234	36.8115	45.7814	55.2192	65.0821	74.5198

Gage	Original Raw Data (N = 900,000)										
	P = 0.00k	P = 9.30k	P = 18.60k	P = 27.90k	P = 37.20k	P = 46.50k	P = 55.80k	P = 65.10k	P = 74.40k	P = 83.70k	P = 93.00k
G01	0	-18.8916	-37.2284	-53.0901	-62.6389	-63.3489	-62.2375	-58.555	-54.1683	-49.2216	-46.0061
G02	0	18.4515	31.6874	45.2865	57.663	71.1291	84.5448	98.3694	112.1461	125.6927	138.6395
G03	0	52.1082	89.6454	128.0205	166.355	205.5245	245.2564	284.8003	324.7669	364.5072	403.7837
G04	0	104.2438	182.4988	259.8836	331.705	399.0296	463.9466	528.2677	591.9466	654.7967	718.3051
G05	0	99.8472	174.0736	247.6615	314.86	377.9398	439.0782	499.3438	558.9658	618.1312	677.1182
G06	0	99.5247	174.1113	248.1049	316.2519	380.5958	442.9949	504.2849	565.7226	626.5163	687.0385
G07	0	49.4333	84.2454	119.7553	156.7945	196.0578	235.6508	275.5237	315.6336	355.7446	395.1185
G08	0	9.2987	13.2316	19.0587	32.0577	51.1167	71.9813	93.8174	116.5813	139.3925	162.1129
G09	0	-27.3904	-51.6013	-73.0962	-80.9363	-81.1722	-78.5028	-73.9913	-68.3285	-62.1089	-56.8081
G10	0	-23.3703	-46.265	-66.8951	-77.5284	-78.8048	-76.6244	-71.867	-65.2653	-58.7559	-52.9372
G11	0	14.3525	21.8793	31.0722	44.2787	61.3191	79.5146	99.5566	120.2455	140.4726	160.0565
G12	0	40.6832	69.7152	99.4898	129.6843	159.5534	189.5664	220.1857	250.8978	281.9837	312.6076
G13	0	97.3417	169.9198	241.0227	305.9151	365.6164	423.1428	479.1428	534.5456	588.7931	641.4206
G14	0	101.9005	178.8728	255.718	326.4516	392.8809	456.9523	520.5223	583.1713	645.6891	707.8901
G15	0	97.8	171.4646	244.8144	312.5531	375.8398	437.3224	497.9754	558.2643	617.9556	677.5151
G16	0	52.0283	88.1515	124.5564	162.6759	201.818	240.6848	280.3386	320.1325	359.8864	399.2257
G17	0	18.7544	26.2669	34.9823	50.427	70.3471	91.7899	114.8445	138.6851	162.2457	185.7208
G18	0	9.575	10.6905	11.5667	15.78	22.5863	29.7218	38.503	47.285	56.3488	64.4679

Gage	Original Raw Data (N = 1,100,000)										
	P = 0.00k	P = 9.30k	P = 18.60k	P = 27.90k	P = 37.20k	P = 46.50k	P = 55.80k	P = 65.10k	P = 74.40k	P = 83.70k	P = 93.00k
G01	0	-19.0817	-39.0644	-56.6631	-66.4004	-68.4691	-66.655	-64.4684	-59.6574	-56.5335	-51.912
G02	0	17.9	30.8622	44.005	56.198	69.4821	83.1279	96.9534	110.3628	123.8662	136.9954
G03	0	51.3635	88.2065	126.0242	164.262	203.5692	243.0629	282.7932	322.1076	361.4736	401.1682
G04	0	103.9519	182.0577	260.1293	332.9636	400.3262	465.7462	529.5019	592.8473	655.6432	718.3537
G05	0	99.6139	173.6075	246.9625	315.134	378.7229	439.907	499.4292	558.7254	617.2408	675.855
G06	0	100.0014	174.9684	249.3897	318.9398	383.8488	446.5813	508.0653	569.0458	629.5215	690.1442
G07	0	49.1025	83.8656	119.2326	156.1727	195.2017	234.9269	274.2862	314.2059	353.8028	393.4497
G08	0	8.2346	11.3348	16.2365	28.2188	46.6762	67.3998	89.145	111.6313	134.4439	156.9316
G09	0	-28.9545	-54.8261	-78.349	-89.6487	-91.1783	-88.8788	-84.6908	-79.6238	-74.1428	-68.7992
G10	0	-24.7958	-49.9024	-72.6492	-85.6317	-88.7986	-86.386	-82.3677	-76.4104	-70.1319	-63.7618
G11	0	13.6166	20.268	28.0313	40.4084	57.0821	75.7413	95.0946	115.3256	135.4644	155.6509
G12	0	41.2063	69.3115	98.4427	128.4565	158.4253	188.8614	219.0665	248.8998	279.0156	309.645
G13	0	96.5469	167.6821	238.8268	303.5299	363.0417	419.6353	474.8427	528.8485	582.1633	635.4842
G14	0	102.3064	179.8265	257.5441	329.8005	396.4548	461.3551	524.7324	587.1428	649.8402	711.988
G15	0	97.9764	172.2374	246.2772	314.8922	378.7775	440.8118	501.5526	561.5568	621.1498	680.6104
G16	0	51.8393	87.8206	124.0834	161.7364	200.6886	239.8272	279.2922	318.8068	358.4643	398.0301
G17	0	17.0916	24.1889	31.6569	45.854	65.0343	86.75	109.6651	132.7172	156.3705	179.9333
G18	0	9.151	10.6471	10.7722	14.42	20.6147	28.5519	36.7246	45.4598	54.7609	63.5419

Gage	Original Raw Data (N = 1,300,000)										
	P = 0.00k	P = 9.30k	P = 18.60k	P = 27.90k	P = 37.20k	P = 46.50k	P = 55.80k	P = 65.10k	P = 74.40k	P = 83.70k	P = 93.00k
G01	0	-23.6177	-43.6876	-63.0608	-74.6683	-76.7335	-76.0917	-74.0444	-70.1254	-65.647	-61.4002
G02	0	17.3511	30.2218	43.2748	55.471	68.3885	81.8501	95.1232	108.3005	121.8486	135.1195
G03	0	51.2731	88.3905	126.3012	164.3537	203.2886	243.3402	282.8374	322.3852	362.3522	401.8157
G04	0	105.9505	185.3114	263.9882	338.1717	406.4649	472.6767	537.5033	600.9903	665.0427	727.8019
G05	0	101.6469	177.6752	252.2778	322.3466	387.4162	450.0355	511.6424	572.375	632.6506	692.8874
G06	0	101.058	176.9927	251.8697	322.3416	388.0346	450.8531	513.5392	574.7459	635.8663	696.0639
G07	0	48.6908	83.7333	118.9633	155.9545	194.9389	234.6685	274.6345	314.5125	354.622	394.4125
G08	0	6.8029	9.6247	13.7408	24.9829	42.749	63.1541	84.9476	106.6512	130.0219	152.2814
G09	0	-31.5868	-58.2443	-82.3695	-95.2864	-97.5075	-95.7622	-92.1742	-87.1528	-81.6718	-76.0029
G10	0	-27.3809	-53.0888	-77.6347	-91.9569	-95.8585	-94.9237	-90.9939	-85.7294	-79.6796	-73.7238
G11	0	12.921	18.8772	26.7807	39.1098	55.5014	73.7433	93.5551	113.5977	134.2417	154.7938
G12	0	40.5482	69.8143	99.8725	130.4875	161.2434	192.2304	223.6454	254.3607	286.1005	317.2879
G13	0	99.2441	173.6782	246.6849	314.1779	376.5263	435.6786	494.5594	550.7533	606.396	662.1846
G14	0	103.6229	181.76	259.6309	332.8749	400.4229	465.9387	530.1169	593.1431	655.8982	718.1973
G15	0	99.5116	174.7505	249.3498	319.1292	384.1318	446.6334	508.3061	568.7312	628.9313	688.7668
G16	0	51.8966	87.7442	123.8734	161.5332	200.9102	240.0092	279.8064	319.3292	359.1763	398.4254
G17	0	16.1737	22.9496	30.3265	44.341	63.3382	84.8262	107.1427	130.5675	154.0378	177.7867
G18	0	8.3532	9.3763	9.1699	12.5348	19.1066	26.9954	35.4511	44.7022	53.9058	63.5816

Gage	Original Raw Data (N = 1,500,000)										
	P = 0.00k	P = 9.30k	P = 18.60k	P = 27.90k	P = 37.20k	P = 46.50k	P = 55.80k	P = 65.10k	P = 74.40k	P = 83.70k	P = 93.00k
G01	0	-23.0565	-44.0136	-63.9019	-76.3007	-81.1788	-80.0201	-77.1307	-73.3049	-68.8249	-63.7828
G02	0	17.584	30.4581	43.745	55.6231	68.4031	82.0053	95.8324	109.2418	122.9743	136.4769
G03	0	50.8131	87.8395	125.5196	163.3889	202.2799	241.6376	281.1348	321.1013	360.5139	400.3018
G04	0	105.2522	184.7051	263.5203	338.0275	407.0174	472.9959	537.7283	601.586	664.9873	728.2574
G05	0	101.3512	177.7375	253.0692	324.61	389.9929	453.1121	515.3115	576.4976	636.9957	698.0576
G06	0	100.5859	176.7006	251.8972	322.8747	388.6552	451.9337	514.1972	575.3527	636.4221	697.0802
G07	0	48.2238	83.2652	118.1693	154.6482	193.4906	233.0327	272.9483	312.868	352.9309	392.902
G08	0	6.5668	9.0654	12.3935	22.2469	39.4992	59.3907	81.3648	103.6654	126.3835	149.0549
G09	0	-31.2631	-58.6599	-84.5378	-100.037	-102.949	-101.989	-98.213	-93.5631	-88.3124	-82.23
G10	0	-27.4677	-53.7257	-79.3251	-95.8566	-100.681	-99.8364	-95.861	-90.5494	-84.7786	-78.5487
G11	0	12.4118	18.5057	25.4865	37.0749	52.9579	71.3835	90.915	111.3713	131.8286	152.7033
G12	0	41.1765	70.7046	100.6511	131.3434	161.8934	192.777	224.03	255.4258	286.7292	318.2677
G13	0	100.6596	176.0056	251.2694	321.2537	384.378	446.6282	505.1254	564.2796	621.908	678.8
G14	0	103.1393	181.725	259.8592	334.0168	402.016	467.1478	531.6852	594.6994	657.2112	720.0087
G15	0	99.3071	174.4386	249.9532	320.2295	385.4526	448.314	509.7427	570.6679	630.8567	691.0063
G16	0	51.4272	87.5948	123.4429	160.959	199.5434	238.6858	278.4322	317.9482	357.607	397.4526
G17	0	15.5703	21.9291	28.6594	41.4269	59.7744	80.4742	103.1105	126.1161	150.0449	173.2333
G18	0	8.4901	9.559	8.7451	11.8269	17.877	25.2465	33.8886	42.9052	52.4827	62.0629

Gage	Original Raw Data (N = 1,900,000)										
	P = 0.00k	P = 9.30k	P = 18.60k	P = 27.90k	P = 37.20k	P = 46.50k	P = 55.80k	P = 65.10k	P = 74.40k	P = 83.70k	P = 93.00k
G01	0	-25.92	-48.4227	-69.9057	-85.8076	-90.737	-91.0798	-88.147	-85.3561	-80.6326	-76.4247
G02	0	17.1285	29.7281	42.6477	54.8563	67.3165	80.7351	94.4272	108.1138	121.848	135.3039
G03	0	50.3503	86.9129	124.2173	161.6208	200.3705	239.5732	279.0231	318.7068	358.6254	398.4561
G04	0	106.284	186.7662	266.89	342.8916	412.9105	480.2438	545.7274	609.9179	674.0234	737.8118
G05	0	102.9713	180.5609	257.4212	330.2126	397.5889	462.3308	525.4573	586.9217	648.9969	710.5233
G06	0	102.2316	178.8841	255.5021	327.577	394.8287	459.3467	522.1062	583.8507	645.4171	706.1997
G07	0	48.3172	82.847	117.9811	154.1823	193.0254	232.5183	272.7127	312.6328	352.8786	392.6648
G08	0	4.9072	6.0635	8.4674	16.562	32.7535	52.3695	73.0971	95.2622	117.8434	140.3341
G09	0	-34.1692	-63.7309	-91.1322	-108.8	-113.88	-114.213	-111.686	-107.128	-102.017	-96.95
G10	0	-29.7315	-58.2039	-85.8791	-104.436	-112.905	-113.811	-111.54	-106.733	-101.101	-95.5596
G11	0	11.5316	16.3335	22.2947	32.4066	47.0879	64.5897	83.6576	103.3734	124.0133	144.6079
G12	0	40.8775	70.014	99.531	129.8789	160.5648	190.971	222.6299	253.7375	285.3109	316.9334
G13	0	101.1344	176.9047	252.1771	322.6796	387.7136	448.8099	507.8705	565.4521	623.2262	680.3565
G14	0	104.4706	183.6841	263.328	338.3912	408.0366	474.443	538.7694	603.0579	666.3794	729.0591
G15	0	100.3313	176.812	252.6544	324.1878	390.9462	454.9719	516.8215	577.8423	638.8704	699.2554
G16	0	51.2416	86.9451	123.2093	160.771	199.4016	238.4952	278.0557	317.803	357.6434	397.5365
G17	0	14.1893	19.4875	25.6188	36.9129	54.3866	74.5826	96.577	119.447	143.1487	166.4782
G18	0	7.7846	8.1005	7.3334	9.6646	15.3847	22.4701	30.7775	39.6517	49.323	58.9929

Gage	Original Raw Data (N = 2,100,000)										
	P = 0.00k	P = 9.30k	P = 18.60k	P = 27.90k	P = 37.20k	P = 46.50k	P = 55.80k	P = 65.10k	P = 74.40k	P = 83.70k	P = 93.00k
G01	0	-25.2176	-48.8042	-70.1022	-86.1534	-93.5269	-94.9944	-92.5189	-89.4347	-85.4156	-80.3605
G02	0	16.4851	28.6725	41.7826	53.5786	65.8601	79.7435	93.3914	106.9415	120.864	134.3691
G03	0	50.0245	86.3564	123.3396	161.2049	199.5893	238.9447	278.4873	317.7559	358.0467	397.5063
G04	0	106.0482	186.0639	266.6029	343.4387	414.6634	481.3447	547.1049	610.8284	674.514	738.2539
G05	0	102.5889	180.448	257.6706	331.5666	399.8631	464.2734	527.7179	589.2689	651.0124	712.3926
G06	0	101.5332	178.3235	255.126	328.6404	396.3094	460.594	523.3985	584.91	646.1495	707.2102
G07	0	47.9454	82.5682	117.4235	153.4859	191.9573	231.451	271.457	311.1431	351.4345	391.4509
G08	0	4.5831	5.6475	7.8669	14.3878	29.2827	48.8073	69.7177	91.9743	114.5558	136.9519
G09	0	-34.2587	-63.8646	-92.0931	-112.481	-119.497	-119.826	-117.252	-112.926	-107.997	-102.747
G10	0	-29.8216	-57.8787	-86.7942	-108.254	-117.179	-118.684	-115.859	-111.377	-105.788	-100.111
G11	0	11.3939	16.5641	21.603	30.7454	44.9195	62.5594	81.721	101.806	122.2142	142.9474
G12	0	40.8069	69.9348	99.8379	130.3569	160.2077	191.4	222.7332	254.1114	286.0075	317.3381
G13	0	101.6372	177.7282	253.8771	326.1385	391.076	451.9831	512.0153	570.5221	628.4321	685.745
G14	0	103.5082	182.499	262.4765	338.6149	408.4075	474.8678	539.5729	602.9403	665.6188	728.5377
G15	0	100.44	176.8401	253.4837	326.7473	393.9349	457.9245	520.342	581.2333	641.8998	702.5733
G16	0	51.3821	86.9451	123.3036	160.3547	199.0807	237.8966	277.1336	316.9274	356.678	396.4768
G17	0	14.7442	20.5484	25.9885	35.7609	52.4513	72.5088	94.5928	117.5544	140.8843	164.1704
G18	0	7.5938	8.4763	7.5705	9.1026	13.9294	20.7318	29.1344	37.7234	47.2524	57.1116

Gage	Original Raw Data (N = 2,300,000)										
	P = 0.00k	P = 9.30k	P = 18.60k	P = 27.90k	P = 37.20k	P = 46.50k	P = 55.80k	P = 65.10k	P = 74.40k	P = 83.70k	P = 93.00k
G01	0	-25.6366	-48.0008	-69.5317	-87.0303	-94.0283	-94.7895	-93.8667	-90.3606	-87.5121	-82.8333
G02	0	17.8737	30.8023	45.3491	55.296	67.4373	81.6944	94.2334	107.5532	120.6883	134.194
G03	0	50.3653	86.7193	123.647	161.3438	199.7248	238.8469	278.2515	317.7519	357.1628	397.088
G04	0	105.9957	186.146	267.0055	344.3012	415.2436	482.4784	547.3055	611.3512	674.568	738.3972
G05	0	102.9206	180.3214	257.8273	332.0998	400.0302	464.0273	526.3167	587.4077	648.4135	709.3804
G06	0	101.7735	179.2203	256.4469	330.5712	398.2457	463.0931	525.7176	587.0946	648.4319	709.1256
G07	0	48.1742	82.7032	117.4635	153.7075	191.8041	231.0177	270.8807	310.9341	350.6686	390.7265
G08	0	4.9064	6.017	7.6801	14.2032	28.7711	47.7387	68.6035	90.5802	112.9755	135.4172
G09	0	-34.223	-63.829	-92.796	-113.273	-120.701	-121.622	-118.718	-114.156	-108.994	-104.108
G10	0	-29.7379	-58.5415	-88.2486	-110.632	-121.264	-123.182	-120.679	-116.06	-110.379	-104.514
G11	0	11.1221	16.2462	20.8732	29.3702	42.3932	59.6249	78.24	98.2869	118.3376	138.7144
G12	0	38.2891	66.5681	93.9843	122.5333	151.8191	181.0259	210.3165	239.3277	253.3365	279.9908
G13	0	99.6847	173.3935	246.1385	314.5753	376.6597	433.6431	487.9851	542.5651	596.2685	649.2344
G14	0	92.0964	167.9752	246.9739	320.9275	383.0122	443.7587	508.5043	582.961	644.5675	707.0173
G15	0	100.458	176.7788	253.9007	327.038	393.7262	456.9371	518.8076	579.3376	639.6426	699.7216
G16	0	51.4232	87.4469	123.1929	160.3333	198.6652	237.1167	277.1034	316.4356	356.101	395.6728
G17	0	14.3283	19.8103	24.7892	34.3775	50.7446	70.2904	92.419	115.6094	138.6622	162.0365
G18	0	7.2715	8.0618	7.817	9.211	13.5203	20.4701	28.642	37.426	46.3498	55.1294

Gage	Original Raw Data (N = 2,500,000)										
	P = 0.00k	P = 9.30k	P = 18.60k	P = 27.90k	P = 37.20k	P = 46.50k	P = 55.80k	P = 65.10k	P = 74.40k	P = 83.70k	P = 93.00k
G01	0	-27.5669	-51.4141	-74.9191	-92.7058	-101.34	-102.802	-101.318	-97.8927	-94.3862	-90.9726
G02	0	16.6721	28.5375	42.0187	53.3102	64.9904	78.553	91.4607	104.7365	118.7502	131.3315
G03	0	49.8795	86.0708	123.4203	160.6834	198.891	239.7316	277.4182	316.6842	356.4179	395.9704
G04	0	106.0873	186.9333	268.4422	345.9232	417.2827	488.1879	549.8084	613.6673	677.2555	740.7124
G05	0	103.6709	181.5426	260.1217	334.9108	403.6358	472.138	532.1608	593.7214	655.151	716.7732
G06	0	102.6685	179.939	257.361	331.4479	399.6884	467.1944	527.0364	588.2809	648.9289	709.9559
G07	0	48.0878	82.3893	117.3846	153.0787	191.1352	232.4853	270.3634	310.192	349.9747	389.9029
G08	0	4.6289	5.2316	6.6173	12.5838	27.1099	46.4027	66.5292	88.5086	111.0892	133.4883
G09	0	-35.5988	-65.4369	-95.2346	-116.268	-124.619	-126.195	-123.297	-118.875	-114.133	-108.603
G10	0	-30.4708	-59.8219	-89.4336	-112.553	-123.642	-126.066	-123.381	-118.205	-113.219	-107.399
G11	0	10.5201	14.9507	19.5736	27.7009	39.9839	57.2545	75.4023	95.3975	115.2059	135.2024
G12	0	39.6252	68.0696	96.714	126.0599	155.7675	186.9075	215.5289	246.0749	276.6116	306.7954
G13	0	101.2092	176.6768	252.7589	324.5348	388.8451	452.5131	507.2246	563.8005	619.9182	675.5776
G14	0	104.6272	184.3643	265.0419	342.1597	412.5131	482.4585	543.8723	606.7792	669.3223	732.1985
G15	0	101.0129	177.5641	255.0558	328.6099	395.8543	462.9217	521.5377	581.9736	642.2307	702.4017
G16	0	51.524	87.1869	123.0343	160.0459	198.0321	239.077	276.418	315.5227	355.6005	394.8494
G17	0	13.8213	18.5188	23.5887	32.9003	48.4368	69.0928	89.7909	112.2427	136.0321	159.2248
G18	0	6.2918	6.3894	5.5438	6.1555	9.9708	16.7127	24.7202	33.3904	42.625	51.2471

Gage	Original Raw Data (N = 2,700,000)										
	P = 0.00k	P = 9.30k	P = 18.60k	P = 27.90k	P = 37.20k	P = 46.50k	P = 55.80k	P = 65.10k	P = 74.40k	P = 83.70k	P = 93.00k
G01	0	-27.8982	-50.9693	-73.7732	-92.9617	-100.189	-102.359	-101.949	-97.594	-94.1816	-90.1116
G02	0	16.1734	27.8141	40.4694	51.8625	63.5511	76.6125	89.8984	103.5486	116.9674	130.3374
G03	0	49.2869	84.8789	122.096	158.9005	197.0517	235.8526	275.4452	315.1318	354.7302	394.0981
G04	0	106.9045	186.7491	267.9543	346.1519	418.2274	486.2229	551.6709	615.8724	679.7564	743.0904
G05	0	103.7292	181.8533	260.9162	336.2372	405.8669	472.0288	535.2774	597.8854	659.6198	720.8046
G06	0	103.0561	179.9789	257.7034	332.6054	401.8952	466.7318	530.1831	592.0142	653.1092	713.9332
G07	0	47.6608	81.7696	117.0349	152.4415	190.7199	230.2076	270.0678	309.9786	350.2628	390.041
G08	0	3.3799	3.7525	5.0918	9.8545	23.0854	41.4521	62.3205	84.0671	106.5115	128.9083
G09	0	-37.5436	-68.9085	-99.2658	-122.794	-132.717	-135.308	-133.47	-129.603	-124.998	-119.466
G10	0	-32.037	-61.8055	-92.9356	-117.759	-130.231	-134.134	-132.184	-128.162	-122.85	-117.125
G11	0	10.4715	14.9009	19.1986	26.4487	39.4701	55.9054	74.7438	94.6408	114.8616	135.5008
G12	0	40.5949	69.1046	98.2711	127.5172	157.8568	188.4182	219.2152	250.5894	282.1184	313.2992
G13	0	100.9029	178.1599	253.6647	326.7673	393.1489	454.943	514.3298	572.3773	630.6634	685.9835
G14	0	104.9328	184.5522	265.5756	343.5959	415.3141	483.0035	547.9624	611.6758	674.9326	736.9896
G15	0	101.2528	177.6709	255.5407	330.1699	398.8142	463.6559	526.2745	587.3674	648.1409	708.1319
G16	0	50.6808	86.4749	122.4097	159.0878	197.5769	236.6683	276.2711	315.5976	355.3895	394.9084
G17	0	12.8046	17.1795	21.6944	30.0834	45.0646	64.3315	85.676	108.217	131.681	154.9174
G18	0	6.6101	6.9737	6.3041	7.2255	11.4411	18.0104	25.8484	34.6281	44.1604	53.7398

Gage	Original Raw Data (N = 2,900,000)										
	P = 0.00k	P = 9.30k	P = 18.60k	P = 27.90k	P = 37.20k	P = 46.50k	P = 55.80k	P = 65.10k	P = 74.40k	P = 83.70k	P = 93.00k
G01	0	-26.726	-50.4601	-74.7172	-94.0959	-102.969	-105.559	-104.679	-102.11	-100.013	-96.6
G02	0	16.5429	28.3215	41.3041	53.2069	67.3955	80.1338	93.5582	106.9778	122.5277	135.7141
G03	0	49.7058	86.3365	122.8199	160.0908	198.1552	237.007	276.327	316.1563	355.4794	395.3172
G04	0	106.7537	187.7982	269.5987	348.1135	420.4605	488.1241	553.4724	617.8529	681.219	744.8259
G05	0	103.6152	182.36	260.9784	336.5026	405.8705	471.4916	534.3379	596.0327	657.4099	718.2847
G06	0	103.1362	181.1988	259.0418	333.7818	403.4198	468.5563	531.4698	592.9498	653.8788	714.9543
G07	0	47.5757	82.2468	116.8709	152.4237	190.3416	229.2804	268.8244	308.6494	348.8498	388.5432
G08	0	3.3785	3.8887	3.9338	8.5581	21.5094	39.458	59.9065	81.79	104.0459	126.394
G09	0	-36.5756	-67.6655	-98.6666	-122.38	-133.179	-135.584	-133.93	-129.737	-124.947	-119.972
G10	0	-31.7152	-61.5767	-93.2141	-118.728	-131.753	-135.56	-133.797	-129.496	-124.231	-118.737
G11	0	10.2402	14.2535	17.6768	24.7432	36.8443	52.5431	70.9696	90.4575	110.4548	130.7273
G12	0	39.7518	68.2126	96.4389	125.5015	154.8047	184.4773	214.5218	245.0385	275.4131	305.8836
G13	0	98.8759	173.6843	248.1792	318.3207	382.2041	441.6381	498.1998	553.5599	608.0903	662.0689
G14	0	104.7397	185.0022	267.1342	345.1486	417.2338	484.8723	549.6869	613.2104	676.1378	739.2127
G15	0	100.9746	177.7176	255.6803	330.2167	398.4892	463.0983	525.0668	586.4843	646.3743	706.5978
G16	0	51.5178	87.3119	123.1581	159.933	197.9148	236.9162	276.2431	315.7579	355.5992	395.2587
G17	0	13.2208	18.1953	22.0673	30.3654	44.6112	63.3298	84.8153	107.3593	130.5503	154.0644
G18	0	6.2847	7.1682	5.8875	6.2473	9.5232	15.7186	23.1373	31.8272	41.0816	50.3827